

Superconductor Discovery in the Emerging Paradigm of Materials Informatics

Huan Tran,* Hieu-Chi Dam, Christopher Kuenneth, Vu Ngoc Tuoc, and Hiori Kino



Cite This: <https://doi.org/10.1021/acs.chemmater.4c01757>



Read Online

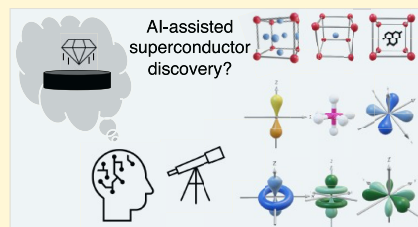
ACCESS |

Metrics & More

Article Recommendations

Supporting Information

ABSTRACT: The past two decades have witnessed a tremendous number of computational predictions of hydride-based (phonon-mediated) superconductors, mostly at extremely high pressures, i.e., hundreds of gigapascals. These discoveries were strongly driven by Migdal–Eliashberg theory (and its first-principles computational implementations) for electron–phonon interactions, the key concept of phonon-mediated superconductivity. Dozens of predictions were experimentally synthesized and characterized, triggering not only enormous excitement in the community but also some debates. In this work, we review the computationally driven discoveries and the recent developments in the field from various essential aspects, including the theoretically based, computationally based, and, specifically, artificial intelligence/machine learning (AI/ML)-based approaches emerging within the paradigm of materials informatics. While challenges and critical gaps can be found in all of these approaches, AI/ML efforts specifically remain in their infancy for good reasons. However, there are opportunities in which these approaches can be further developed and integrated in concerted efforts, in which AI/ML approaches could play more important roles.



1. INTRODUCTION

Superconductivity was discovered by H. Kamerlingh Onnes in 1911.¹ When cooling some ordinary substances such as mercury and lead down to a critical temperature T_c near absolute zero, Onnes found that their electrical resistance R completely disappears, signaling that they can carry a current indefinitely without losing any energy. In this state, a superconducting material is a perfect diamagnet; i.e., it completely repels external magnetic fields in the phenomenon known as the Meissner effect.² Although the T_c discovered for the first superconductors is generally very low, e.g., just a few Kelvin,^{3–5} the discovery of superconductivity triggered not only the development of a new branch of condensed matter physics^{6–30} but also significant interest from society^{31–33} in the century to come. The ultimate research goal is a material that “superconducts” electricity under ambient conditions, i.e., at room temperature and above ($T_c \geq 300$ K) and at atmospheric pressure ($P \simeq 0.1$ GPa). If such a material was to be discovered, it would unlock many technologies previously confined to science fiction, potentially transforming human civilization as we know it.^{34,35} Before the 21st century, numerous new superconductors were discovered,^{36–51} pushing the record for T_c to $\simeq 150$ K^{45,46} under (nearly) ambient pressure (see Figure 1). This period was largely propelled by experimental efforts, often performed in combination with profound physics expertise and intuition.

Concurrently with experimental advancements, a new branch of theoretical condensed matter physics emerged, dedicated to the understanding of superconductivity, “a manifestation of the quantum world on a macroscopic scale”,²² from the atomic level.^{6–23,25–27} The first solid

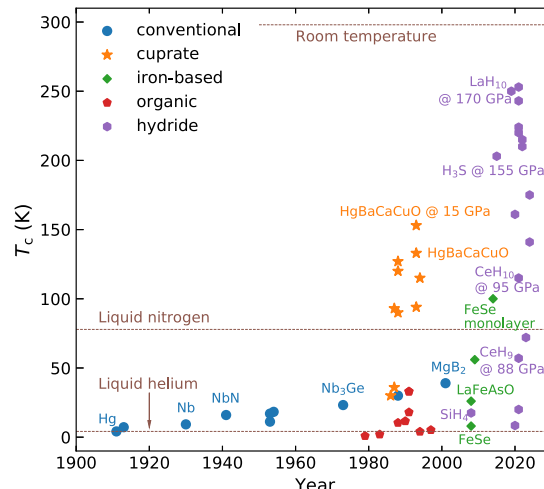


Figure 1. Time evolution of T_c for some classes of superconductors.

microscopic theory of superconductivity was developed by Bardeen, Cooper, and Schrieffer (BCS) in 1957.^{12–14} Briefly, lattice phonons can mediate a net attractive interaction between certain pairs of electrons in the neighborhood of

Received: June 25, 2024

Revised: October 28, 2024

Accepted: October 29, 2024

the Fermi surface, fusing them into a bound state called a Cooper pair.¹² Below T_c , the Cooper pairs can form a robust quantum condensation that can flow without dissipation. Some years later, Migdal–Éliashberg theory was developed,^{19–24} providing a more complete, truly many-body approach for the simplified model of instantaneous electron–phonon (EP) interactions in the BCS theory. From another perspective, theoretical endeavors^{25–30} have expanded far beyond the phonon-mediated pairing mechanism, which applies to approximately one-third of known (conventional) superconductors.⁵² For the remaining two-thirds of (unconventional) superconductors, in which this pairing mechanism does not apply, dozens of new mechanisms were suggested, involving possible roles of screened Coulomb interactions,⁵³ polarons,⁵⁴ anyons,⁵⁵ Majorana Fermions,⁵⁶ topology,⁵⁷ spin fluctuations,⁵⁸ resonating valence bond states,⁵⁹ and more. Unconventional superconductors are arranged into numerous classes, e.g., cuprates,³⁸ iron-based,^{48–51} heavy Fermion materials,^{60,61} and organic materials,^{62–65} and each may be associated with one or more pairing mechanisms. Theoretically, the proposed mechanisms impose no inherent limits on T_c ; in fact, the Kohn–Luttinger theorem⁵³ allows for an arbitrarily small T_c . After all, superconductivity remains one of the most challenging and enigmatic topics of physics, with much yet to be understood.

Starting from the 2000s, first-principles computational approaches and the required infrastructure have progressed^{66–72} to the point where they can provide, within the framework of Migdal–Éliashberg theory, some valuable guidance in the search for new phonon-mediated superconductors.^{73–97} Two classes of first-principles-based methods that are critical for superconductor discovery are structure prediction methods^{66,67} and density functional perturbation theory (DFPT).^{71,72} The former is used to explore the configuration space, while the latter is used to approximate the EP interactions. Equipped with these tools, one may start from a hypothetical chemical formula, predicting the lowest-enthalpy atomic structures at specific pressures, examining their thermodynamic and dynamical stability, evaluating the EP interactions, and, finally, estimating their T_c . This generic workflow (shown in Figure 2a) was used predominantly during the past two decades, leading to thousands of predictions for high- T_c materials.^{73–92} Dozens of them, including SiH_4 ,⁹⁸ H_3S ,⁹⁹ LaH_{10} ,^{100,101} ThH_{10} ,¹⁰² BaH_{12} ,¹⁰³ YH_6 ,^{104,105} YH_9 ,¹⁰⁵ CeH_9 , and CeH_{10} ,¹⁰⁶ CaH_6 ,^{107,108} and LaBeH_8 ,¹⁰⁹ were synthesized and tested experimentally (see Table 1 for a summary), increasing T_c to a record of ≈ 250 K, but at the cost of ultrahigh pressures (P) of ≈ 100 –200 GPa. Despite these achievements, critical gaps remain in various stages of the workflow, possibly impacting its predictive power, which is one of the points raised⁵² in the ongoing debates in the field.^{52,110–116}

Figure 1 provides a snapshot of the evolution of T_c during the past century. New discoveries, labeled as “hydride superconductors” in Figure 1 and summarized in Table 1, were synthesized and tested experimentally, while some of them were reproduced independently. The highest- T_c conventional superconductor is MgB_2 with a T_c of ≈ 39 K,⁴⁷ while the T_c values of unconventional superconductors reach ≈ 150 K.^{45,46} The discoveries of hydride superconductors push the boundary to ≈ 250 K at hundreds of gigapascals. Some points should be noted here on them. First, the discoveries are strongly driven by the Migdal–Éliashberg theory-based first-

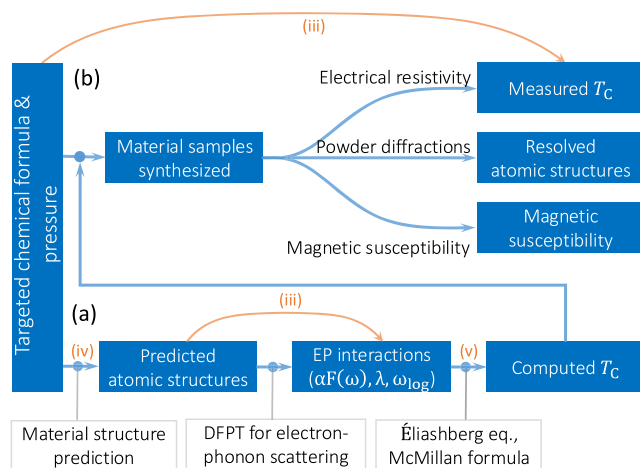


Figure 2. Typical (a) computational and (b) experimental workflows for superconductor discovery. ML efforts are divided into five groups (see section 4). Three of them are (iii) predicting superconductivity-related properties, (iv) accelerating the structure predictions by ML potentials, and (v) deriving new formulas of T_c . Some computational predictions were advanced to experimental synthesis and characterization.

principles computational workflow, suggesting the growing role of this non-experimental method. Second, hydride superconductors are predominant in the discoveries,⁸⁰ perhaps because the field is strongly inspired by Ashcroft, who, in 2004, predicted^{117,118} that high- T_c superconductivity may be found in hydrogen-dominant alloys, probably at high pressure. The main rationale is that such materials may feature high vibrational frequencies involving the hydrogen atoms, thus enhancing the electron–phonon interactions. Finally, some extraordinary experimental claims were retracted in the past several years after facing valid concerns from the community.^{52,110–116} We believe that transparency and healthy debates are important for the scientific integrity of all fields, including superconductivity.

The surge in computation-inspired superconductor discoveries^{73–92} is occurring almost simultaneously with the emergence of materials informatics,^{119–126} a new frontier of materials research. Within this paradigm, artificial intelligence/machine learning (AI/ML)-based methods are developed to learn past data and accelerate the understanding, discovery, and design of new materials. Given their nature, AI/ML approaches may, in principle, complement any physics-based experimental and computational methods that can produce reliable data. Despite considerable efforts,^{91,92,127–165} materials informatics approaches for superconductor discovery remain in their infancy.^{142,157} Upon examination of other branches of materials informatics where concerted efforts with traditional physics-based methods are blossoming, it is obvious that superconductor discovery would greatly benefit if the informatics-related developments were to gain more momentum.

In this work, we will review the recent computation-driven discoveries of hydride superconductors with an eye to the emerging paradigm of materials informatics, which can, in principle, be useful for the future discovery of superconductors in any classes. For this goal, section 2 is devoted to the essential background of superconductor discovery, including the Migdal–Éliashberg theory, the first-principles computations of phonon-mediated superconductivity-related proper-

Table 1. Notable Hydride Superconductors, Given in Terms of Chemical Formula, That Were Discovered Computationally and Then Confirmed Experimentally from the 2000s^a

formula	T_c^{\max} (K)	$P@T_c^{\max}$ (GPa)	experimental discovery	computer prediction	short summary
SiH ₄	17.5	90	2008 ⁹⁸	2006 ^{230,231} 2007 ²³²	electrical resistance measured, P_6 structure resolved, not matched with predictions, multiple structure searches follow, refining the structure
H ₃ S	203	155	2015 ⁹⁹	2014 ⁸²	electrical resistance and magnetic susceptibility measured, $Im\bar{3}m$ structure resolved and matched with predictions, superconductivity replicated ^{233–237}
LaH ₁₀	250	170	2019 ^{100,101}	2017 ^{87,88}	electrical resistance measured, $Fm\bar{3}m$ structure resolved and matched with predictions, superconductivity replicated ²³⁸
ThH ₉	146	170	2020 ¹⁰²	N/A	electrical resistance measured, $P6_3/mmc$ structure resolved
ThH ₁₀	161	174	2020 ¹⁰²	2018 ⁸⁹	electrical resistance measured, $Fm\bar{3}m$ structure resolved and matched with predictions
PrH ₉	8.4	120	2020 ²³⁹	2020 ²³⁹	electrical resistance measured, $P6_3/mmc$ structure resolved and matched with predictions
BaH ₁₂	20	140	2021 ¹⁰³	2021 ¹⁰³	electrical resistance measured, $Cmc2_1$ structure resolved and matched with predictions
(La,Y)H ₁₀	253	199	2021 ²¹¹	2021 ²¹¹	electrical resistance measured, $Fm\bar{3}m$ structure resolved and matched with predictions
YH ₆	224	168	2021 ¹⁰⁴	2015 ^{86,88}	electrical resistance measured, $Im\bar{3}m$ structure resolved and matched with predictions, superconductivity replicated ¹⁰⁵
	220	183	2021 ¹⁰⁵	2015 ^{86,88}	
YH ₉	243	201	2021 ¹⁰⁵	2017 ⁸⁸	electrical resistance measured, $P6_3/mmc$ structure resolved and matched with predictions, superconductivity replicated ²⁴⁰
CeH ₉	57	88	2021 ¹⁰⁶	2017 ⁸⁸	electrical resistance measured, $P6_3/mmc$ structure resolved and matched with predictions, T_c replicated and diamagnetism of the Meissner effect probed ²⁴¹
CeH ₁₀	115	95	2021 ¹⁰⁶	2017 ⁸⁸	electrical resistance measured, $Fm\bar{3}m$ structure resolved and matched with predictions
ScH ₃	18.5	131	2021 ²⁴²	2010, ²⁴³ 2016 ²⁴⁴	electrical resistance measured, $Fm\bar{3}m$ structure resolved and matched with predictions
LuH ₃	12.4	122	2021 ²⁴²	N/A	electrical resistance measured, $Fm\bar{3}m$ structure resolved
CaH ₆	215/210	172/160	2022 ^{107,108}	2012 ^{81,148}	electrical resistance measured, $Im\bar{3}m$ structure resolved and matched with predictions, superconductivity replicated ¹⁰⁸
SnH ₄	72	180	2023 ²⁴⁵	2023 ²⁴⁵	electrical resistance measured, $Fm\bar{3}m$ structure resolved and matched with predictions
LaBeH ₈	110	80	2023 ¹⁰⁹		electrical resistance measured, $Fm\bar{3}m$ structure resolved
NbH ₃	42	187	2024 ²⁴⁶	N/A	electrical resistance measured, $Fm\bar{3}m$ structure resolved
La _{0.5} Ce _{0.5} H ₁₀	175	155	2024 ²⁴⁷	2024 ²⁴⁷	electrical resistance measured, $Fm\bar{3}m$ structure resolved
Y _{0.5} Ce _{0.5} H ₉	141	130	2024 ²⁴⁸	N/A	electrical resistance measured, $P6_3/mmc$ structure resolved
La ₄ H ₂₃	90	95	2024 ²⁴⁹	NA	electrical resistance measured, $Pm\bar{3}m$ structure resolved

^aFor each, maximum observed critical temperature T_c^{\max} , $P@T_c^{\max}$ at which T_c^{\max} was observed, years and references of (experimental) discoveries and (computational) predictions, and a short summary of the discoveries are provided.

ties, and the computational workflow used widely for the discoveries. Section 2 also includes a minimal coverage of some experimental methods needed for the discussions, although the main theme of this work is non-experimental. Then, in section 3, major computation-driven experimental discoveries that were reproduced and confirmed at some levels are reviewed. Next, an introduction of materials informatics is given in section 4, followed by a review of the materials informatics works that have been completed in this field. Finally, we offer in section 5 some opinions on the remaining challenges and some forward-looking next steps, specifically in terms of what materials informatics can do to further contribute to the future of superconductor discovery.

2. FUNDAMENTALS OF SUPERCONDUCTOR DISCOVERY

2.1. Migdal–Éliashberg Theory. In BCS theory,^{8,13} the phonon-mediated interaction between certain pairs of electrons residing within an energy cutoff ω_c from the Fermi surface is assumed to be instantaneous and constant, while vanishing beyond ω_c . This simplified picture does not include enough of the physics of interacting electron–phonon systems. Migdal–Éliashberg theory is more complete,^{19–24} taking into account the retarded nature of the EP interactions, considering the first order of vertex corrections,²¹ while relying on the Migdal theorem²⁰ to treat the damping of the excitations. Central to this theory are the anisotropic nonlinear integral

Éliashberg equations involving Matsubara gap $\Delta(\mathbf{k}, i\omega_n)$ and renormalization factor $Z(\mathbf{k}, i\omega_n)$. On the imaginary axis, they are¹⁶⁶

$$Z(\mathbf{k}, i\omega_n) = 1 + \frac{\pi T}{N_F \omega_n} \sum_{\mathbf{k}', n'} \frac{\omega_{n'}}{\sqrt{\omega_{n'}^2 + \Delta^2(\mathbf{k}, i\omega_n)}} \times \lambda(\mathbf{k}, \mathbf{k}', n - n') \quad (1)$$

and

$$Z(\mathbf{k}, i\omega_n) \Delta(\mathbf{k}, i\omega_n) = \frac{\pi T}{N_F} \sum_{\mathbf{k}', n'} \frac{\Delta(i\omega_{n'})}{\sqrt{\omega_{n'}^2 + \Delta^2(\mathbf{k}, i\omega_n)}} \times [\lambda(\mathbf{k}, \mathbf{k}', n - n') - N_F V(\mathbf{k} - \mathbf{k}')] \quad (2)$$

where N_F is the density of states (DOS) at Fermi level ε_F , $i\omega_n = \pi T(2n - 1)$ is the n th Matsubara frequency where $n = 0, \pm 1, \pm 2, \dots$, T is the temperature, and $V(\mathbf{k} - \mathbf{k}')$ is the screened Coulomb interaction between electronic states \mathbf{k} and \mathbf{k}' . Furthermore

$$\lambda(\mathbf{k}, \mathbf{k}', n - n') = 2 \int_0^\infty d\omega \frac{\omega}{\omega^2 + (\omega_n - \omega_{n'})^2} \times \alpha^2 F(\mathbf{k}, \mathbf{k}', \omega) \quad (3)$$

is the EP coupling, determined from the EP spectral function

$$\alpha^2 F(\mathbf{k}, \mathbf{k}', \omega) = N_F \sum_{\nu} |g_{\mathbf{k}, \mathbf{k}'}^{\nu}|^2 \delta(\omega - \omega_{\mathbf{k}-\mathbf{k}'}^{\nu}) \quad (4)$$

In eq 4, $g_{\mathbf{k}, \mathbf{k}'}$ is the EP matrix elements, ν is the polarization index of the phonon with frequency ω , and δ is the delta-Dirac function. When the anisotropy of the Fermi surface is weak, the isotropic spectral function

$$\alpha^2 F(\omega) = \frac{1}{N_F^2} \sum_{\mathbf{k}, \mathbf{k}'} \alpha^2 F(\mathbf{k}, \mathbf{k}', \omega) \delta(\epsilon_{\mathbf{k}}) \delta(\epsilon_{\mathbf{k}'}) \quad (5)$$

can be used to suppress the \mathbf{k} dependence in eqs 1–3, yielding two isotropic Eliashberg equations and an isotropic EP coupling $\lambda(n - n')$. Within this approximation, the BCS gap equation can be reproduced by setting $\lambda(n - n') = \lambda$ for both $|\omega_n|, |\omega_{n'}| < \omega_c$ and 0 otherwise,¹⁸ where

$$\lambda = 2 \int_0^{\infty} d\omega \frac{\alpha^2 F(\omega)}{\omega} \quad (6)$$

is the dimensionless isotropic EP coupling $\lambda(n - n')$ at $n = n'$ that will be used extensively in the literature.

One way to examine the superconductivity of a material is to solve the Eliashberg equations (eqs 1 and 2) self-consistently^{166–168} at multiple values of T for a nontrivial solution $\Delta(\mathbf{k}, i\omega_n)$ and the highest T at which $\Delta(\mathbf{k}, i\omega_n) \neq 0$ defines T_c . In this procedure, two main inputs are spectral function $\alpha^2 F(\mathbf{k}, \mathbf{k}', \omega)$ and dimensionless Coulomb pseudopotential μ^* , introduced as a treatment for the last term of eq 2. It is defined by^{166,167,169}

$$\mu^* = \frac{N_F \langle \langle V(\mathbf{k} - \mathbf{k}') \rangle \rangle}{1 + N_F \langle \langle V(\mathbf{k} - \mathbf{k}') \rangle \rangle \ln(\epsilon_F / \omega_c)} \quad (7)$$

where the double angle brackets denote the double average of the screened Coulomb interaction over \mathbf{k} and \mathbf{k}' on the Fermi surface. With μ^* defined in eq 7 and precomputed, $\lambda(\mathbf{k}, \mathbf{k}', n - n') - N_F V(\mathbf{k} - \mathbf{k}')$ becomes $\lambda(\mathbf{k}, \mathbf{k}', n - n') - \mu^*$ before eqs 1 and 2 are solved numerically.^{166,167}

To bypass the cumbersome step of solving the Eliashberg equations (eqs 1 and 2), in 1968, McMillan¹⁷⁰ started from some solutions of these equations to develop a direct, empirical formula for T_c , given that isotropic spectral function $\alpha^2 F(\omega)$ is known. It was then modified by Allen and Dynes^{171,172} in 1975 to be

$$T_c = \frac{\omega_{\log}}{1.2} \exp \left[-\frac{1.04(1 + \lambda)}{\lambda - \mu^*(1 + 0.62\lambda)} \right] \quad (8)$$

where

$$\omega_{\log} = \exp \left[\frac{2}{\lambda} \int_0^{\infty} d\omega \ln(\omega) \frac{\alpha^2 F(\omega)}{\omega} \right] \quad (9)$$

is the first logarithmic moment of $\alpha^2 F(\omega)$. In the McMillan approach, μ^* is an empirical parameter typically ranging from 0.10 to 0.20.^{117,118} The empirical eq 8 is good for $\lambda \leq 1.5$, while additional empirical parameters are needed for larger values.¹⁷² Recently, there have been some efforts^{133,134} to derive alternative formulas of eq 8, and they will be reviewed in section 4.5. Because of its simplicity, the McMillan formula (eq 8) and some related versions¹⁷² were used extremely widely in the literature to estimate T_c given the computed $\alpha^2 F(\omega)$.

The domain of applicability is an essential aspect of a mathematical model. According to the Migdal theorem,²⁰ Migdal–Eliashberg theory is believed¹⁹ to be valid if the

phonon energy scale is much smaller than the electronic energy scale, i.e., $\lambda \omega_c / \epsilon_F \ll 1$, even in the strong coupling regime, i.e., $\lambda \geq 1$. Subsequent examinations^{173–178} suggest a more complex picture. Among others, a common conclusion of these works is that Migdal–Eliashberg theory may be inaccurate when λ exceeds a certain value, which can be 0.4,¹⁷³ 1.0,^{174,175} 1.3,¹⁷⁶ or 3.7.¹⁷⁷ Given that $\lambda \geq 1.0$ in most of the published reports employing this theory to predict T_c ^{73–92} we believe that extra care is needed for the predictions. Readers who are interested in the validity and the possible breakdown of Migdal–Eliashberg theory are referred to some recent beautiful reviews^{21,22} and original articles.^{173–177}

2.2. First-Principles Computations. Computing EP matrix element $g_{\mathbf{k}, \mathbf{k}'}$ from first principles, and thus $\alpha^2 F(\mathbf{k}, \mathbf{k}', \omega)$ and $\alpha^2 F(\omega)$, is crucial for using Migdal–Eliashberg theory in practice.²⁴ The standard method for such computations is DFPT,^{71,72} a perturbation treatment for the response of quantum systems described at the level of density functional theory (DFT).^{179,180} Notable implementations of DFPT can be found in QUANTUM ESPRESSO^{181,182} and ABINIT,^{183–185} two major DFT tools for calculating phonon-related properties of solids. Using these packages, thousands of predictions of superconductors have been reported since the 2000s.^{73–95} While the calculations of $\alpha^2 F(\mathbf{k}, \mathbf{k}', \omega)$ and $\alpha^2 F(\omega)$ are computationally demanding, some high-throughput efforts^{140,141,148–150} have made significant strides in this area.

In practice, $\alpha^2 F(\mathbf{k}, \mathbf{k}', \omega)$ and its isotropic version, $\alpha^2 F(\omega)$, are computed on two finite-size Γ -centered grids, one for the (electronic) \mathbf{k} points and one for the (phononic) \mathbf{q} points defined as $\mathbf{q} = \mathbf{k} - \mathbf{k}'$, while the \mathbf{q} grid must be a subgrid of the \mathbf{k} grid. Once $\alpha^2 F(\mathbf{k}, \mathbf{k}', \omega)$ and $\alpha^2 F(\omega)$ are computed, there are two ways to estimate T_c as discussed in section 2.1. In the first approach, eqs 1 and 2 are solved iteratively, e.g., on the imaginary axis, for a nontrivial solution of $\Delta(\mathbf{k}, i\omega_n)$ using a designated code like Electron–Phonon Wannier (EPW).^{166–168} Then, real-axis superconducting gap function $\Delta_0(T)$ is approximated from $\Delta(\mathbf{k}, i\omega_n)$, e.g., using Páde continuation.¹⁸⁶ Finally, T_c is determined as the maximum temperature at which order parameter $\Delta_0(T)$ remains non-zero. The second, and more commonly employed, method uses empirical formulas for T_c from prior solutions to the Eliashberg equations, such as the McMillan formula (eq 8). Having $\alpha^2 F(\omega)$, λ and ω_{\log} can be computed using some postprocessing tools¹⁸⁷ of the QUANTUM ESPRESSO suite^{181,182} and ABINIT^{183–185} for eqs 6 and 9. Unfortunately, both approaches need an empirical value of μ^* for some reasons,^{167,181–185} while efforts to derive more rational values of μ^* , e.g., using eq 7, are limited.¹⁸⁸

Although the DFT-based calculations may be exact in principle, practical calculations of superconductivity-related quantities require certain finite-size \mathbf{k} - and \mathbf{q} -point grids, pseudopotentials, exchange-correlation functionals, finite-energy cutoffs, finite smearing widths for the δ functions in eqs 4 and 5, empirical values of μ^* , whether to include anharmonic effects¹⁰⁴ and/or spin–orbit couplings,¹⁸⁹ and more.^{142,190,191} In many cases, the desired convergence, e.g., with respect to the \mathbf{k} - and \mathbf{q} -point grids, may be computationally prohibitive, and some affordable parameters must be assumed. In fact, controlling these factors is challenging in phonon-related calculations, because acceptable numerical errors in energy and force evaluations are several orders of magnitude smaller than those deemed sufficient for standard DFT calculations. Despite

the established reliability of DFT in regular electronic structure problems,¹⁹² the factors described above present potential sources of numerical error when computing $\alpha^2 F(\mathbf{k}, \mathbf{k}', \omega)$, $\alpha^2 F(\omega)$, and, ultimately, T_c . A more detailed discussion of these challenges is presented in section 5.1.

2.3. A Practical Computational Discovery Workflow.

Targeted materials discovery, often termed “inverse design”, involves the guided exploration of the vast materials space to find synthesizable materials possessing the desired properties.^{193–198} In a broad sense, the materials space is truly infinite, containing all possible chemical compositions, external conditions, microscopic details, macroscopic morphologies, additives, and processing parameters needed to describe and fabricate a material. Due to this immense complexity and space, a trial-and-error approach is impractical, even with highly efficient evaluation and decision-making processes. Instead, an effective inverse design strategy must involve an “intelligent” protocol that rationally directs the exploration toward the targeted properties. Limited versions of this protocol were developed,^{193–198} actively contributing to the recent discovery of various functional materials.^{199–206} One strategy, which is widely used for discovering superconductors,^{73–95} is depicted in Figure 2a. In this strategy, computational methods for predicting atomic structures have reached an advanced level of maturity.^{66–68}

The computational workflow for discovering new superconductors, as shown in Figure 2a, consists of several steps. First, usually guided by chemical intuition and expertise, a targeted chemical formula and external conditions (e.g., a range of pressures) are selected. Subsequently, employing a DFT-level structure prediction method, the atomic structures that are both thermodynamically and dynamically stable are predicted. In this step, a pressure–temperature phase diagram of the targeted chemical formula is usually needed.^{85,207,208} For this purpose, one may need very expensive computations for the Gibbs free energy of different atomic phases, e.g., using advanced tools like PHONOPY²⁰⁹ and SSCHA.²¹⁰ Next, the superconducting properties of these atomic structures are computed, by either solving the Éliashberg equations or using the McMillan formula, to identify those with respectable predicted T_c values. While most of the computational works conclude at this juncture, some proceed to experimental synthesis and testing of these new materials, confirming the predicted superconductivity, as sketched in Figure 2b.

If we put the computations of phonon-mediated superconducting properties aside, atomic structure prediction is a very time-consuming step. Its goal is to find a thermodynamically stable arrangement of atoms for a given chemical formula at a given pressure, considering its potential decomposition into all possible related materials. This requires, at least, a convex hull analysis,^{84–89,208,211} which necessitates the prediction of the lowest-enthalpy atomic structure, i.e., the global minimum of the multidimension potential energy surface (PES), for each related formula. Given the exponential increase in the number of local minima on a PES with the system size,²¹² the global optimization problem for each formula presents a formidable challenge. Despite its computational costs, an advanced first-principles-based materials structure search is strongly desired to explore unknown domains of the materials space in which unknown chemistries and atomic structures are expected, and relying on the known prototype structures is insufficient. In fact, unconstrained structure prediction endeavors have uncovered numerous

novel (non-existing) atomic structures^{207,213–215} that were then confirmed experimentally.^{216–218} For superconductor discovery, the structure prediction step is critical, especially when the searches extend to the territories no one has ever explored, e.g., at hundreds of gigapascals. Current state-of-the-art structure prediction methods, which were used widely in superconductor discovery, are USPEX,^{219,220} CALYPSO,²²¹ *ab initio* random structure search (AIRSS),²²² XtalOpt,²²³ MAISE,²²⁴ and minima hopping.^{225,226}

2.4. Experimental Synthesis and Characterizations.

Some computationally discovered hydride superconductors were synthesized and tested experimentally.^{98–109} For those advanced to this step, the targeted formulations are typically synthesized by reacting pure metals with excess hydrogen or hydrogen-rich gases, e.g., ammonia borane and hydrocarbons, often using laser heating in diamond anvil cells (DACs) under the desired pressure.

With the samples in hand, electrical resistance R was always examined, typically using the four-point probe technique.^{250,251} By definition, the presence of a superconducting transition is implied when R decreases sharply to zero at critical temperature T_c . The isotope effect,^{252,253} a footprint of the lattice dynamics on the phonon-mediated superconductivity, can then be observed in the dependence of T_c on the average isotope mass of the material. Magnetic susceptibility measurements are more challenging but critical^{254,255} because they can help probing the Meissner effect,² a hallmark of superconductivity, while providing other essential information such as the critical field, penetration depth, and critical current density. Four methods that may be used are alternating-current (AC) susceptibility measurements using a pickup/compensating coil architecture,²³⁴ a superconducting quantum interference device (SQUID) magnetometer,⁹⁹ the synchrotron Mössbauer technique,²⁵⁶ and a quantum sensing approach involving nitrogen-vacancy centers implanted in DACs.^{241,257} As performing these techniques under hundreds of gigapascals in a DAC is nontrivial, only a few magnetic susceptibility measurements have been reported.^{234,238} Instead, the most widely used approach is to measure the dependence of T_c on the external magnetic field, the behavior that could reveal the upper critical field, ultimately linking to the coherence length of the superconducting state.^{7,258} A new method,²⁵⁹ measuring the magnetic flux trapped inside the superconducting samples, i.e., the incomplete Meissner effect, seems to be useful. Finally, resolving the atomic structure of the synthesized samples is desirable. For this goal, the X-ray diffraction (XRD) pattern and sometimes Raman scattering are powerful methods. Overall, tremendous challenges remain for the experimental techniques in superconductor discovery, specifically magnetic susceptibility measurements at extremely high pressures in a DAC, and readers are referred to refs 241, 257, and 259 for more information.

Figure 2b summarizes the aforementioned measurements, among others, desired and used for probing the possible superconductivity. All of the discovered hydride superconductors discussed in section 3 have been experimentally synthesized, and at least one of the three characteristics is examined.

3. COMPUTATION-DRIVEN SUPERCONDUCTOR DISCOVERIES

We now turn to the discoveries of hydride superconductors in the past two decades, mostly driven by the first-principles

computational methods and workflow. It is interesting to note that Ashcroft's prediction^{117,118} about the possible superconductivity in hydrides came more than three decades after his similar prediction about compressed hydrogen.²⁶⁰ One way to view the difference between the two predictions is that hydrogen atoms in solid materials are "chemically precompressed";²³⁰ thus, realizing the prediction in these materials could be technically more feasible. This may be a reason why the latter^{117,118} was soon followed by thousands of computational and dozens of experimental discoveries.

Table 1 and **Figure 3** provide a (likely incomplete) summary of the computational and experimental discoveries reported

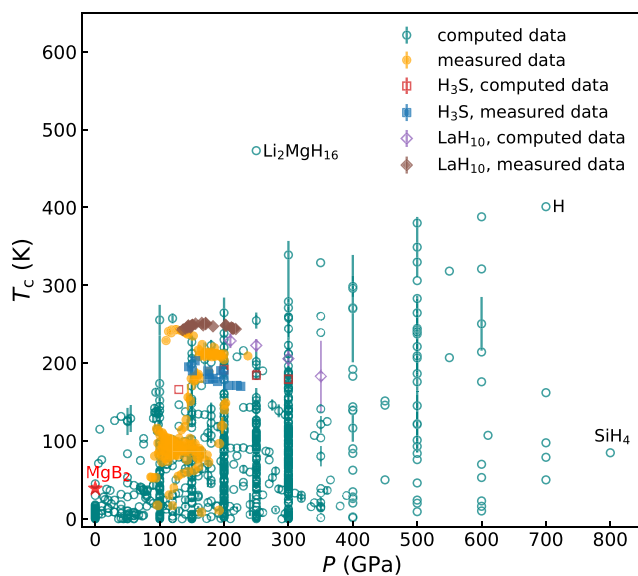


Figure 3. Incomplete snapshot of the phonon-mediated superconductors discovered computationally. For some of them, e.g., H_3S and LaH_{10} , experimental data are available and also shown. Highlighted in the figure, data for MgB_2 at 0 GPa, $\text{Li}_2\text{MgH}_{16}$ at 250 GPa, H at 700 GPa, and SiH_4 at 800 GPa are taken from refs 47, 227, 228, and 229, respectively. Some of the data used for this figure were used for Figure 2c of ref 142.

starting from the 2000s. Not surprisingly, most of the materials are rich in hydrogen, predicted to be superconductors at very high pressures, reaching ≈ 800 GPa. One of the most striking computational predictions is the superconductivity of $\text{Li}_2\text{MgH}_{16}$ at 250 GPa with a T_c of ≈ 473 K, or 200 °C,²²⁷ while the first major experimental discovery is the superconductivity of H_3S at 155 GPa with a T_c of 203 K.⁹⁹ This discovery is remarkable because it reproduced a majority of the computational predictions reported one year earlier.⁸²

The remaining part of this section is devoted to a detailed discussion of some superconducting materials that were predicted computationally and then synthesized and tested. Given the scope and the limited length of this work, and an extensive list of experimental discoveries presented in **Table 1**, we will examine a few of them that were reproduced independently and/or sparked significant interest and follow-up works from the community. For other discoveries, readers are referred to **Table 1** in which a short summary and relevant references are given for each.

3.1. Silane SiH_4 . Silane SiH_4 is the first hydride superconductor computationally predicted in 2006^{230–232} and experimentally reported in 2008,⁹⁸ shortly after Ashcroft's

later prediction.^{117,118} Upon examination of multiple atomic structures of SiH_4 and computation of frequency cutoff ω_c at a first-principles level, the orthorhombic $Pman$ structure stands out with a predicted $T_c \approx 1.13\hbar\omega_c/k_B \exp(-1/N_FV) \approx 166$ K at 202 GPa.²³⁰ In the same year, after a search for high-pressure structures of SiH_4 , a qualitative assessment of the possible superconductivity, specifically involving a monoclinic $C2/c$ phase, was conducted with a preferable conclusion at pressures of ≤ 50 GPa.²³¹ From 50 to 250 GPa, an insulating tetragonal $I4_1/a$ phase was predicted²³¹ to be thermodynamically stable and then confirmed experimentally.^{261,262} One year later, the computational workflow based on Migdal–Éliashberg theory was used²³² for another monoclinic $C2/c$ structure, visualized in **Figure 4a**, predicting a $T_c \approx 45–55$ K at 90 and 125 GPa. Spectral function $\alpha^2F(\omega)$ and the accumulated $\lambda(\omega)$ of this phase are shown in **Figure 4b**.

The computational predictions were followed by an experimental discovery,⁹⁸ in which SiH_4 samples, shown in **Figure 4c**, were fabricated. Electrical resistance measurements (one of them is given in **Figure 4b**) clearly show the superconducting-like decreases at a pressure-dependent critical temperature T_c . Between 65 and 90 GPa, T_c increases from 7 to 17.5 K before decreasing and increasing again in the regime of 120–200 GPa, as shown in **Figure 4e**. This behavior suggests the involvement of more than one phase of SiH_4 . Upon examination of Raman scattering and the XRD pattern, a superconducting hexagonal $P6_3$ phase was resolved in the first regime and the predicted $I4_1/a$ phase²³¹ was confirmed again in the second regime, in which both phases coexist.

While the superconducting hexagonal $P6_3$ phase was not predicted computationally, the discovery of the predicted superconductivity in SiH_4 and the verification of the predicted $I4_1/a$ phase are intriguing. In fact, they motivated multiple computational structure searches for SiH_4 ^{229,263,264} and disilane, a related compound with a formula of Si_2H_6 .^{265,266} As the $P6_3$ phase was found²⁶³ to be dynamically unstable, a related orthorhombic $Cmca$ phase was suggested as a candidate for the superconducting phase of SiH_4 . Among the structures subsequently found²⁶⁴ for SiH_4 , an orthorhombic $Pbcn$ phase is not only thermodynamically more stable than the $Cmca$ phase but also related to the $P6_3$ phase through its dynamical instability. Furthermore, the computed λ and ω_{\log} of the $Pbcn$ phase lead to a T_c of ≈ 16.5 K by using the McMillan formula.²⁶⁴ To close this section, we refer readers to ref 262 for a summary of such SiH_4 -related efforts.

3.2. Sulfur Hydride H_3S . In 2014, a structure prediction effort⁸² was performed to search for possible stable atomic structures of $(\text{H}_2\text{S})_2\text{H}_2$ at increased pressures of ≤ 300 GPa. This work was partially motivated by an early experimental report,²³³ showing that H_2S and H_2 , both gases under ambient conditions, can form stoichiometric compound H_3S near 3.5 GPa. The computational examination⁸² reveals that when P increases, the H_3S compound undergoes a series of structural phase transitions from $P1$ to $Cccm$ at 37 GPa, then to $R3m$ at 111 GPa, and finally to $Im\bar{3}m$ at 180 GPa. Upon examination of the simulated XRD pattern at 22 GPa, the stable $P1$ phase of H_3S was found⁸² to match with that experimentally reported.²³³ As the $R3m$ and $Im\bar{3}m$ phases are metallic at the pressures at which they are stable, superconducting-related calculations suggest that at 130 GPa, the $R3m$ phase has a λ of 2.07 and an ω_{\log} of 1125.1 K, which can be translated to a T_c range of $\approx 155–166$ K using eq 8 with μ^* ranging from 0.10 to 0.13. Likewise, at 200 GPa, the $Im\bar{3}m$ phase has a λ of 2.19, an

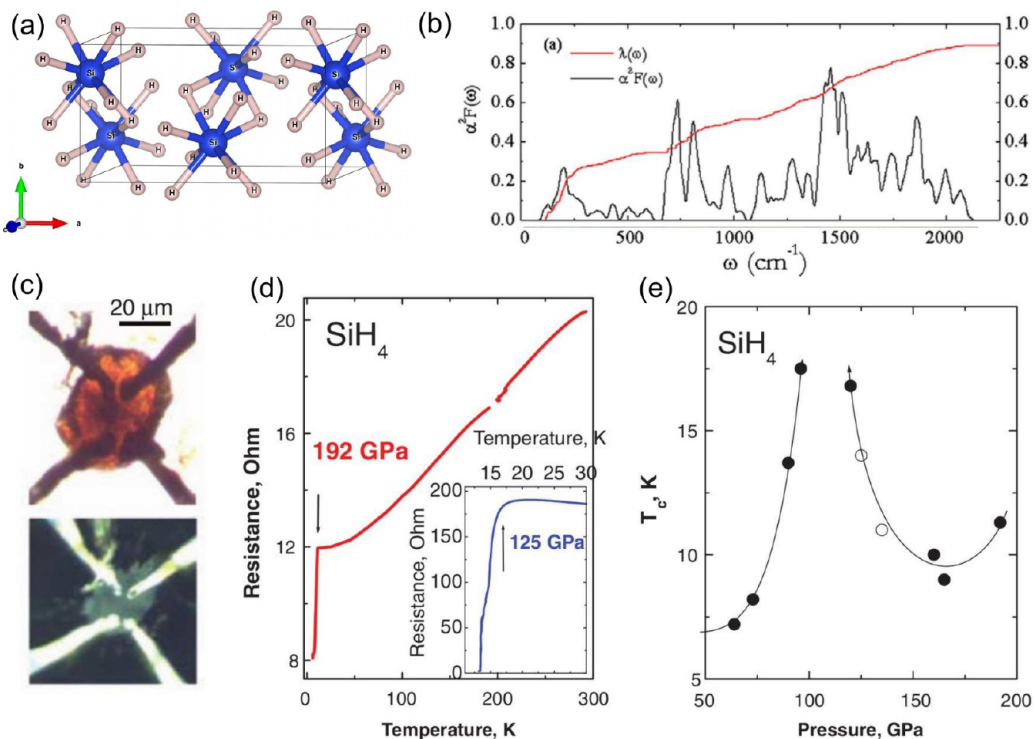


Figure 4. (a) Predicted C_2/c structure of silane SiH_4 .²³² (b) Spectral function $\alpha^2 F(\omega)$ and accumulated $\lambda(\omega)$ of the C_2/c structure. (c) Fabricated sample placed within the four-point probe. (d) Representative superconducting step in measured resistance. (e) Pressure-dependent T_c measured for silane. Panel b and panels c–e were reprinted with permission from ref 232 (Copyright 2007 IOP Publishing) and ref 98 (Copyright 2008 The American Association for the Advancement of Science), respectively.

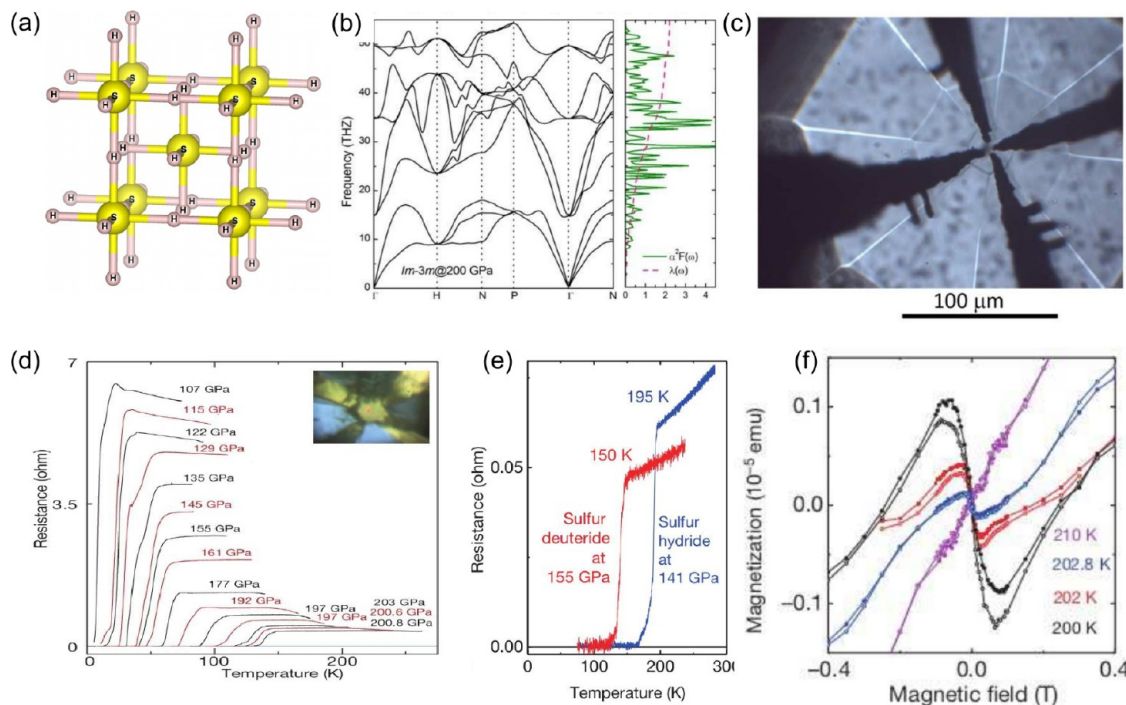


Figure 5. (a) Predicted $Im\bar{3}m$ structure of H_3S . (b) Phonon band structure, spectral function $\alpha^2 F(\omega)$, and accumulated $\lambda(\omega)$ of the $Im\bar{3}m$ structure at 200 GPa. (c) Four Ti electrodes sputtered on a diamond anvil, i.e., a four-point probe; at the center of them is the sample. (d) R – T dependence measured for H_3S at different pressures. (e) R – T dependence measured for H_3S and H_3D , which reveals the isotope effect. (f) Magnetization measured as a function of external field, showing the diamagnet and paramagnet characteristics below and above the T_c of ≈ 203 K, respectively. Panel b and panels c–f were reprinted with permission from ref 82 (under a Creative Commons license) and ref 99 (Copyright 2015 Springer Nature), respectively.

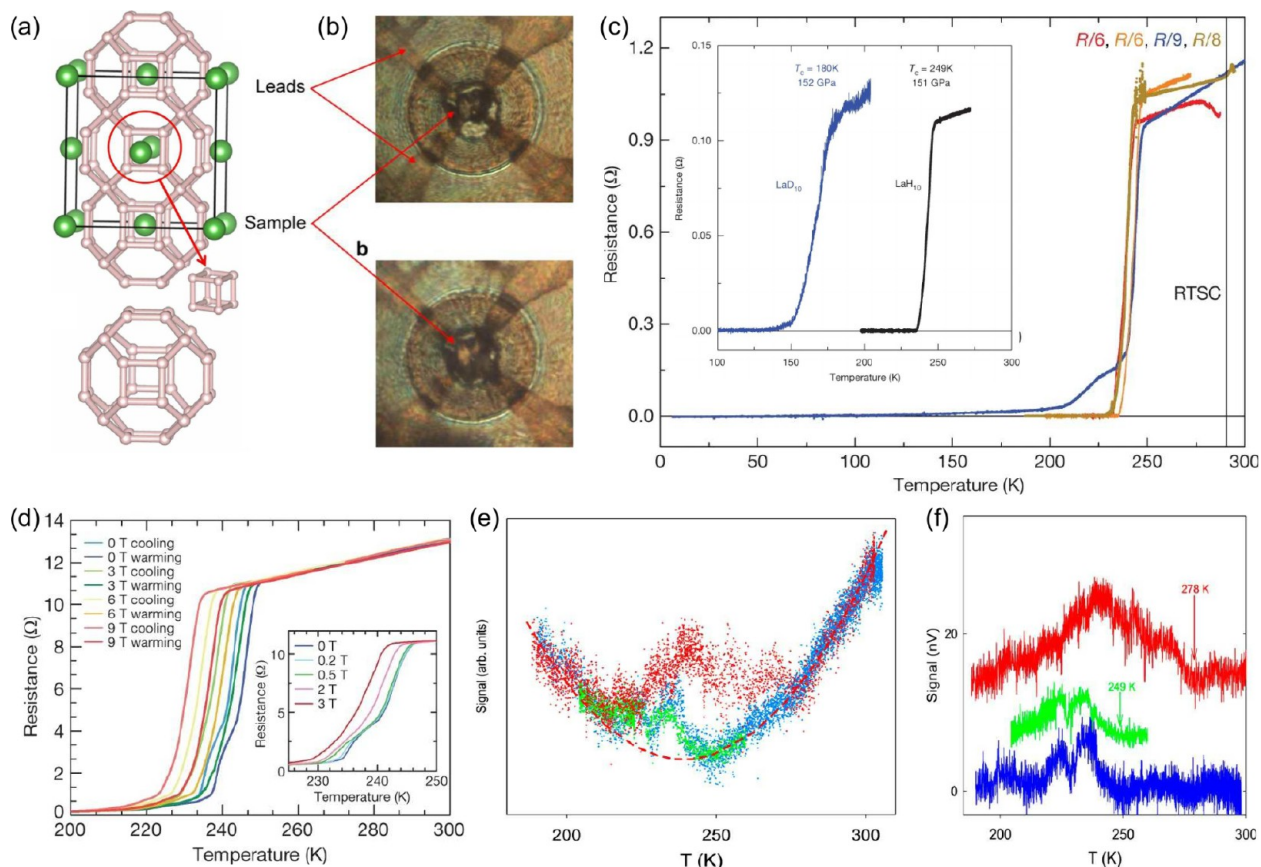


Figure 6. (a) $Fm\bar{3}m$ clathrate-like structure predicted for LaH_{10} . (b) LaH_{10} samples fabricated and placed among four probes. (c) $R-T$ dependence measured for LaH_{10} samples at zero external magnetic field. (d) $R-T$ dependence measured for LaH_{10} samples at varying external magnetic fields of ≤ 9 T. (e) Magnetic response signals from LaH_{10} samples in a DAC, whose the background is shown as a dashed line. (f) Magnetic response after the removal of the background signal. The inset of panel c shows the $R-T$ curves measured for LaH_{10} and LaD_{10} , which reveal the isotope effect. Panel a, panels b-d, and panels e and f were reprinted with permission from ref 87 (Copyright 2017 National Academy of Sciences of the United States of America), ref 101 (Copyright 2019 Springer Nature), and ref 238 (under a Creative Commons CC BY license), respectively.

ω_{\log} of 1334.6 K, and finally a T_c range of ≈ 191 – 204 K. The phonon band structure, spectral function $\alpha^2 F(\omega)$, and the accumulated $\lambda(\omega)$ of the $Im\bar{3}m$ phase of H_3S at 200 GPa are reproduced in Figure 5a.

In 2015, the superconductivity with a record-breaking T_c of 203 K at 155 GPa was observed on synthesized samples of H_3S (see Figure 5c) and reported.⁹⁹ Figure 5d shows the sharp decreases in electrical resistance to zero when T is decreased to a critical value that depends on the pressure. A strong isotope effect was also observed⁹⁹ and is shown in Figure 5e, implying a link to the lattice phonons. Magnetic susceptibility measurements were performed using SQUID,⁹⁹ revealing a transition from the diamagnetic to the paramagnetic state at ≈ 203.5 K, as shown in Figure 5f.

The superconductivity in H_3S was reproduced by some other groups.^{234–237,256} In one effort,²³⁴ the superconductivity of H_3S was probed in a range of P using AC magnetic susceptibility measurements. As P increases, the superconductivity appears at 117 GPa with a T_c of 38 K. The critical temperature then increases to 183 K at 149 GPa before decreasing to 140 K at 171 GPa. This nonmonotonic behavior may come from the change in stoichiometry and the effects of P on λ .

At first, the H_2S compound might be involved in the observation,⁹⁹ but the predicted T_c of ≈ 80 K of H_2S in this pressure range²⁶⁷ is far from the measured data. Although the

reported pressure (155 GPa) is in the regime where the $R3m$ phase of H_3S was predicted,⁸² the $Im\bar{3}m$ phase was anticipated⁹⁹ and then experimentally confirmed.^{190,235–237} The values of T_c that were computed⁸² and measured⁹⁹ for H_3S at different pressures are summarized in Figure 3, indicating an overall good agreement.

The discovery⁹⁹ and confirmation^{234–237} of the superconductivity in H_3S with a strikingly high T_c came soon after the prediction.⁸² Moreover, the predicted superconducting $Im\bar{3}m$ phase was confirmed, while the predicted T_c agrees well with the measured values. These factors make the superconductivity of H_3S a major discovery, sparking significant excitement not only in the science community but also in media and society.²⁶⁸

3.3. Lanthanum Hydride LaH_{10} . The discovery of the superconductivity in lanthanum hydride LaH_{10} was also initiated by computational structure prediction endeavors. In 2017, dozens of clathrate-like structures of hydrides were discovered computationally^{87,88} at high pressures with very high predicted T_c values. In these prototype structures, rare-earth elements like La and Y are located at the center of hydrogen cavities, linked together throughout the space (see Figures 6a and 7d for visualizations). Among the examined rare-earth hydrides, LaH_{10} in its cubic $Fm\bar{3}m$ clathrate-like structure was predicted to have an estimated T_c of ≈ 288 K at 200 GPa⁸⁸ and a T_c of ≈ 274 – 286 K at 210 GPa.⁸⁷ Quickly,

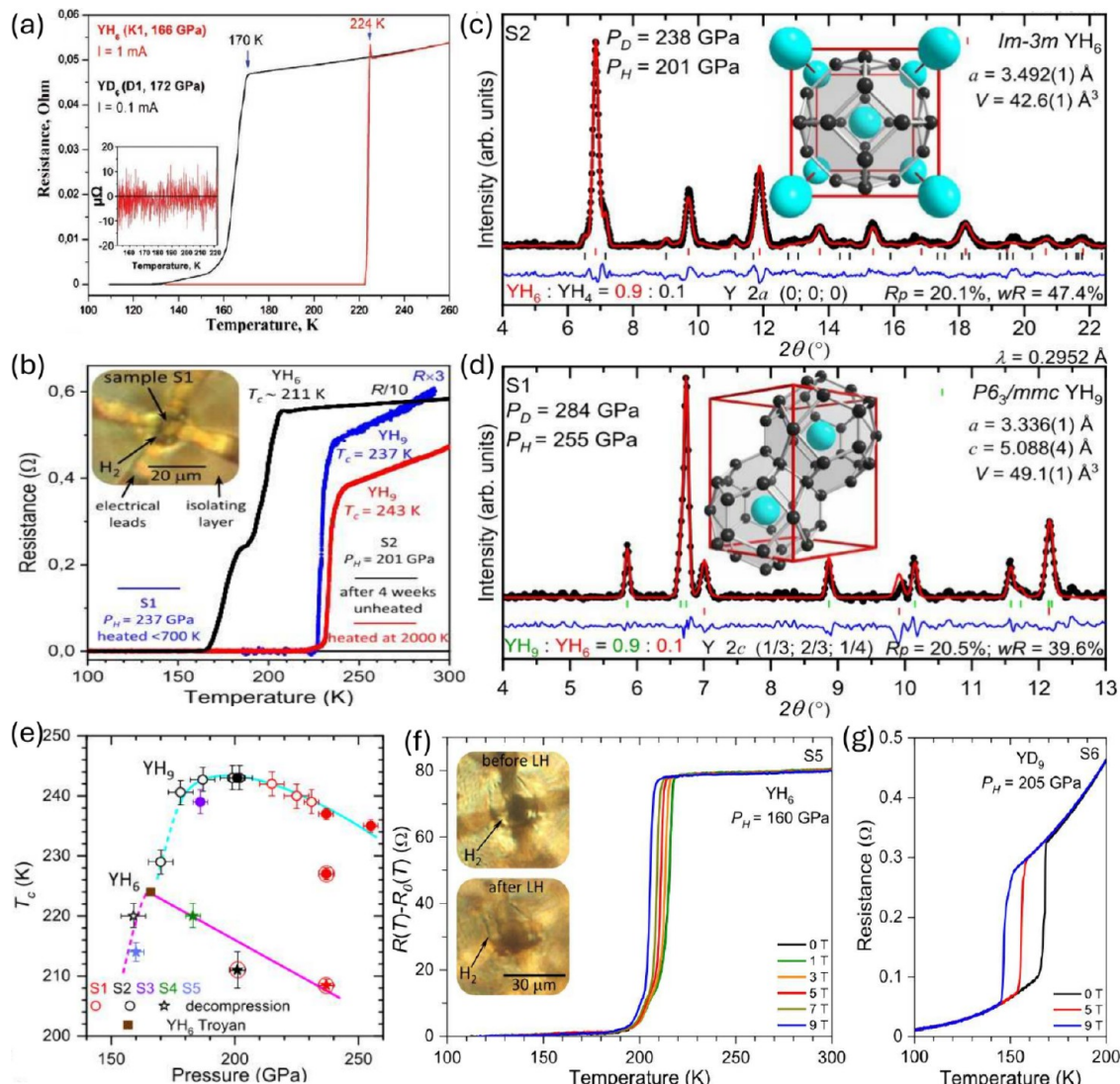


Figure 7. (a) $R-T$ dependence measured for YH_6 (166 GPa) and YD_6 (172 GPa). (b) $R-T$ dependence measured for YH_6 (237 GPa) and YH_9 (201 GPa). (c) XRD-resolved $\text{Im}-3\bar{m}$ clathrate-like structure of YH_6 . (d) XRD-resolved $\text{P}6_3/\text{mmc}$ clathrate-like structure of YH_9 . (e) P -dependent T_c measured for YH_6 and YH_9 and $R-T$ dependence measured for (f) YH_6 and (g) YH_9 at varying external magnetic fields. Panel a and panels b–g were reprinted with permission from ref 104 (Copyright 2021 John Wiley and Sons) and ref 105 (under a Creative Commons CC BY license), respectively.

LaH_{10} was synthesized²⁶⁹ in the predicted $\text{Fm}\bar{3}m$ clathrate structure at 170 GPa, the pressure at which it was predicted computationally to be dynamically unstable.⁸⁷ The small discrepancy between computations and experiments was then attributed to lattice vibrations,²⁷⁰ which had been neglected in early computations.⁸⁷ Nevertheless, the experimental synthesis of LaH_{10} in the predicted structure is a success.

The superconductivity of LaH_{10} was observed in 2019.^{100,101} Superconducting-like decreases in measured electrical resistance R of the synthesized samples were reported to be at a T_c of $\approx 260 \text{ K}$ under 180–200 GPa¹⁰⁰ and a T_c of $\approx 250 \text{ K}$ under 170 GPa,¹⁰¹ as shown in Figure 6c. In ref 101, the cubic $\text{Fm}\bar{3}m$ structure of LaH_{10} was confirmed while other characteristics of superconductivity, including the isotope effect, shown in the inset of Figure 6c, and a decrease in T_c at increasing magnetic fields, shown in Figure 6d, were also observed. By obtaining the upper critical field as a function of T and fitting the data into the Ginzburg–Landau model,⁷ Drozdov et al. extracted a coherence length of approximately 1.56–1.86 nm.¹⁰¹ However,

magnetization measurements from the DAC cannot be performed using SQUID because of the small volume and size (10–20 μm) of the samples.

One year later, the synthesis of LaH_{10} was repeated.²³⁸ The samples are not larger, but using the pickup/compensating coil technique, weak but measurable signals from magnetic susceptibility measurements, as shown in Figure 6e, were obtained.²³⁸ After the removal of the background, the final data, shown in Figure 6f, point to superconducting transitions at a T_c range of ≈ 250 –280 K and a P range of ≈ 170 –180 GPa.²³⁸ In 2021, the cubic $\text{Fm}\bar{3}m$ phase was confirmed again while some other key superconducting characteristics such as the upper critical fields and coherence lengths were established.²⁷¹

The clathrate structures realized in LaH_{10} , in which the hydrogen cavities are interconnected and distributed continuously throughout the space (see Figures 6a), allow for unusually high hydrogen content. For that reason, it can be viewed a close realization of metallic hydrogen, for which high

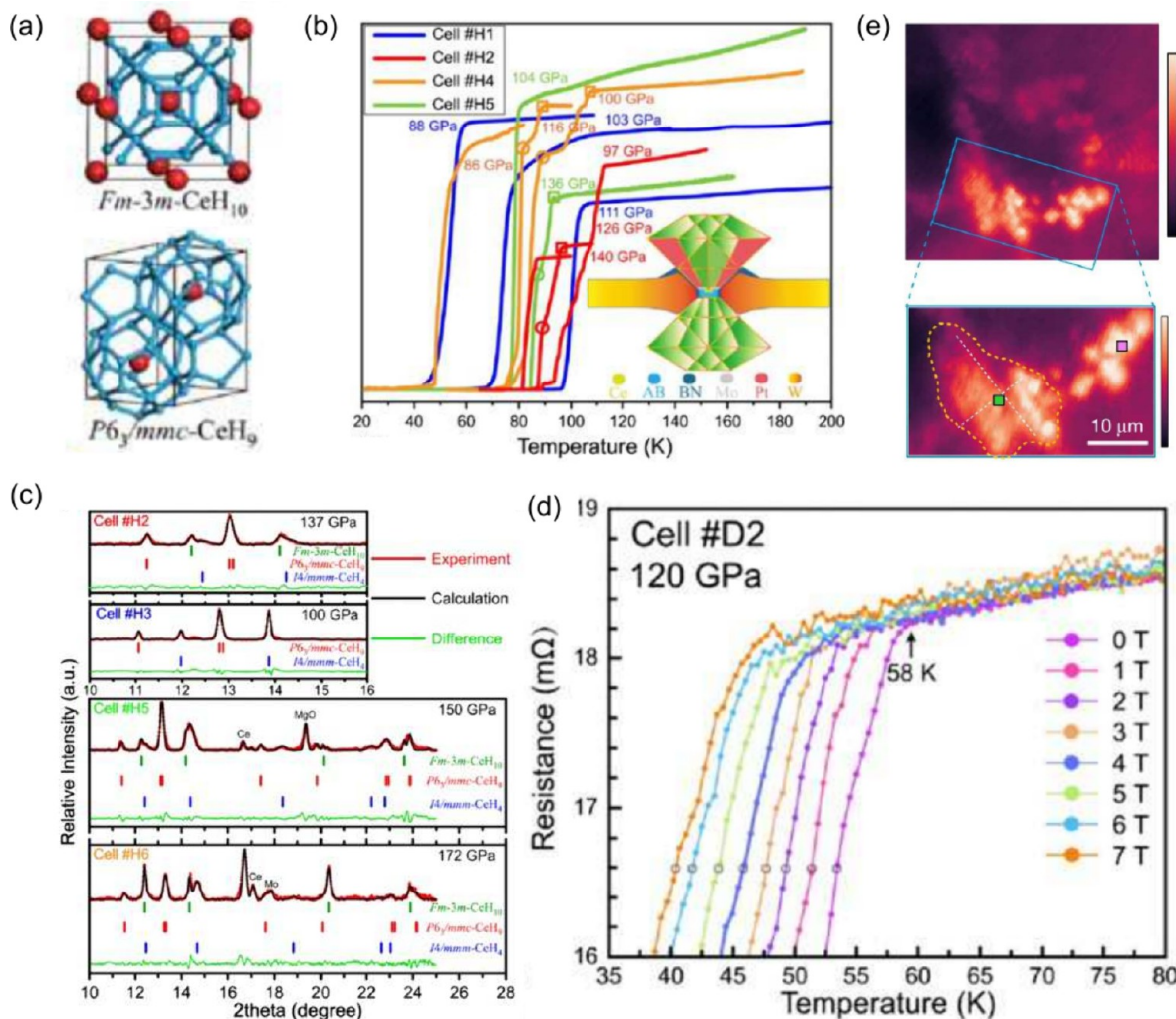


Figure 8. (a) Predicted *Fm* $\bar{3}$ *m* structure of CeH₁₀ and *P*6₃/*mmc* structure of CeH₉. (b) *R*–*T* dependence measured for CeH₉ and CeH₁₀. (c) XRD-resolved *Fm* $\bar{3}$ *m* structure of CeH₁₀ and *P*6₃/*mmc* structure of CeH₉. (d) *R*–*T* dependence measured for CeH₉ and CeH₁₀ at varying external magnetic fields. (e) Confocal fluorescence image of CeH₉ in which the diamagnet domains are brightly colored. Panels a–d and panel e were reprinted with permission from ref 106 (Copyright 2021 American Physical Society) and ref 241 (Copyright 2024 Springer Nature), respectively.

T_c values were predicted in 1968, also by Ashcroft.²⁶⁰ Remarkably, this host-atoms-in-hollows motif has been predicted computationally^{75,81,86,88} and then realized experimentally^{104,105} for many superconducting hydrides such as YH₆, YH₉, CeH₉, and CeH₁₀, as discussed below. Some computational works follow this promising lead, suggesting even hydrogen-richer clathrate structures of superhydrides, e.g., LaH₁₆,²⁷² LaH₁₈, YH₁₈, AcH₁₈, CeH₁₈, and ThH₁₈,^{228,273} with a predicted T_c of \gtrsim 200 K.

3.4. Yttrium Hydrides YH₆ and YH₉. Yttrium hydrides YH₆ and YH₉ are included in the list of 10 high- T_c superconducting rare-earth hydrides, including LaH₁₀, computationally predicted in 2017.⁸⁸ The common feature of this series is their clathrate-like structure, which, as mentioned above, is interesting in the context of high- T_c superconductivity.⁷⁵ The predicted T_c values of YH₆ (in its cubic *Im* $\bar{3}$ *m* phase) and YH₉ (in its hexagonal *P*6₃/*mmc* phase) are \approx 250 K at 120 GPa and \approx 260 K at 150 GPa, respectively.⁸⁸ In fact, the cubic *Im* $\bar{3}$ *m* phase of YH₆ was also predicted to be a superconductor with a T_c of \approx 251–264 K at 164 GPa in 2015 in a structure prediction campaign.⁸⁶

The experimentally observed superconductivity of YH₆ and YH₉ was reported in refs 104 and 105, both in 2021. First, YH₆ was synthesized and observed in the predicted *Im* $\bar{3}$ *m* phase.¹⁰⁴ Measured electrical resistance *R*, shown in Figure 7a, has a superconducting-like decrease at a T_c of \approx 224 K at 168 GPa. The isotope effect was also observed, suggesting a link between the superconductivity and the lattice phonons. This discovery was reproduced in ref 105, in which a T_c of \approx 220 K at 183 GPa was reported for the *Im* $\bar{3}$ *m* phase of YH₆ as shown in panels b, c, and e of Figure 7. The superconductivity of YH₉ in its predicted hexagonal *P*6₃/*mmc* phase (see Figure 7d) was also reported in ref 105, exhibiting a pressure-dependent T_c peaking at \approx 243 K at 201 GPa (see Figure 7e). The dependence of T_c on the external magnetic field is shown in panels f and g of Figure 7, pointing to an upper critical field and a coherence length. Fitting the measured *T*-dependent upper critical fields to the Ginzburg–Landau⁷ and Werthamer–Helfand–Hohenberg²⁵⁸ models, we found coherence lengths at 0 K of YH₆ and YH₉ of 1.45–1.75 and 2.3–2.7 nm, respectively.

The superconducting-like decreases in electrical resistance *R*, the dependence of T_c on the external magnetic field, and the atomic structure of both YH₆ and YH₉ were reproduced

recently.²⁴⁰ Nevertheless, magnetic susceptibility measurements have not been reported thus far, perhaps because of known technical challenges. In this context, emerging techniques for visualizing the local domain of diamagnetism²⁴¹ or measuring the trapped flux²⁵⁹ could be useful, as demonstrated²⁴¹ for CeH₉ and mentioned in section 3.5.

3.5. Cerium Hydrides CeH₉ and CeH₁₀. Similar to LaH₁₀, YH₆, and YH₉, CeH₉ and CeH₁₀ are also in the series of rare-earth hydrides predicted in ref 88. The predicted structures of CeH₉ and CeH₁₀, visualized in Figure 8a, are both clathrate-like and belong to the *P6₃/mmc* and *Fm̄3m* space groups, respectively. Although the predicted T_c of CeH₉ and CeH₁₀ is lower than others, i.e., \approx 50–60 K, the pressure at which the superconductivity was predicted is relatively lower, i.e., 100 GPa for CeH₉ and 200 GPa for CeH₁₀.⁸⁸ Given that the superconductivity of H₃S, LaH₁₀, YH₆, and YH₉ was reported to be close to 200 GPa, this prediction stimulates some interest. Amid the search, CeH₉ was synthesized,²⁷⁴ confirming the predicted *P6₃/mmc* phase. A structure prediction campaign was then launched,²⁷⁴ recovering the predicted *P6₃/mmc* and *Fm̄3m* phases of CeH₉ and CeH₁₀, respectively. Calculations performed return a λ of 2.3 and an ω_{\log} of 740 K for the *P6₃/mmc* phase of CeH₉ at 200 GPa, which were translated to a T_c of 105–117 K using the McMillan formula with a μ^* of 0.10–0.13.²⁷⁴

In 2021, the superconductivity of CeH₉ and CeH₁₀ was reported at 88 and 95 GPa, respectively.¹⁰⁶ The critical temperature, extracted from measured electrical resistance R (shown in Figure 8b), is 57 K for CeH₉ and 115 K for CeH₁₀.¹⁰⁶ The *P6₃/mmc* phase of CeH₉ is predominant in the synthesized samples, while CeH₁₀ in its *Fm̄3m* phase plays a minor role, as shown in Figure 8c. Using the Ginzburg–Landau⁷ and Werthamer–Helfand–Hohenberg²⁵⁸ models for the measured magnetic field-dependent T_c data (see Figure 8d), the upper critical field at 0 K of CeH₉ was estimated to be 17.7–22.9 T at 140 GPa while the coherence length is 3.4 nm at 120 GPa, 4.3 nm at 150 GPa, and 5.1 nm at 150 GPa.¹⁰⁶ An isotope effect was observed for CeH₉,¹⁰⁶ but no magnetic susceptibility measurements were reported.

Recently, local diamagnetic domains of CeH₉ were observed²⁴¹ using a new technique that can perform local magnetometry with submicrometer spatial resolution inside a DAC.²⁴¹ These domains, brightly colored in Figure 8e, are \sim 10 μ m in size and small for SQUID. This result is intriguing, suggesting that the new technique would be useful for probing the superconductivity in small samples, the scenario that is common in superconductor discovery.¹⁰¹

4. MATERIALS INFORMATICS IN SUPERCONDUCTOR DISCOVERY

Emerging in the early 2010s and partly driven by the Materials Genome Initiative,²⁷⁵ materials informatics has rapidly developed into a widely used tool in materials research.^{119–126} This approach employs AI/ML techniques to learn materials data, creating models that can generate rapid predictions and complement traditional approaches in accelerating materials discovery. Synergetic approaches involving materials informatics methods, simulations, and physical experimentations have proactively driven numerous recent materials discoveries. Many of these newly discovered materials have been synthesized and tested. Notable examples include battery materials,¹⁹⁹ green energy materials,²⁰⁰ functional and sustainable polymers,²⁰¹ alloys,^{202,203} and more.

Data are the cornerstone of materials informatics. In this field, data can originate from different sources such as experimental measurements and/or physics-based computations, be represented in different formats, contain different amounts and details of information, and possess different levels of fidelity. An ideal data set for ML model training should be sufficiently large, diverse in the chemical, configuration, and parameter spaces, and complete in terms of the relevant information. The development of major DFT-based materials databases like Materials Project,²⁷⁶ OQMD,²⁷⁷ AFLOWLIB,²⁷⁸ and NOMAD^{122,123} is important for the future progress of materials informatics.

For problems related to superconductivity, a typical model development procedure, sketched in Figure 9, starts with

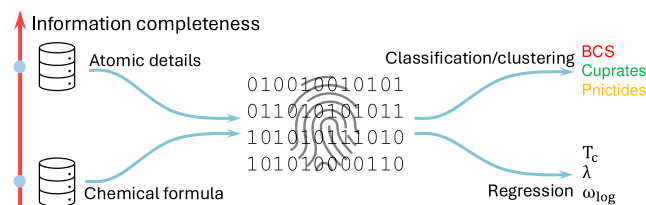


Figure 9. Widely adopted schematic pipeline for ML predictive models of superconductivity.

collecting and preparing training data for related materials. These data include both the structural information of the materials and the target labels or properties of interest. In a next step, the materials, represented by their chemical formulas or atomic structures, are converted into numerical “hand-crafted” features that can be readily interpreted and utilized by ML algorithms.^{119,125,126} This step is required from the early days of materials informatics, but recent advances in deep-learning techniques^{138,139,279–285} signal that the materials features may also be “learned”. Subsequently, a suitable ML algorithm learns the features, establishing a clustering, classification, or regression model capable of rapidly predicting or evaluating new materials.

As the model input, a chemical formula inherently provides less detailed information than a fully specified atomic structure. On the spectrum of information completeness, as previously discussed²⁸⁶ and sketched in Figure 9, the information content of a chemical formula is lower than that of an atomic structure. From the physics standpoint, each formula corresponds to an infinite number of metastable atomic structures (local minima on the PES).²¹² Many of these structures may be energetically close to the global minimum, implying that they can be stabilized in experiments or appear in computational models. Importantly, these low-energy structures may have completely different atomic arrangements and properties, e.g., with one being insulating and another conducting.²⁸⁷ Superconductivity, as discussed in section 2.1, is highly sensitive to the atomic arrangements. Thus, describing a superconductor by only its chemical formula entails the risk of inaccurate results. Eventually, models relying on only formulas as inputs inevitably encounter a degree of irreducible (aleatoric) uncertainty in their predictions that cannot be simply reduced by increasing the amount of data.^{286,288} As early superconductor databases provide only chemical formulas, recent efforts to introduce atomic details, as discussed in section 4.1, have become a focal point of research.

Table 2. Summary of the Currently Available Databases of Superconductors That Have Been or Can Be Used for Machine-Learning Techniques

name	description	URL (https://+)	refs
NIMS SuperCon	≈31 000 records of chemical formula and T_c at 0 GPa	supercon.nims.go.jp/index_en.html	
MDR SuperCon	originated from NIMS SuperCon, 26 323 records of chemical formula and T_c at 0 GPa	mdr.nims.go.jp/collections/5712mb227	
SuperCon	originated from NIMS SuperCon, 16 400 records of chemical formula and T_c at 0 GPa	github.com/vstanev1/Supercon	136, 137
3DSC _{ICSD}	9150 records of atomic structure at 0 GPa (from ICSD) “matched” with experimental T_c (from NIMS SuperCon) via chemical formula; license needed for ICSD	github.com/aimat-lab/3DSC	165
3DSC _{MP}	5759 records of atomic structure at 0 GPa (from Materials Project) “matched” with experimental T_c (from NIMS SuperCon) via chemical formula	github.com/aimat-lab/3DSC	165
Jarvis_EPC	626 records of atomic structure and λ and ω_{log} computed at 0 GPa using DFPT	doi.org/10.6084/m9.figshare.21370572	140
N/A	≈7000 records of atomic structure and λ and ω_{log} computed at 0 GPa using DFPT		141
CompSC	587 atomic structures for which 584 values of λ and 567 values of ω_{log} were computed at ≤500 GPa; data from literature, reoptimized using DFT, and validated visually	github.com/huantd/matsdata	142
SC-CoMics	1000 annotated abstracts, developed and tailored for extracting superconductivity-related information, e.g., using NLP	data.mendeley.com/data-sets/xc9fjz2p3h/2 github.com/tti-coin/sc-comics	160, 161
SuperMat	142 articles, 16 052 entities, and 1398 links, for NLP	github.com/lfoppiano/SuperMat	163
SuperCon ²	40 324 records of superconductors, T_c , applied pressure, measurement method	github.com/lfoppiano/supercon	164

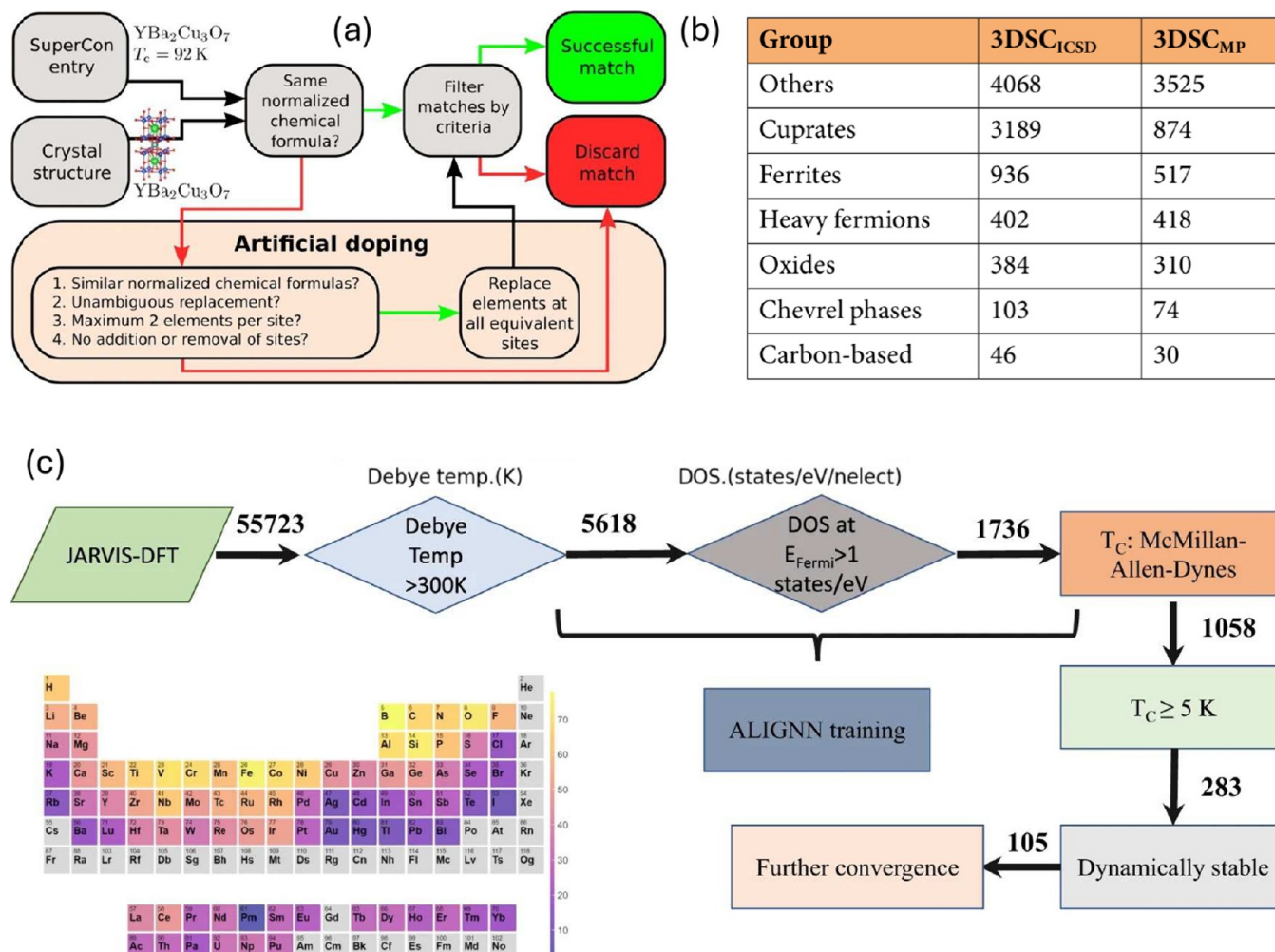


Figure 10. Workflows used to develop (a) 3DSC_{ICSD} and 3DSC_{MP} and (c) Jarvis_EPC, three data sets of superconductivity-related parameters and atomic structures. A summary of 3DSC_{ICSD} and 3DSC_{MP} is given in panel b. Panels a and b and panel c were taken from ref 165 (under a Creative Commons CC BY license) and ref 140 (under a Creative Commons CC BY license), respectively.

Extending some previous discussions,^{142,157} one can categorize materials informatics efforts in superconductor discovery into five groups. The first group (i) includes those

fully devoted to^{160–165} or partially involved in^{136,137,140–142} data generation, extraction, and dissemination. The other groups are (ii) classifying superconductors,^{135,137,159} (iii)

predicting superconducting-related properties,^{136,137,139–148} (iv) accelerating the structure prediction step with ML potentials,^{127–129} and (v) refining empirical formulas for T_c .^{133,134,148} Groups iii–v are sketched in Figure 2. Due to the integrated nature of the materials informatics approaches, the availability of the data, and specifically the forward-looking aspiration of the field, subsequent discussions in this section will involve all classes of superconductors, including those mediated by phonons. The current status, challenges, and critical next steps of the materials informatics efforts in superconductor discovery will be discussed in section 5.

4.1. Data Generation, Extraction, and Dissemination.

The Superconducting Material Database maintained by Japan's National Institute for Materials Science (NIMS) provides data for many efforts in the field.^{135–137,159} This database, named NIMS SuperCon, records the chemical formula of ~32 000 known conventional (phonon-mediated) and unconventional superconductors; not all of them have (measured) T_c values included. Recently, NIMS SuperCon was cleaned, re-edited, and released as MDR SuperCon, containing 26 323 records. Parallel cleaning and curation efforts^{136,137} resulted in another version, presently known as SuperCon, containing ~16 400 records; among them, 4000 records have no T_c values. Details about NIMS SuperCon, MDR SuperCon, and SuperCon are listed in Table 2.

Some approaches were used to introduce atomic-level information. First, the chemical formula of superconductors are looked up in the available databases like ICSD²⁸⁹ and Materials Project²⁷⁶ for the most reasonable structures.^{135,137,143} Figure 10a details the procedure¹⁶⁵ used to create 3DSC_{ICSD} and 3DSC_{MP}, two superconductor data sets in which the T_c from NIMS SuperCon is paired with the atomic structures from ICSD and Materials Project by matching the chemical formula. In this procedure, an “artificial doping” step was used to obtain complete matches in the chemical formula from “nearly complete” matches. A summary of 3DSC_{ICSD} and 3DSC_{MP} is given in Figure 10b.

In the second approach, superconductivity-related parameters such as $\alpha^2 F(\omega)$, λ , ω_{\log} , and T_c are computed (see section 2.2) for the atomic structures obtained from existing databases and/or predicted computationally.^{140,141,148} JARVIS-EPC is a data set generated¹⁴⁰ using such a computationally demanding approach (its technical details are shown in Figure 10c). Starting from JARVIS-DFT, a database of 55 645 materials, screening steps involving some accessible data, e.g., debye temperature and N_F , were used.¹⁴⁰ Then, $\alpha^2 F(\omega)$, λ , and ω_{\log} were computed for 1058 materials, identifying 626 dynamically stable structures; 105 of them have McMillan T_c values of ≥ 5 K. More recently, a data set of >7000 records of atomic structures and their computed λ , ω_{\log} , and T_c values were obtained in a ML-driven computational discovery effort, whose workflow is shown in Figure 14e.¹⁴¹ The two computational data sets are summarized in Table 2.

The third approach is inspired by the presence of thousands of computational reports for possible superconductivity at multiple ranges of pressure. Most of them start from the atomic structures predicted computationally, thus being highly expensive and trustworthy. The main challenge in this approach is how to collect and validate the literature data in a reliable and scalable manner. In an initial effort, a few hundred atomic structures and their λ and ω_{\log} values, computed at pressures of ≤ 500 GPa, were manually collected.¹⁴² The curation involves constructing the reported

atomic structures, uniformly optimizing them using DFT, and inspecting them visually. Resulting data set CompSC, summarized in Table 2, contains 587 atomic structures for which 584 values of computed λ and 567 values of computed ω_{\log} are available.¹⁴² This approach can create a reliable and highly diverse data but is laborious and obviously unscalable.

Using natural language processing (NLP) tools to automatically extract superconductor-related data from scientific literature, a largely unexplored data reservoir, is more scalable and sustainable. This approach has emerged and recently gained some momentum.^{160–164} SC-CoMics is a corpus of 1000 annotated abstracts, created^{160,161} for extracting superconductivity-related information using NLP-based tools like named entity recognition (NER). Beyond abstracts, SuperMat is an annotated corpus, supplying 142 full texts, which contain 16 052 entities and 1398 links.¹⁶³ Such efforts were further elevated to Grobid-superconductors, a module designed to automatically extract superconductor names and properties from text, and finally to SuperCon², a database containing 40 324 records of superconductor chemical formulas, T_c values, applied pressures, and measurement methods.¹⁶⁴

4.2. Categorizing Superconductors from Data. The developed databases could be useful for two categorical questions: (1) whether a material is a superconductor and (2) if yes, what class, e.g., cuprates and iron-based, to which it belongs. In an endeavor to address the first question, SuperCon (with 16 400 records) was augmented by 300 materials found⁵⁰ to be nonsuperconducting. For these materials, the T_c was set to zero.¹³⁷ Then, an adjustable parameter T_{sep} was introduced to separate the combined data set into two groups. The “below- T_{sep} ” group includes the nonsuperconductors ($T_c = 0$ K), ≈ 4000 records without T_c values, and those for which $T_c < T_{sep}$, while the “above- T_{sep} ” group hosts records for which $T_c \geq T_{sep}$. By using the Magpie features²⁹⁰ for chemical formulas, setting $T_{sep} = 10$ K, and employing the Random Forest algorithm,²⁹¹ the classification model developed, shown in Figure 11a, can reach an accuracy of $\approx 92\%$.¹³⁷

Upon inclusion of nonsuperconducting materials in the “below- T_{sep} ” group, the problem of superconductor recognition was just partially addressed.¹³⁷ The reason is that T_c is not the only measurable characteristic of a superconductor but is the only superconductivity-related property available in NIMS SuperCon. Moreover, as T_c may be arbitrarily low,⁵³ some materials currently classified as nonsuperconducting may be discovered to exhibit superconductivity as technological advancements enable us to probe lower temperature regimes. An example of such a (very rare) finding is the discovery of superconductivity in elemental Li below 4×10^{-3} K,²⁹² despite a long-standing belief that Li would not exhibit superconductivity.^{293,294}

In fact, the first attempt to categorize superconductors on the basis of T_c emerged slightly earlier, starting from ≈ 700 chemical formula– T_c records collected from the literature, handbooks, and NIMS SuperCon.¹³⁵ The chemical formulas were then matched with suitable atomic structures in AFLOWLIB,²⁷⁸ creating a data set of 464 structure– T_c records. The data were featurized by SiRMS, a fragment-based Simplex representation,²⁹⁵ before being learned using the Random Forest algorithm. When temperature separator T_{sep} was set to 20 K, an accuracy of ≈ 0.97 was searched by the obtained classification model, as visualized in Figure 11b.

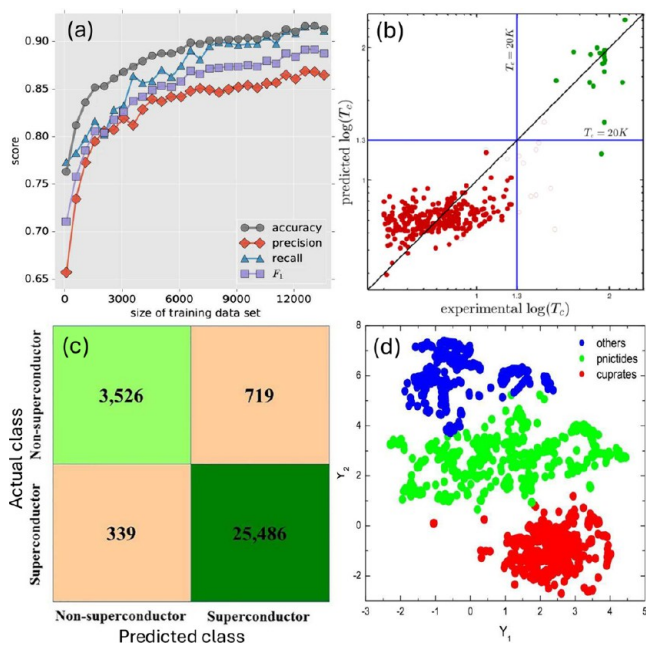


Figure 11. (a) Four accuracy-related scores of the superconductor/nonsuperconductor classification model. (b) Predictions of a classification model (colored red and green) and a regression model (given on the y -axis) on a data set of 464 structure– T_c records. (c) Confusion matrix for the classification model for superconductors that can reach an accuracy of 96.5%. (d) t-SNE plot of 4500 randomly selected superconductors from SuperCon, showing distinct clusters for different classes of superconductors. Panels a–d were reprinted with permission from ref 137 (under a Creative Commons CC BY license), ref 135 (Copyright 2015 American Chemical Society), ref 158 (Copyright 2020 Elsevier), and ref 159 (Copyright 2022 Elsevier), respectively.

In an effort to distinguish superconductors from non-superconductors, NIMS SuperCon was cleaned and augmented by 3000 nonsuperconducting materials, including insulators, semiconductors, and metals.¹⁵⁸ Then, each chemical formula was represented by a row vector formed by the composition (contribution) of the constituent species. These vectors were aggregated in a chemical composition matrix that has 96 columns for 96 available species and $\approx 30\,000$ rows for the data set size. Figure 11c shows that the classification model trained using the k-Nearest Neighbors algorithm performs very well¹⁵⁸ with an overall accuracy of $\approx 96\%$. It is worth noting that the augmented 3000 materials were assumed¹⁵⁸ to be nonsuperconductors, skipping the aforementioned small possibility that some (metals) of them may be superconductors at very low temperatures.

The second question involves recognizing superconductors of different classes, i.e., those governed by different pairing mechanisms. To address this problem, NIMS SuperCon was cleaned and represented¹⁵⁹ by the chemical composition matrix.¹⁵⁸ Several clustering algorithms were tested before Self-Organizing Map²⁹⁶ was selected. Figure 11d shows the t -distributed Stochastic Neighbor Embedding (t -SNE)²⁹⁷ of 4500 superconductors randomly selected from SuperCon, in which iron-based compounds, cuprates, and those in other classes are distinguished.¹⁵⁹ It seems that data, when curated and learned properly, could be useful for recognizing a superconductor and the governing mechanism, if applicable.

4.3. Predicting Superconducting-Related Properties.

ML efforts in this class aim to accelerate the predictions of superconducting-related properties such as T_c , traditionally obtained by expensive computations (section 2.2) and/or physical measurements (section 2.4). The critical role of NIMS SuperCon and its descendants, evidenced in section 4.2, is also visible here. In fact, most of the works aiming at predicting T_c from the chemical formula rely on NIMS SuperCon. Efforts to introduce atomic-level information into the development of ML models for λ and ω_{\log} have emerged recently. This section is devoted to not only the ML efforts in the two subcategories but also the ML-driven searches for superconductors. An in-depth discussion of the remaining challenges and opportunities of ML efforts in this class is given in section 5.2.2.

4.3.1. Predictions from Chemical Formula. In an early ML work starting from NIMS SuperCon, a data set of 21 263 records was curated, containing multiple classes of superconductors.¹³⁶ For each material, the chemical formula was featurized by some simple functions, e.g., mean, weighted mean, entropy, etc., of the basic properties of the constituent species, e.g., atomic mass, electron affinity, etc. Some algorithms were tested, and XGBoost²⁹⁸ was selected. The developed ML model for T_c with an averaged out-of-sample error of ≈ 9.5 K is visualized in Figure 12a.¹³⁶

Following the classification between low- T_c and high- T_c superconductors, T_c predictive models were developed for

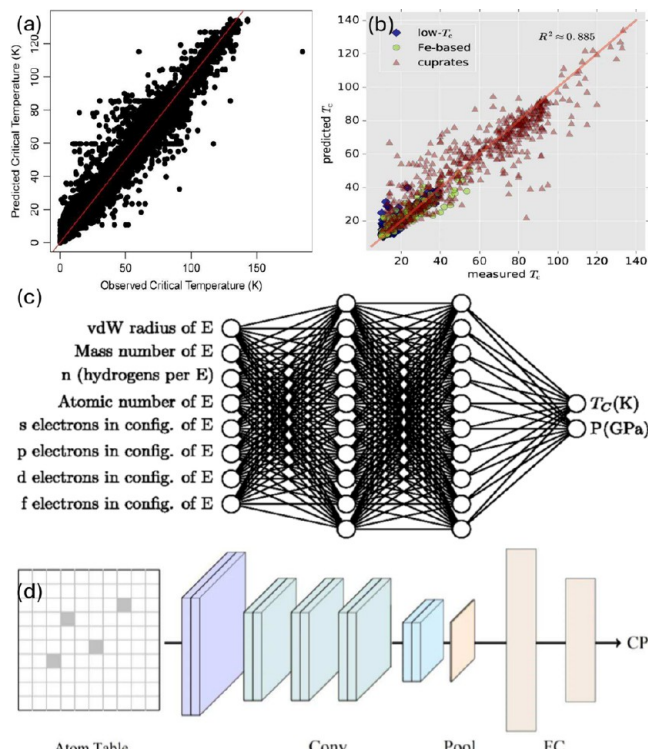


Figure 12. (a and b) Two ML models for predicting T_c from chemical formula. (c) Fully connected neural network created to predict T_c and P from chemical formula. (d) Atom table convolutional neural network used to train the ML predictive model for T_c on the data sets whose chemical formulas are represented as 10×10 images. Panels a–d were reprinted with permission from ref 136 (Copyright 2018 Elsevier), ref 137 (under a Creative Commons CC BY license), ref 147 (Copyright 2020 American Physical Society), and ref 138 (under a Creative Commons CC BY license), respectively.

the high- T_c group.¹³⁷ The materials data were represented by Magpie (composition) features²⁹⁰ and learned by the Random Forest (regression) algorithm. One of the models developed is visualized in Figure 12b, showing the performance on low- T_c , Fe-based, and cuprate superconductors with a coefficient of determination (R^2) of ≈ 0.88 .¹³⁷ Screening the ICSD database by a combination of a classification and a regression model identified ≈ 2000 materials with predicted T_c values of > 20 K at 0 GPa.¹³⁷ While most of them contain copper and oxygen, i.e., they may be related to cuprates, a subset of 35 materials without obvious connection to known high- T_c families was compiled and reported.¹³⁷

Roughly 2000 records of AlB_2 -, Chevrel-, Cr_3Si -, spinel-, NaCl -, and skutterudite-type superconductors were extracted from NIMS SuperCon and augmented with elemental superconductors.¹⁴⁴ This data set was believed to include phonon-mediated superconductors, for which MgB_2 ⁴⁷ is the highest- T_c material; the averaged T_c of MgB_2 in this data set is 38.6 K. Featurizing the data by some simple functions of the fundamental attributes of existing species, the trained Random Forest model could reach an R^2 of 0.98 on the training data (80% of the data set) and an R^2 of 0.92 on the test data (the remaining 20% of the data set). This model was used to create the predicted T_c map for three families of ternary materials, namely, Mg–B–Ti, Fe–Te–Se, and Ca–B–C. In the Mg–B–Ti map, the region containing MgB_2 was predicted to exhibit the highest T_c values, while in the Fe–Te–Se map, the high T_c was predicted along the line connecting FeTe and FeSe.¹⁴⁴ For the Ca–B–C system, materials with formula close to CaB_6 and B_{13}C_2 were also predicted¹⁴⁴ to exhibit high T_c values.

Focusing on the recent discoveries, a few hundred binary hydride superconductors EH_n were collected from the literature.¹⁴⁷ For each material, its chemical formula, T_c , and pressure at which superconductivity was predicted are available. A set of features, including hydrogen content n and some fundamental attributes of species E such as the atomic number, the van der Waals radius, and the electron configurations of E, was used to describe EH_n . The featurized data were then fed into a fully connected neural network, as visualized in Figure 12c, whose output layer has two nodes, one for T_c and the other for P . This network is an example of a multitask learning architecture, which can be trained with multiple data sets to exploit the hidden correlations among them and leverage the performance.^{288,299,300} The T_c predictivity of the model reaches an R^2 of 0.88 with a root-mean-square error (RMSE) of ≈ 33.7 K for T_c predictions.

Nevertheless, the main objective of the developed neural network model is to screen over the periodic table for the species E that minimize the “distance” from the predicted T_c and P to the ambient conditions, i.e., 0 GPa and 293 K.¹⁴⁷ The analysis suggests that alkali- and alkaline-earth metal hydrides could be the best candidates for superconductivity near ambient conditions. Next, the AIRSS method²²² was used, identifying dozens of atomic structures of alkali- and alkaline-earth metal hydrides with respectable computed T_c values. Specifically for the predicted $\text{C}2/\text{m}$, Cmcm , and Immm phases of RbH_{12} , the computed T_c could be as high as 126 K at ≤ 100 GPa.¹⁴⁷

Materials informatics endeavors relying on NIMS SuperCon were extended into the deep-learning territory, where high-level features may be learned directly from raw data. In the atom table Convolutional Neural Network (ATCNN), each chemical formula was represented by an image of 10×10

pixels, visualized at the left end of Figure 12d. Each pixel corresponds to a species, and its value is the composition (contribution) of this species in the chemical formula. As there are 86 species that appear in the data set, $10 \times 10 = 100$ pixels is sufficient for the representation. Then, the “atom tables” are accepted by an architecture, sketched in Figure 12d, which consists of several convolutional layers to process the images.¹³⁸ Two models for T_c , i.e., ATCNN-I and ATCNN-II, were developed, one trained on a cleaned version of NIMS SuperCon containing 13 598 records and the other trained on the same data set after being augmented by 9399 energetically stable insulators, the obvious nonsuperconductors. Both models show good performance with a mean absolute error (MAE) of ≈ 4.2 K, a RMSE of ≈ 8.2 K, and an R^2 of ≈ 0.97 . Compared to the measured T_c values of some well-known superconductors such as Hg , MgB_2 , and $\text{YBa}_2\text{Cu}_3\text{O}_7$, the predictions of these two models are accurate.¹³⁸

The idea of using a convolutional neural network (CNN) architecture in superconductor discovery has evolved from recognizing “atom tables”¹³⁸ to “reading periodic tables”.¹³⁹ In the latter, the species composition of each superconductor in NIMS SuperCond is “written” directly to the periodic table. Then, the table was separated into four “channels” for recording those with s, p, d, and f valence electrons. A CNN was trained on 95% of NIMS SuperCond and tested on the remaining 5% of the data, yielding an R^2 of 0.92 in T_c predictions.¹³⁹ This model predicts $\sim 17\,000$ materials (of $\sim 48\,000$ records) in Crystallography Open Database (COD)³⁰¹ to have T_c values of > 10 K. The obtained result is unreasonable, perhaps because the training data have almost no nonsuperconductors. After it is augmented by a synthetic data set of nonsuperconductors (assumed $T_c = 0$ K), the final (new) model becomes more reliable. Testing on 400 materials (including 330 nonsuperconductors) reported in ref 50, the model reaches a precision of 62%, an accuracy of 76%, a recall of 67%, and an f1 score of 63% in predicting materials with T_c values of > 0 K. Using it for COD, 70 materials, including CaBi_2 and $\text{Hf}_{0.5}\text{Nb}_{0.2}\text{V}_2\text{Zr}_{0.3}$ (both are not in NIMS SuperCond), were predicted to have T_c values of > 10 K. One of them, CaBi_2 , is indeed a superconductor.³⁰²

We close this section by noting the connection from the “atom table” and the “periodic table” in these CNN approaches to the chemical composition row vector¹⁵⁸ discussed in section 4.2. In particular, the former is the latter rearranged in a two-dimensional image so that it can be used in a CNN architecture. The main information encoded in these images is the composition of the constituent species, the highest level of information that can be extracted from a chemical formula.

4.3.2. Predictions from Atomic Structure. In fact, attempts to introduce atomic-level details into ML models for T_c emerged quite early.¹³⁵ By matching ≈ 700 formulas collected for superconductors with AFLOWLIB and excluding those for which $T_c < 2$ K, we obtained a data set of 295 atomic structure– T_c records. The atomic structures were represented using SiRMS²⁹⁵ before being mapped onto T_c by Random Forest and Partial Least Squares³⁰³ algorithms. The obtained models for T_c could reach an R^2 of ≈ 0.66 , and one of them is shown in Figure 11b. As SiRMS is a fragment-based representation,²⁹⁵ an analysis was performed, compiling a catalog of fragments that may likely present in materials with low and high values of T_c .¹³⁵

An atomic structure matching procedure was also used in ref 143. Upon examination of the ICSD database for which atomic

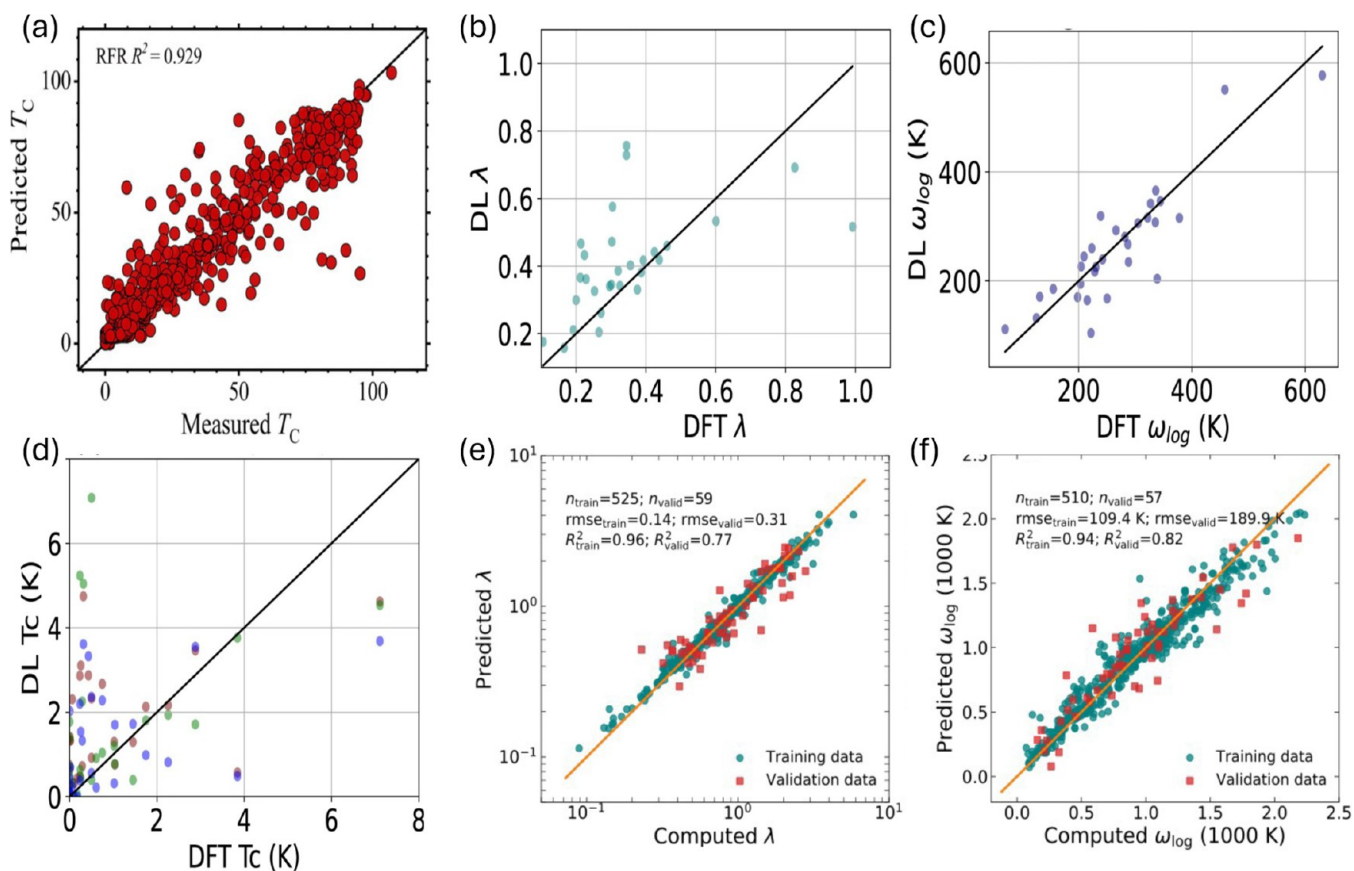


Figure 13. Six ML predictive models starting from atomic structures to predict (a and d) T_c , (b and e) λ , and (c and f) ω_{log} . Panel a, panels b–d, and panels e and f were reprinted with permission from ref 143 (Copyright 2019 American Chemical Society), ref 140 (under a Creative Commons CC BY license), and ref 142 (Copyright 2023 American Physical Society), respectively.

structures are available, ≈ 1700 superconductors were obtained. Next, by identifying suitable (close-matched) structures and “doping” them to recover the chemical formulas in NIMS SuperCon, Zhang et al.¹⁴³ finally obtained a data set of 5713 atomic structure– T_c records. Then, the atomic structures were featurized using the “Smooth Overlap of Atomic Position” (SOAP) scheme.³⁰⁴ Finally, three models were trained using Random Forest, XGBoost, and Support Vector Regression.³⁰⁵ One of them, the Random Forest regression model with an R^2 of ≈ 0.92 , is visualized in Figure 13a.¹⁴³ These models were used to screen over the ICSD database, compiling the 10 most promising superconductors whose averaged T_c (predicted by three models) is at least ≈ 20 K at 0 GPa.¹⁴³ Among them, $\text{Ba}_4\text{Ca}_4\text{Cu}_6\text{O}_{19}\text{Tl}_3$ was predicted to have a T_c of ≈ 103 K.¹⁴³

Starting from JARVIS-EPC, two learning methods were used to develop predictive models for λ , ω_{log} , and T_c .¹⁴⁰ The first relies on some force field-inspired features and the Gradient Boosting Decision tree algorithm.³⁰⁶ The second, termed “Atomistic Line Graph Neural Network” (ALIGNN), is a deep-learning architecture, in which a graph convolutional layer was designed to describe two- and three-body interactions among the atoms of an atomic structure.³⁰⁷ Panels b–d of Figure 13 visualize three ALIGNNN models¹⁴⁰ trained on JARVIS-EPC to predict λ , ω_{log} , and T_c , respectively.

Two ML models trained¹⁴² on CompSC to predict λ and ω_{log} are shown in panels e and f, respectively, of Figure 13. In this work, the atomic structures predicted at pressures of ≤ 500 GPa and reported in the literature were collected, uniformly reoptimized, visually validated, represented using MATMINER,³⁰⁸

and learned using the Gaussian Process Regression (GPR) algorithm.^{309,310} The training data are highly diverse, containing numerous (“unusual”) atomic details realized at different pressures and computationally linked to the values of λ and ω_{log} that lead to high values of T_c . Therefore, the models are expected to be capable of recognizing at any P , including 0 GPa, the atomic structures that resemble the “unusual” atomic-level details to which they were exposed.¹⁴² Using these models to screen the hydrides from the Materials Project database, an $Fm\bar{3}m$ structure of CrH and another $Fm\bar{3}m$ structure of CrH₂ were identified with computed T_c values of 15.7 and 10.7 K, respectively, at 0 GPa.¹⁴²

4.3.3. ML-Driven Search for High- T_c Superconductors. An efficient materials discovery strategy, even powered by ML models, should be target-driven, extending beyond a brute-force screening, as discussed in section 2.3. One such workflow was developed,¹⁴⁶ utilizing an evolutionary algorithm and a GPR model to discover hydrogen-containing superconductors. In this ML-driven strategy, visualized in Figure 14a, mating and mutation operate directly on the atomic structures while the space group, hydrogen concentration, atomic mass, pressure, and μ^* were used as descriptors to train the GPR model.¹⁴⁶ With new candidates, new data are computed, the ML model is retrained, and the workflow cycles. Some hydride superconductors were discovered, including a $C2/m$ structure of KScH_{12} with a computed T_c of 122 K at 300 GPa and a $Pm\bar{3}$ structure of GaAsH_6 , as shown in Figure 14b, with a computed T_c of 98 K at 180 GPa.

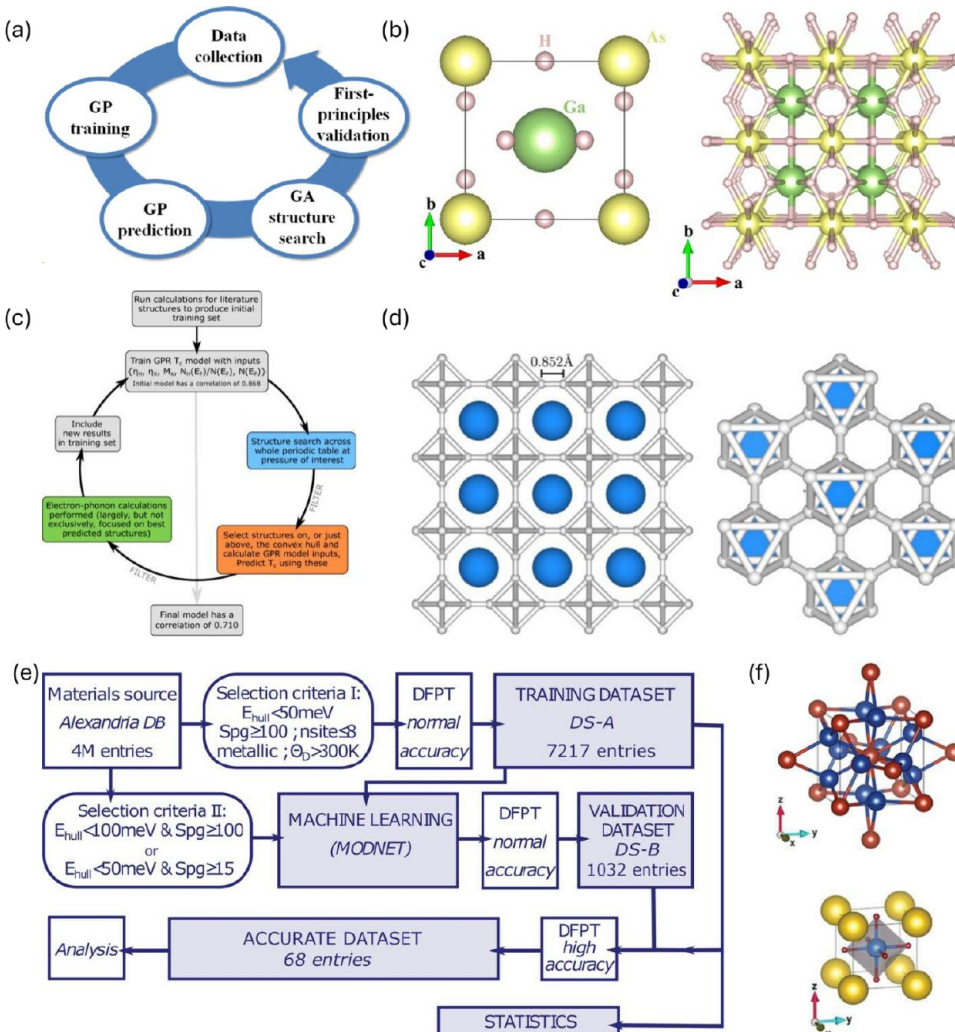


Figure 14. (a) Discovery loop using a ML predictive model to search for high- T_c superconductors. (b) The atomic structure of GaAsH₆ discovered using the strategy (a). (c) A ML-driven strategy for superconductor discovery, (d) the atomic structure of discovered NaH₆ at 100 GPa using the strategy visualized in (c). (e) A ML-driven workflow to search for superconductors and generate a significant volume of computed data. (f) The atomic structure discovered for Ti₃Te and KCdH₃ using the workflow in (e). Panels a and b, panels c and d, and panels e and f were taken from ref 146 (under a Creative Commons Attribution 4.0 International license), ref 148 (Copyright 2021 American Physical Society), and ref 141 (Copyright 2024 John Wiley and Sons), respectively.

Another ML-powered discovery strategy for hydride superconductors was recently developed¹⁴⁸ and is visualized in Figure 14c. In this procedure, the GPR model was trained on some formula-based features like the Gaspari–Gyorffy electron–phonon coupling estimates of available species, the atomic mass of non-hydrogen species, and N_F; all of them were normalized appropriately. In this strategy, the atomic structures of the formula candidates were searched using AIRSS,²²² and as the workflow cycles, 27 new superconductors were discovered at pressures of \leq 500 GPa. Among them, NaH₆, shown in Figure 14d, was predicted to have a T_c in the range of 228–279 K at 100 GPa.¹⁴⁸

Figure 14e visualizes the workflow used to create the data set of \approx 7000 records discussed in section 4.1 and summarized in Table 2.¹⁴¹ In this workflow, a deep-learning model trained on a “Material Optimal Descriptor Network”, or MODNet³¹¹ was used to select candidates from the Alexandria database³¹² for λ , ω_{log} , and T_c computations. MODNet accepts features computed using MATMINER³⁰⁸ for the atomic structures before passing them through a series of successive blocks for feature

selection, encoding, decoding, and splitting to learn multiple properties concurrently. Among \approx 7000 data records produced using this workflow, 541 materials with T_c values of >10 K (at 0 GPa) were identified. Two of them, a $Pm\bar{3}n$ structure of Ti₃Te (computed T_c of 16.3 K) and a $Pm\bar{3}m$ structure of KCdH₃ (computed T_c of 12.3 K), are visualized in Figure 14f.¹⁴¹

4.4. Accelerated Structural Prediction with ML Potentials.

In the computational discovery workflow discussed in section 2.3, the structure prediction step is computationally very demanding. For each chemical formula, hundreds of thousands of energy evaluations are typically needed to search for its stable atomic structures, and they must be performed at a first-principles level. The development of ML potentials,³¹³ mostly in the context of molecular dynamics (MD) simulations, offers an approach for accelerating this step. A ML potential is a ML model, generally based on a neural network, accepting an atomic structure and returning its potential energy faster than a normal DFT calculation by multiple orders of magnitude. State-of-the-art ML potentials

such as the Gaussian Approximation Potential (GAP),^{314,315} Spectral Neighbor Analysis Potential (SNAP),^{316,317} Moment Tensor Potentials (MTP),^{318,319} and Deep Potential,³²⁰ trained on millions of atomic environments, are expected to be comparable with DFT in terms of accuracy, i.e., a few millielectronvolts per atom. However, like any ML models, out-of-domain energy predictions (on unseen atomic environments) should be treated with care. In superconductor discovery, ML potentials started leaving discernible trails.^{127–129,131,132}

A reliable atomic structure predicted computationally should be thermodynamically, dynamically, and kinetically stable. In the context of superconductor discovery, the dynamical stability of a structure, i.e., whether it is a local minimum, not a saddle point of the PES, can be accessed during the calculations of spectral function $\alpha^2 F(\omega)$ using DFPT. Examining the kinetic stability of a structure, i.e., if the kinetic (energy) barrier protecting this local minimum is high enough so that its lifetime could be reasonable, is much harder than inspecting its thermodynamic stability. The reason is that the former is nonlocal in nature, especially when the configuration space is extremely high in dimensionality, which is ~ 3 times the system size, i.e., on the order of 10^2 .

In most cases, ML potentials were used to accelerate the energy evaluations during the search; i.e., their role is on the side of thermodynamic stability. Some results of these efforts are the discoveries at 0 GPa of C₄K (in *P4/mmm* symmetry with a predicted T_c of 30.4 K),¹²⁷ *c*-B₂₄ (in *Pm3* symmetry with a predicted T_c of 13.8 K),¹²⁸ and Mg₂IrH₆ (in *Fm3m* symmetry with a predicted T_c of 160 K).¹²⁹ At a slightly higher pressure (20 GPa), a series of 14 La–N–H ternary materials were predicted with support from the universal neural network potential developed by MATLANTIS.³²¹ Upon examination of their possible superconductivity by DFPT calculations,¹³⁰ the predicted T_c of this series spans from 0.49 to 14.41 K. In another interesting effort,¹³¹ ephemeral data-derived (ML) potentials³²² were used in a large-scale structure prediction campaign, which ended up disproving an early claim of ambient-condition superconductivity in the Lu–N–H systems. Compared with positive conclusions, such a negative conclusion requires much more computational effort because all of the attainable possibilities, e.g., chemical formulas and system sizes, should be considered. ML potentials are particularly useful for this purpose.

ML potentials have also been used to accelerate the examination of the kinetic stability, which connects with kinetic barriers. A typical approach is to perform long first-principles MD simulations at and above room temperature to examine the stability of the long-range order against increased thermal energies.¹²⁷ Directly accessing the kinetic barriers, e.g., using stochastic self-consistent harmonic approximation, requires sufficiently large supercells and numerous randomly displaced structures.¹³² With help from MTP, such a computationally expensive analysis was completed, suggesting the stability of the *Fm3m* phase of BaSiH₈, whose predicted T_c is ~ 90 K.¹³²

4.5. Refining Empirical Formulas for T_c . The empirical McMillan formula (eq 8) of T_c was developed¹⁷⁰ and refined^{171,172} by “manually learning” small data sets generated from the Eliashberg equations. This formula, and some other variants, are particularly useful in the search for new superconductors. Recent ideas^{133,134} have suggested that these formulas may be refined further using advanced symbolic

ML techniques and larger data sets of the solutions of the Eliashberg equations, which become available thanks to new generations of computational infrastructures.

One such symbolic ML technique is “Sure Independence Screening and Sparsifying Operator” (SISSO).³²³ By defining some physically meaningful operators and functions of the primary variables, which are λ , ω_{\log} , and μ^* , it generated millions of features (expressions). Training a linear regression model using these features with L_0 regularization afforded some expressions for T_c ; among them, the simplest version is¹³³

$$T_c = 0.0953 \frac{\lambda^4 \omega_{\log}}{\lambda^3 + \sqrt{\mu^*}} \quad (10)$$

In a subsequent effort,¹³⁴ a modified version of the McMillan formula (eq 8) was assumed as

$$T_c = \frac{f_\omega f_\mu \omega_{\log}}{1.2} \exp \left[-\frac{1.04(1+\lambda)}{\lambda - \mu^*(1+0.62\lambda)} \right] \quad (11)$$

in which two prefactors f_ω and f_μ are learned from the data to be

$$f_\omega = 1.92 \frac{\lambda + \omega_{\log}/\bar{\omega}_2 - \sqrt{[3]\mu^*}}{\sqrt{\lambda} \exp(\omega_{\log}/\bar{\omega}_2)} - 0.08 \quad (12)$$

and

$$f_\mu = \frac{6.86 \exp(-\lambda/\mu^*)}{1/\lambda - \mu^* - \omega_{\log}/\bar{\omega}_2} + 1 \quad (13)$$

where¹⁷²

$$\bar{\omega}_2 = \left[\frac{2}{\lambda} \int_0^\infty d\omega \omega \alpha^2 F(\omega) \right]^{1/2} \quad (14)$$

Likewise, data obtained from the ML-powered discovery strategy developed¹⁴⁸ for hydride superconductors offer an opportunity to test and improve the McMillan formula (eq 8). Assuming

$$T_c = \frac{\omega_{\log}}{1.2} \exp \left[-\frac{1.04(1+\lambda)}{\lambda - \mu^*(1+0.62\lambda)} \right] (a + b\lambda) \quad (15)$$

data fitting yields an a of 1.0061 and a b of 0.0663,¹⁴⁸ slightly modifying the McMillan formula (eq 8).

5. CHALLENGES, OPPORTUNITIES, AND CRITICAL NEXT STEPS

5.1. Theoretical and Computational Methods. Despite thousands of computational discoveries reported in the past two decades, only approximately 20–30 materials were synthesized and reported. This small fraction ($\lesssim 1\%$) may suggest that we simply do not have a “silver bullet” for such a tough problem like understanding, predicting, and discovering superconductivity. In the future, this situation may change, but some major challenges must be resolved. Apparently, phonon-mediated pairing is one of many mechanisms proposed for superconductivity, and an exact and/or well-controlled theory for this mechanism is not readily available. It is known that Migdal–Eliashberg theory may become inaccurate,^{173–178} and one reason could be the fact that it accounts for only the first order of vertex corrections.²¹ Challenges in pushing the

theoretical front in superconductivity understanding are obviously enormous.

In the computational front, two major steps of the workflow discussed in section 2.3, namely the atomic structure prediction and the computations of $\alpha^2 F(\omega)$, λ , and ω_{\log} are highly nontrivial. The former faces truly infinite, extremely high-dimensional configuration spaces. For the latter, implications of the possible breakdown of Migdal–Éliashberg theory have not been well understood while the desirable accuracy and convergence are hard to control and obtain.^{140–142,148} Technically, even a numerical error that is comparable with the best attainable level of accuracy, i.e., approximately 10^{-4} to 10^{-3} eV/Å in the atomic force calculations, could be translated into a sizable change in the computed phonon frequencies and, thus, in the superconductivity-related properties.

For a more quantitative assessment, we show in Figure 15 some computed and measured data of T_c of some notable

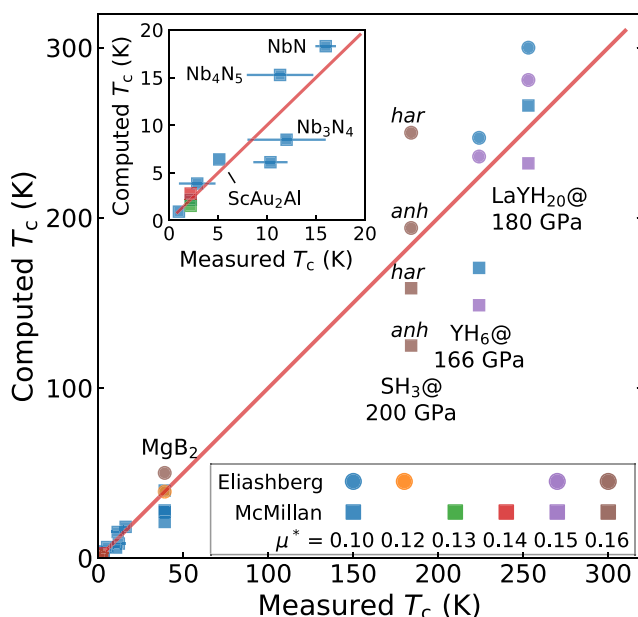


Figure 15. Critical temperature T_c computed for some notable superconductors using the McMillan formula and solving the Éliashberg equations, given in comparison with measured T_c values. The value of μ^* and the question of anharminicity, labeled by *anh* and *har*, are shown. The inset is used for the small- T_c regime. The *x*-axis error bars were obtained from different measured values of T_c , while different computed values of T_c are shown separately for further discussions.

superconductors, obtained from the same atomic structure under the same pressure. Four materials with the highest T_c shown in this figure are MgB₂ at ambient pressure,^{47,166,324–328} H₃S at 200 GPa,^{99,190} YH₆ at 166 GPa,¹⁰⁴ and LaYH₂₀ at 180 GPa.²¹¹ For each of them, multiple computational schemes were used, involving different values of μ^* and whether anharmonicity is included. These empirical treatments allow the computed T_c to spread over a sizable range, i.e., ≈ 29 K for MgB₂, ≈ 125 K for H₃S, ≈ 100 K for YH₆, and ≈ 70 K for LaYH₂₀. Considering the significant challenges in both experimental and computational techniques, the moderate agreement is reasonable and understandable, highlighting important cautions for future works.

Some emerging techniques may be useful for these challenges. Given that the atomic structure predictions can

be effectively coupled with powerful ML potentials,^{127–132} they are expected to be further accelerated by the next developments of this fast-evolving field.^{313–320} In the future, when deep learning can be used to accelerate the essential quantum mechanics-based calculations like DFT^{329–333} and DFPT³³⁴ in practice, significant advancements may be envisioned. On the contrary, some advanced physics-based computational approaches are also under development. Among them are SuperConducting DFT,^{335–337} a fully *ab initio* approach for T_c , and a GW perturbation theory-based scheme for computing electron–phonon coupling.³³⁸ Once these methods can be fully demonstrated, further advances in this field may be anticipated.

5.2. Materials Informatics Approaches. Different from the experimental and theoretical efforts with a century of history and the computational approaches that have blossomed for two decades, materials informatics has less than a decade of development in terms of understanding and discovering superconductivity. Compared to the DFPT-based computational approaches, the driving force behind almost all of the discoveries of hydride superconductors discussed in section 3, materials informatics remains in its early stage, in terms of the methodology development and the impacts to the field. Nevertheless, opportunities exist on the horizon for the informatics-based methods to efficiently complement the traditional (computational and experimental) approaches. With an eye on the future, some critical challenges, discussed below, are waiting to be resolved.

5.2.1. Generation and Accumulation of Data. Data development is the most critical challenge of materials informatics approaches in superconductor discovery. In this area, available data are scarce and insufficient. The largest superconductor data set is SuperCon², developed in 2023 with $\approx 40\,000$ records. The most widely used data set, i.e., NIMS SuperCon, in its cleaned version (SuperCon), has $\approx 16\,000$ records.¹³⁷ For both of them, only the chemical formula is available for the description of the materials. Attempts to augment the chemical formula with atomic details using the structure matching/lookup method produced data sets with up to ≈ 5700 records,¹⁴³ as they rely on NIMS SuperCon for the experimental values of T_c . Such data sets are small and less informative than other branches of materials informatics.

Besides a few high-throughput computational efforts that can generate hundreds to thousands of data records of λ , ω_{\log} and computed T_c ,^{140,141,148–150} the vast majority of the literature can only report results from works of structure prediction performed for a handful of materials. This is the main limitation of the available computational data in the field. An initial attempt to collect atomic-level data from the literature¹⁴² returns nearly 600 records, but more efficient and scalable methods are needed. Given some known limits of the computational approaches, computed data, when developed, should be combined with (more trustworthy) experimental data and “machine” learned in a collective and complementary manner.

The scientific literature also hosts a huge, yet essentially untouched, experimental data reservoir. During the past decade, NLP-based approaches such as NER have demonstrated their power in creating SC-COMICS,^{160,161} SuperMat,¹⁶³ and SuperCon².¹⁶⁴ Significant future developments are anticipated for these methods can be used to extract the crystallographic information, typically distributed throughout

the full text and in tables, supporting information material, and, in few cases, some atomic structure formats. In such a challenging endeavor, large language models (LLMs) like ChatGPT³³⁹ and Meta Llama 2 and 3³⁴⁰ could be useful, as recently demonstrated.^{341,342} Nevertheless, there are enormous challenges before this approach can become mature and efficient in literature data extraction.

5.2.2. Deep Learning for the Physics of Superconductivity. Superconductivity is highly collective and nonlocal in nature. The coherence length of the Cooper pairs can range from a few nanometers as in LaH_{10} ,¹⁰¹ YH_6 and YH_9 ,¹⁰⁵ and CeH_9 ,¹⁰⁶ to several hundred nanometers as in many known superconductors.³⁴³ Chemical formulas do not include such information and, thus, are insufficient for informatics techniques. Even when the atomic structures are used to describe the materials, recognizing such behaviors is impossible for local-environment- and fragment-based featurizing schemes like SOAP³⁰⁴ and SiRMS.²⁹⁵ In such “hand-crafted” featurizing schemes, the typical “neighboring” distance cutoff of $\sim 10 \text{ \AA}$ is far too small for the physics of superconductivity. However, bringing this length scale to the order of hundreds of nanometers will certainly (and exponentially) increase the size and the complexity of feature vectors, making them impractical.

In this context, deep-learning techniques that can directly accept the atomic structures (of course, when data are available) to understand both the local atomic environments and the long-range orders of the materials could be useful. Deep neural network-based architectures¹³⁹ like ATCNN¹³⁸ and ALIGNN³⁰⁷ have been developed and used in some cases with encouraging results. Nevertheless, further developments for this challenging problem, going beyond these initial steps, are needed and anticipated. Equivariant neural networks, in which essential physics-inspired invariances are respected, have begun to emerge and show their applicability in materials informatics.^{281–283}

5.3. ML-Guided Search for Ambient-Pressure Superconductors. After two decades of discoveries at hundreds of gigapascals, recently attention has gradually shifted to the search for possible high- T_c superconductivity at lower pressures.^{97,129,140–142,147} Given the infinite materials space and the complexity of the traditional physics-based approaches, rapid ML models for predicting superconductivity, as discussed in section 4, could be useful, but not without challenges. Adding to the challenges outlined in sections 5.2.1 and 5.2.2 for developing the ML models, another notable problem is that inferences made outside, or far from, the scope of their experience are generally not good.³⁴⁴ Thus, if a ML model is trained on superconductors whose $T_c \leq 150 \text{ K}$ (at ambient pressure), it may not be able to recognize superconductors with higher T_c values.

One possible way to expand the “domain of applicability” is to include in the training data the atomic-level details of the (computational and experimental) discoveries at any pressures, for which T_c could be much higher (e.g., $\simeq 200 \text{ K}$ for H_3S and $\simeq 250 \text{ K}$ for LaH_{10}).¹⁴² Trained on such a data set, the obtained models may recognize the atomic details related to high- T_c superconductivity at any pressures, including ambient pressure. In this approach, external pressure P is assumed to connect with the superconductivity indirectly; i.e., P determines the atomic structures, which, in turn, determines the superconductivity. This assumption has its roots in thermodynamics, where P , a macroscopic concept, determines the atomic

structures through the equation $P = -\partial H/\partial V$, given that both enthalpy H and volume V of a unit cell are solely functions of the atomic structures. The current edition of such a training data set, i.e., CompSC, is small, containing 587 atomic structures with 584 values of λ and 567 values of ω_{\log} .¹⁴² When a substantially larger and more diverse version is available and advanced deep-learning techniques are developed, the ML models trained on this data set may be more effective and useful.

Along another dimension, potential non-hydrogen high- T_c superconductors have not been explored appropriately. Although hydrides may have a favorable vibrational frequency spectrum for high- T_c superconductors, this field remains full of other enigmas and wonders. As CompSC currently contains mostly hydrides,¹⁴² the inclusion of non-hydrogen superconductors would be critical to an exploration beyond the hydride-related boundary.

6. SUMMARY

Research efforts devoted to superconductor discovery in the past two decades have been massive and incredible. Among thousands of superconductors predicted computationally at hundreds of gigapascals, a few dozen were synthesized and characterized experimentally. The inspiring results have somehow rekindled the dream of room-temperature superconductors. Nevertheless, this “holy grail” remains far from being attainable while technical challenges are numerous and enormous. Many of them are related to conducting measurements at hundreds of gigapascals in a DAC and then analyzing and/or interpreting the obtained data.^{52,110–116} Theoretical foundations and computational approaches, on the contrary, have their own inherent hard limits that are not easy to overcome.

Materials informatics approaches, emerging as a new frontier of materials research, could be useful to complement the traditional approaches. In the past decade, some essential components of materials informatics for superconductor discovery have been developed, reaching an inspiring level of maturity. Tremendous opportunities will become available in the future when the enormous challenges can be resolved. The most notable challenges are, but not limited to, those related to data generation and curation, deep-learning techniques that can capture the physics of superconductivity, and a reliable ML-guided search protocol for high- T_c superconductors at ambient pressures. Looking at other branches of materials informatics where tremendous advancements have been made, we believe that superconductor discovery may be significantly advanced with the new developments in this new frontier of materials research.

■ ASSOCIATED CONTENT

Data Availability Statement

These data files are also available at https://github.com/huantd/matsdata/tree/main/papers/supercond_2024_01.

SI Supporting Information

The Supporting Information is available free of charge at <https://pubs.acs.org/doi/10.1021/acs.chemmater.4c01757>.

Files supercond_history_Figure 1.csv, supercond_data_Figure 3.csv, and supercond_data_Figure 15.csv for creating Figures 1, 3, and 15, respectively (ZIP)

■ AUTHOR INFORMATION

Corresponding Author

Huan Tran – School of Materials Science and Engineering, Georgia Institute of Technology, Atlanta, Georgia 30332, United States;  orcid.org/0000-0002-8093-9426; Email: huan.tran@mse.gatech.edu

Authors

Hieu-Chi Dam – Japan Advanced Institute of Science and Technology, Nomi, Ishikawa 923-1292, Japan;  orcid.org/0000-0001-8252-7719

Christopher Kenneth – Faculty of Engineering Science, University of Bayreuth, 95447 Bayreuth, Germany;  orcid.org/0000-0002-6958-4679

Vu Ngoc Tuoc – Hanoi University of Science & Technology, Hanoi 10000, Vietnam;  orcid.org/0000-0002-5749-1483

Hiori Kino – Research Center for Electronic and Optical Materials, National Institute for Materials Science, Tsukuba, Ibaraki 305-0044, Japan;  orcid.org/0000-0002-8912-686X

Complete contact information is available at:
<https://pubs.acs.org/10.1021/acs.chemmater.4c01757>

Notes

The authors declare no competing financial interest.

■ ACKNOWLEDGMENTS

Some data used for Figures³ were prepared with support from the San Diego Supercomputer Center (Expanse) within XSEDE/ACCESS Allocation DMR170031. Work by V.N.T. is supported by the Vietnam National Foundation for Science and Technology Development under Grant 103.01-2021.12.

■ REFERENCES

- (1) Onnes, H. K. Further experiments with liquid helium. C. On the change of electric resistance of pure metals at very low temperatures etc. IV. The resistance of pure mercury at helium temperatures. *Commun. Phys. Lab. Univ. Leiden* **1911**, *119*, 120–122.
- (2) Meissner, W.; Ochsenfeld, R. Ein neuer effekt bei eintritt der supraleitfähigkeit. *Naturwissenschaften* **1933**, *21*, 787–788.
- (3) Smith, H. G.; Wilhelm, J. O. Superconductivity. *Rev. Mod. Phys.* **1935**, *7*, 237–271.
- (4) Eisenstein, J. Superconducting Elements. *Rev. Mod. Phys.* **1954**, *26*, 277–291.
- (5) Matthias, B. T.; Geballe, T. H.; Compton, V. B. Superconductivity. *Rev. Mod. Phys.* **1963**, *35*, 1–22.
- (6) London, F. On the problem of the molecular theory of superconductivity. *Phys. Rev.* **1948**, *74*, 562.
- (7) Landau, L. D.; Ginzburg, V. L. On the theory of superconductivity. *Zh. Eksp. Teor. Fiz.* **1950**, *20*, 1064.
- (8) Fröhlich, H. Electrons in lattice fields. *Adv. Phys.* **1954**, *3*, 325–361.
- (9) Fröhlich, H. On the theory of superconductivity: the one-dimensional case. *Proc. R. Soc. A* **1954**, *223*, 296–305.
- (10) Bardeen, J.; Pines, D. Electron-phonon interaction in metals. *Phys. Rev.* **1955**, *99*, 1140.
- (11) Bardeen, J. Theory of the Meissner effect in superconductors. *Phys. Rev.* **1955**, *97*, 1724.
- (12) Cooper, L. N. Bound electron pairs in a degenerate Fermi gas. *Phys. Rev.* **1956**, *104*, 1189.
- (13) Bardeen, J.; Cooper, L. N.; Schrieffer, J. R. Microscopic theory of superconductivity. *Phys. Rev.* **1957**, *106*, 162.
- (14) Bardeen, J. Electron-phonon interactions and superconductivity. *Science* **1973**, *181*, 1209–1214.
- (15) Schrieffer, J. R. *Theory of superconductivity*; CRC Press, 2018.
- (16) Tinkham, M. *Introduction to superconductivity*; Courier Corp., 2004.
- (17) Ginzburg, V. L.; Andryushin, E. A. *Superconductivity (Revised Edition)*; World Scientific, 2004.
- (18) Carbotte, J. Properties of boson-exchange superconductors. *Rev. Mod. Phys.* **1990**, *62*, 1027.
- (19) Eliashberg, G. Interactions between electrons and lattice vibrations in a superconductor. *Sov. Phys. J. Exp. Theor. Phys.* **1960**, *11*, 696.
- (20) Migdal, A. B. Interaction between electrons and lattice vibrations in a normal metal. *Sov. Phys. J. Exp. Theor. Phys.* **1958**, *7*, 996.
- (21) Chubukov, A. V.; Abanov, A.; Esterlis, I.; Kivelson, S. A. Eliashberg theory of phonon-mediated superconductivity - When it is valid and how it breaks down. *Ann. Phys.* **2020**, *417*, No. 168190.
- (22) Marsiglio, F. Eliashberg theory: A short review. *Ann. Phys.* **2020**, *417*, No. 168102.
- (23) Allen, P. B.; Mitrović, B. Theory of superconducting T_c . *Solid State Phys.* **1983**, *37*, 1–92.
- (24) Pellegrini, C.; Sanna, A. Ab initio methods for superconductivity. *Nat. Rev. Phys.* **2024**, *6*, 509–523.
- (25) Kresin, V. Z.; Morawitz, H.; Wolf, S. A. *Mechanisms of conventional and high T_c superconductivity*; Oxford University Press, 1993; Vol. 84.
- (26) Stewart, G. Unconventional superconductivity. *Adv. Phys.* **2017**, *66*, 75–196.
- (27) Anderson, P. W. *The theory of superconductivity in the high- T_c cuprate superconductors*; Princeton University Press, 1997.
- (28) Blatter, G.; Feigel'man, M. V.; Geshkenbein, V. B.; Larkin, A. I.; Vinokur, V. M. Vortices in high-temperature superconductors. *Rev. Mod. Phys.* **1994**, *66*, 1125.
- (29) Lee, P. A.; Nagaosa, N.; Wen, X.-G. Doping a Mott insulator: Physics of high-temperature superconductivity. *Rev. Mod. Phys.* **2006**, *78*, 17.
- (30) Orenstein, J.; Millis, A. Advances in the physics of high-temperature superconductivity. *Science* **2000**, *288*, 468–474.
- (31) Johnson, C. Y. A superconductor claim blew up online. Science has punctured it. *The Washington Post*, 2023.
- (32) Cartlidge, E. Superconductivity record sparks wave of follow-up physics. *Nature* **2015**, *524*, 277–277.
- (33) Jin, C.; Ceperley, D. Hopes raised for room-temperature superconductivity, but doubts remain. *Nature* **2023**, *615*, 221.
- (34) Little, W. Superconductivity at room temperature. *Sci. Am.* **1965**, *212*, 21–27.
- (35) Sleight, A. W. Room temperature superconductors. *Acc. Chem. Res.* **1995**, *28*, 103–108.
- (36) Matthias, B.; Hulm, J. A search for new superconducting compounds. *Phys. Rev.* **1952**, *87*, 799.
- (37) Müller, K. A.; Bednorz, J. G. The discovery of a class of high-temperature superconductors. *Science* **1987**, *237*, 1133–1139.
- (38) Bednorz, J. G.; Müller, K. A. Possible high T_c superconductivity in the Ba-La-Cu-O system. *Z. Phys. B* **1986**, *64*, 189–193.
- (39) Bednorz, J. G.; Müller, K. A. Perovskite-type oxides The new approach to high-T c superconductivity. *Rev. Mod. Phys.* **1988**, *60*, 585.
- (40) Chu, C.; Hor, P.; Meng, R.; Gao, L.; Huang, Z.; Wang, Y. Q. Evidence for superconductivity above 40 K in the La-Ba-Cu-O compound system. *Phys. Rev. Lett.* **1987**, *58*, 405.
- (41) Cava, R. J.; van Dover, R. B.; Batlogg, B.; Rietman, E. A. Bulk superconductivity at 36 K in $\text{La}_{1.8} \text{Sr}_{0.2} \text{CuO}_4$. *Phys. Rev. Lett.* **1987**, *58*, 408–410.
- (42) Wu, M. K.; Ashburn, J. R.; Torng, C. J.; Hor, P. H.; Meng, R. L.; Gao, L.; Huang, Z. J.; Wang, Y. Q.; Chu, C. W. Superconductivity at 93 K in a new mixed-phase Y-Ba-Cu-O compound system at ambient pressure. *Phys. Rev. Lett.* **1987**, *58*, 908–910.
- (43) Cava, R. J.; Batlogg, B.; van Dover, R. B.; Murphy, D. W.; Sunshine, S.; Siegrist, T.; Remeika, J. P.; Rietman, E. A.; Zahurak, S.; Espinosa, G. P. Bulk superconductivity at 91 K in single-phase

- oxygen-deficient perovskite $\text{Ba}_2 \text{YC}_{\delta} \text{O}_{9-\delta}$. *Phys. Rev. Lett.* **1987**, *58*, 1676–1679.
- (44) Hazen, R. M.; et al. Superconductivity in the high- T_c Bi-Ca-Sr-Cu-O system: Phase identification. *Phys. Rev. Lett.* **1988**, *60*, 1174–1177.
- (45) Schilling, A.; Cantoni, M.; Guo, J.; Ott, H. Superconductivity above 130 K in the Hg-Ba-Ca-Cu-O system. *Nature* **1993**, *363*, 56–58.
- (46) Chu, C.; Gao, L.; Chen, F.; Huang, Z.; Meng, R.; Xue, Y. Superconductivity above 150 K in $\text{HgBa}_2\text{Ca}_2\text{Cu}_3\text{O}_8 + \delta$ at high pressures. *Nature* **1993**, *365*, 323–325.
- (47) Nagamatsu, J.; Nakagawa, N.; Muranaka, T.; Zenitani, Y.; Akimitsu, J. Superconductivity at 39 K in magnesium diboride. *Nature* **2001**, *410*, 63–64.
- (48) Kamihara, Y.; Hiramatsu, H.; Hirano, M.; Kawamura, R.; Yanagi, H.; Kamiya, T.; Hosono, H. Iron-based layered superconductor: LaOFeP . *J. Am. Chem. Soc.* **2006**, *128*, 10012–10013.
- (49) Kamihara, Y.; Watanabe, T.; Hirano, M.; Hosono, H. Iron-based layered superconductor $\text{La}[\text{O}_{1-x}\text{F}_x]\text{FeAs}$ ($x = 0.05$ –0.12) with $T_c = 26$ K. *J. Am. Chem. Soc.* **2008**, *130*, 3296–3297.
- (50) Hosono, H.; Tanabe, K.; Takayama-Muromachi, E.; Kageyama, H.; Yamanaka, S.; Kumakura, H.; Nohara, M.; Hiramatsu, H.; Fujitsu, S. Exploration of new superconductors and functional materials, and fabrication of superconducting tapes and wires of iron pnictides. *Sci. Technol. Adv. Mater.* **2015**, *16*, No. 033503.
- (51) Hosono, H.; Kuroki, K. Iron-based superconductors: Current status of materials and pairing mechanism. *Physica C* **2015**, *514*, 399–422.
- (52) Hirsch, J. Superconducting materials: Judge and jury of BCS-electron-phonon theory. *Appl. Phys. Lett.* **2022**, *121*, 080501.
- (53) Kohn, W.; Luttinger, J. New mechanism for superconductivity. *Phys. Rev. Lett.* **1965**, *15*, 524.
- (54) Mott, N. Polaron models of high-temperature superconductors. *J. Phys.: Condens. Matter* **1993**, *5*, 3487.
- (55) Chen, Y.-H.; Wilczek, F.; Witten, E.; Halperin, B. I. On anyon superconductivity. *Int. J. Mod. Phys. B* **1989**, *3*, 1001–1067.
- (56) Beenakker, C. Search for Majorana fermions in superconductors. *Annu. Rev. Condens. Matter Phys.* **2013**, *4*, 113–136.
- (57) Leijnse, M.; Flensberg, K. Introduction to topological superconductivity and Majorana fermions. *Semicond. Sci. Technol.* **2012**, *27*, 124003.
- (58) Scalapino, D. Superconductivity and spin fluctuations. *J. Low Temp. Phys.* **1999**, *117*, 179–188.
- (59) Anderson, P. W. The resonating valence bond state in La_2CuO_4 and superconductivity. *Science* **1987**, *235*, 1196–1198.
- (60) Petrovic, C.; Pagluso, P.; Hundley, M.; Movshovich, R.; Sarrao, J.; Thompson, J.; Fisk, Z.; Monthoux, P. Heavy-fermion superconductivity in CeCoIn_5 at 2.3 K. *J. Condens. Matter Phys.* **2001**, *13*, L337.
- (61) Steglich, F.; Bredl, C.; Lieke, W.; Rauchschwalbe, U.; Sparn, G. Heavy fermion superconductivity. *Physica B+C (Amsterdam)* **1984**, *126*, 82–91.
- (62) Jérôme, D. The physics of organic superconductors. *Science* **1991**, *252*, 1509–1514.
- (63) Saito, G.; Yoshida, Y. Organic superconductors. *Chem. Rec.* **2011**, *11*, 124–145.
- (64) Ardavan, A.; Brown, S.; Kagoshima, S.; Kanoda, K.; Kuroki, K.; Mori, H.; Ogata, M.; Uji, S.; Wosnitza, J. Recent topics of organic superconductors. *J. Phys. Soc. Jpn.* **2012**, *81*, No. 011004.
- (65) Lebed, A. G. *The physics of organic superconductors and conductors*; Springer, 2008; Vol. 110.
- (66) Oganov, A. R., Ed. *Modern Methods of Crystal Structure Prediction*; Wiley-VCH: Weinheim, Germany, 2011.
- (67) Oganov, A. R.; Pickard, C. J.; Zhu, Q.; Needs, R. J. Structure prediction drives materials discovery. *Nat. Rev. Mater.* **2019**, *4*, 331–348.
- (68) Needs, R. J.; Pickard, C. J. Perspective: Role of structure prediction in materials discovery and design. *APL Mater.* **2016**, *4*, 053210.
- (69) Zhang, L.; Wang, Y.; Lv, J.; Ma, Y. Materials discovery at high pressures. *Nat. Rev. Mater.* **2017**, *2*, 17005.
- (70) Xu, M.; Li, Y.; Ma, Y. Materials by design at high pressures. *Chem. Sci.* **2022**, *13*, 329–344.
- (71) Baroni, S.; de Gironcoli, S.; Dal Corso, A.; Giannozzi, P. Phonons and related crystal properties from density-functional perturbation theory. *Rev. Mod. Phys.* **2001**, *73*, 515.
- (72) Giustino, F. Electron-phonon interactions from first principles. *Rev. Mod. Phys.* **2017**, *89*, No. 015003.
- (73) Pickett, W. E. Colloquium: Room temperature superconductivity: The roles of theory and materials design. *Rev. Mod. Phys.* **2023**, *95*, No. 021001.
- (74) Zurek, E.; Bi, T. High-temperature superconductivity in alkaline and rare earth polyhydrides at high pressure: A theoretical perspective. *J. Chem. Phys.* **2019**, *150*, 050901.
- (75) Sun, Y.; Zhong, X.; Liu, H.; Ma, Y. Clathrate metal superhydrides at high-pressure conditions: enroute to room-temperature superconductivity. *Natl. Sci. Rev.* **2024**, *11*, No. nwad270.
- (76) Hilleke, K. P.; Zurek, E. Tuning chemical precompression: Theoretical design and crystal chemistry of novel hydrides in the quest for warm and light superconductivity at ambient pressures. *J. Appl. Phys.* **2022**, *131*, 070901.
- (77) Gao, G.; Wang, L.; Li, M.; Zhang, J.; Howie, R. T.; Gregoryanz, E.; Struzhkin, V. V.; Wang, L.; Tse, J. S. Superconducting binary hydrides: Theoretical predictions and experimental progresses. *Mater. Today Phys.* **2021**, *21*, 100546.
- (78) Zhao, W.; Huang, X.; Zhang, Z.; Chen, S.; Du, M.; Duan, D.; Cui, T. Superconducting ternary hydrides: Progress and challenges. *Natl. Sci. Rev.* **2024**, *11*, No. nwad307.
- (79) Boeri, L.; Bachelet, G. B. The road to room-temperature conventional superconductivity. *J. Condens. Matter. Phys.* **2019**, *31*, No. 234002.
- (80) Pickard, C. J.; Errea, I.; Eremets, M. I. Superconducting hydrides under pressure. *Annu. Rev. Condens. Matter Phys.* **2020**, *11*, 57–76.
- (81) Wang, H.; Tse, J. S.; Tanaka, K.; Iitaka, T.; Ma, Y. Superconductive sodalite-like clathrate calcium hydride at high pressures. *Proc. Natl. Acad. Sci. U.S.A.* **2012**, *109*, 6463–6466.
- (82) Duan, D.; Liu, Y.; Tian, F.; Li, D.; Huang, X.; Zhao, Z.; Yu, H.; Liu, B.; Tian, W.; Cui, T. Pressure-induced metallization of dense $(\text{H}_2\text{S})_2\text{H}_2$ with high- T_c superconductivity. *Sci. Rep.* **2014**, *4*, 6968.
- (83) Errea, I.; Belli, F.; Monacelli, L.; Sanna, A.; Koretsune, T.; Tadano, T.; Bianco, R.; Calandra, M.; Arita, R.; Mauri, F.; Flores-Livas, J. A. Quantum crystal structure in the 250-kelvin superconducting lanthanum hydride. *Nature* **2020**, *578*, 66–69.
- (84) Shah, S.; Kolmogorov, A. N. Stability and superconductivity of Ca-B phases at ambient and high pressure. *Phys. Rev. B* **2013**, *88*, 014107.
- (85) Huan, T. D. Pressure-stabilized binary compounds of magnesium and silicon. *Phys. Rev. Mater.* **2018**, *2*, 023803.
- (86) Li, Y.; Hao, J.; Liu, H.; Tse, J. S.; Wang, Y.; Ma, Y. Pressure-stabilized superconductive yttrium hydrides. *Sci. Rep.* **2015**, *5*, 9948.
- (87) Liu, H.; Naumov, I. I.; Hoffmann, R.; Ashcroft, N.; Hemley, R. J. Potential high- T_c superconducting lanthanum and yttrium hydrides at high pressure. *Proc. Natl. Acad. Sci. U.S.A.* **2017**, *114*, 6990–6995.
- (88) Peng, F.; Sun, Y.; Pickard, C. J.; Needs, R. J.; Wu, Q.; Ma, Y. Hydrogen clathrate structures in rare earth hydrides at high pressures: possible route to room-temperature superconductivity. *Phys. Rev. Lett.* **2017**, *119*, 107001.
- (89) Kvashnin, A. G.; Semenok, D. V.; Kruglov, I. A.; Wrona, I. A.; Oganov, A. R. High-temperature superconductivity in a Th-H system under pressure conditions. *ACS Appl. Mater. Interfaces* **2018**, *10*, 43809–43816.
- (90) Zhang, Z.; Cui, T.; Hutcheon, M. J.; Shipley, A. M.; Song, H.; Du, M.; Kresin, V. Z.; Duan, D.; Pickard, C. J.; Yao, Y. Design principles for high-temperature superconductors with a hydrogen-based alloy backbone at moderate pressure. *Phys. Rev. Lett.* **2022**, *128*, 047001.

- (91) Boeri, L.; et al. The 2021 Room-Temperature Superconductivity Roadmap. *J. Phys.: Condens. Matter* **2022**, *34*, 183002.
- (92) Yazdani-Asrami, M.; Sadeghi, A.; Song, W.; Madureira, A.; Murta-Pina, J.; Morandi, A.; Parizh, M. Artificial intelligence methods for applied superconductivity: material, design, manufacturing, testing, operation, and condition monitoring. *Supercond. Sci. Technol.* **2022**, *35*, No. 123001.
- (93) Ribeiro, F. J.; Cohen, M. L. Possible superconductivity in hole-doped BC₃. *Phys. Rev. B* **2004**, *69*, 212507.
- (94) Saniz, R.; Medvedeva, J. E.; Ye, L.-H.; Shishidou, T.; Freeman, A. J. Electronic structure properties and BCS superconductivity in β -pyrochlore oxides: KOs₂O₆. *Phys. Rev. B* **2004**, *70*, No. 100505.
- (95) Di Cataldo, S.; Heil, C.; von der Linden, W.; Boeri, L. LaBH₈: Towards high- T_c low-pressure superconductivity in ternary superhydrides. *Phys. Rev. B* **2021**, *104*, No. L020511.
- (96) Zhang, S.; Yu, H.; Wei, J.; Zhong, T.; Sun, J.; Wang, Q.; Liu, L.; Xu, H.; Ma, J.; Liu, H. High-T c superconductivity in squeezed cubic CS₂H₆ and C₂TeH₈ ternary polyhydrides. *Phys. Rev. B* **2024**, *109*, No. 174507.
- (97) Sanna, A.; Cerqueira, T. F.; Fang, Y.-W.; Errea, I.; Ludwig, A.; Marques, M. A. Prediction of ambient pressure conventional superconductivity above 80 K in hydride compounds. *npj Comput. Mater.* **2024**, *10*, 44.
- (98) Eremets, M.; Trojan, I.; Medvedev, S.; Tse, J.; Yao, Y. Superconductivity in hydrogen dominant materials: Silane. *Science* **2008**, *319*, 1506–1509.
- (99) Drozdov, A.; Eremets, M.; Troyan, I.; Ksenofontov, V.; Shylin, S. Conventional superconductivity at 203 K at high pressures in the sulfur hydride system. *Nature* **2015**, *525*, 73–76.
- (100) Somayazulu, M.; Ahart, M.; Mishra, A. K.; Geballe, Z. M.; Baldini, M.; Meng, Y.; Struzhkin, V. V.; Hemley, R. J. Evidence for superconductivity above 260 K in lanthanum superhydride at megabar pressures. *Phys. Rev. Lett.* **2019**, *122*, 027001.
- (101) Drozdov, A. P.; Kong, P. P.; Minkov, V. S.; Besedin, S. P.; Kuzovnikov, M. A.; Mozaffari, S.; Balicas, L.; Balakirev, F. F.; Graf, D. E.; Prakapenka, V. B.; Greenberg, E.; Knyazev, D. A.; Tkacz, M.; Eremets, M. I. Superconductivity at 250K in lanthanum hydride under high pressures. *Nature* **2019**, *569*, 528–531.
- (102) Semenok, D. V.; Kvashnin, A. G.; Ivanova, A. G.; Svitlyk, V.; Fominski, V. Y.; Sadakov, A. V.; Sobolevskiy, O. A.; Pudalov, V. M.; Troyan, I. A.; Oganov, A. R. Superconductivity at 161K in thorium hydride ThH₁₀: Synthesis and properties. *Mater. Today* **2020**, *33*, 36–44.
- (103) Chen, W.; Semenok, D. V.; Kvashnin, A. G.; Huang, X.; Kruglov, I. A.; Galasso, M.; Song, H.; Duan, D.; Goncharov, A. F.; Prakapenka, V. B.; Oganov, A. R.; Cui, T. Synthesis of molecular metallic barium superhydride: pseudocubic BaH₁₂. *Nat. Commun.* **2021**, *12*, 273.
- (104) Troyan, I. A.; et al. Anomalous high-temperature superconductivity in YH₆. *Adv. Mater.* **2021**, *33*, 2006832.
- (105) Kong, P.; Minkov, V. S.; Kuzovnikov, M. A.; Drozdov, A. P.; Besedin, S. P.; Mozaffari, S.; Balicas, L.; Balakirev, F. F.; Prakapenka, V. B.; Chariton, S.; Knyazev, D. A.; Greenberg, E.; Eremets, M. I. Superconductivity up to 243K in the yttrium-hydrogen system under high pressure. *Nat. Commun.* **2021**, *12*, 5075.
- (106) Chen, W.; Semenok, D. V.; Huang, X.; Shu, H.; Li, X.; Duan, D.; Cui, T.; Oganov, A. R. High-Temperature Superconducting Phases in Cerium Superhydride with a Tc up to 115 K below a Pressure of 1 Megabar. *Phys. Rev. Lett.* **2021**, *127*, 117001.
- (107) Ma, L.; Wang, K.; Xie, Y.; Yang, X.; Wang, Y.; Zhou, M.; Liu, H.; Yu, X.; Zhao, Y.; Wang, H.; Liu, G.; Ma, Y. High-Temperature Superconducting Phase in Clathrate Calcium Hydride CaH₆ up to 215 K at a Pressure of 172 GPa. *Phys. Rev. Lett.* **2022**, *128*, 167001.
- (108) Li, Z.; et al. Superconductivity above 200 K discovered in superhydrides of calcium. *Nat. Commun.* **2022**, *13*, 2863.
- (109) Song, Y.; Bi, J.; Nakamoto, Y.; Shimizu, K.; Liu, H.; Zou, B.; Liu, G.; Wang, H.; Ma, Y. Stoichiometric ternary superhydride LaBeH₈ as a new template for high-temperature superconductivity at 110 K under 80 GPa. *Phys. Rev. Lett.* **2023**, *130*, 266001.
- (110) Hirsch, J.; Marsiglio, F. Unusual width of the superconducting transition in a hydride. *Nature* **2021**, *596*, E9–E10.
- (111) Wang, T.; Hirayama, M.; Nomoto, T.; Koretsune, T.; Arita, R.; Flores-Livas, J. A. Absence of conventional room-temperature superconductivity at high pressure in carbon-doped H₃S. *Phys. Rev. B* **2021**, *104*, 064510.
- (112) Hirsch, J.; Marsiglio, F. Nonstandard superconductivity or no superconductivity in hydrides under high pressure. *Phys. Rev. B* **2021**, *103*, 134505.
- (113) Gubler, M.; Flores-Livas, J. A.; Kozhevnikov, A.; Goedecker, S. Missing theoretical evidence for conventional room-temperature superconductivity in low-enthalpy structures of carbonaceous sulfur hydrides. *Phys. Rev. Mater.* **2022**, *6*, 014801.
- (114) Eremets, M. I.; Minkov, V. S.; Drozdov, A. P.; Kong, P. P.; Ksenofontov, V.; Shylin, S. I.; Bud'ko, S. L.; Prozorov, R.; Balakirev, F. F.; Sun, D.; Mozaffari, S.; Balicas, L. High-temperature superconductivity in hydrides: experimental evidence and details. *J. Supercond. Novel Magn.* **2022**, *35*, 965.
- (115) Xing, X.; et al. Observation of non-superconducting phase changes in nitrogen doped lutetium hydrides. *Nat. Commun.* **2023**, *14*, 5991.
- (116) Chen, S. Muted Response to New Claim of a Room-Temperature Superconductor. *Physics* **2023**, *16*, 39.
- (117) Ashcroft, N. W. Hydrogen dominant metallic alloys: high temperature superconductors? *Phys. Rev. Lett.* **2004**, *92*, 187002.
- (118) Ashcroft, N. W. Bridgman's high-pressure atomic destructibility and its growing legacy of ordered states. *J. Phys.: Condens. Matter* **2004**, *16*, S945.
- (119) Ramprasad, R.; Batra, R.; Pilania, G.; Mannodi-Kanakkithodi, A.; Kim, C. Machine Learning and Materials Informatics: Recent Applications and Prospects. *npj Comput. Mater.* **2017**, *3*, 54.
- (120) Agrawal, A.; Choudhary, A. Perspective: Materials informatics and big data: Realization of the fourth paradigm of science in materials science. *APL Mater.* **2016**, *4*, No. 053208.
- (121) Jain, A.; Hautier, G.; Ong, S. P.; Persson, K. New opportunities for materials informatics: resources and data mining techniques for uncovering hidden relationships. *J. Mater. Res.* **2016**, *31*, 977–994.
- (122) Draxl, C.; Scheffler, M. NOMAD: The FAIR concept for big data-driven materials science. *MRS Bull.* **2018**, *43*, 676–682.
- (123) Draxl, C.; Scheffler, M. The NOMAD laboratory: from data sharing to artificial intelligence. *J. Phys.: Mater.* **2019**, *2*, No. 036001.
- (124) Draxl, C.; Scheffler, M. Big data-driven materials science and its FAIR data infrastructure. *Handbook of Materials Modeling: Methods: Theory and Modeling* **2020**, 49–73.
- (125) Ghiringhelli, L. M.; Vybiral, J.; Levchenko, S. V.; Draxl, C.; Scheffler, M. Big Data of Materials Science: Critical Role of the Descriptor. *Phys. Rev. Lett.* **2015**, *114*, No. 105503.
- (126) Damewood, J.; Karaguesian, J.; Lunger, J. R.; Tan, A. R.; Xie, M.; Peng, J.; Gómez-Bombarelli, R. Representations of materials for machine learning. *Annu. Rev. Mater. Res.* **2023**, *53*, 399–426.
- (127) Gu, Q.; Xing, D.; Sun, J. Superconducting single-layer T-graphene and novel synthesis routes. *Chin. Phys. Lett.* **2019**, *36*, No. 097401.
- (128) Yang, Q.; Lv, J.; Tong, Q.; Du, X.; Wang, Y.; Zhang, S.; Yang, G.; Bergara, A.; Ma, Y. Hard and superconducting cubic boron phase via swarm-intelligence structure prediction driven by a machine-learning potential. *Phys. Rev. B* **2021**, *103*, No. 024505.
- (129) Dolui, K.; Conway, L. J.; Heil, C.; Strobel, T. A.; Prasankumar, R. P.; Pickard, C. J. Feasible route to high-temperature ambient-pressure hydride superconductivity. *Phys. Rev. Lett.* **2024**, *132*, No. 166001.
- (130) Ishikawa, T.; Tanaka, Y.; Tsuneyuki, S. Evolutionary search for superconducting phases in the lanthanum-nitrogen-hydrogen system with universal neural network potential. *Phys. Rev. B* **2024**, *109*, No. 094106.
- (131) Ferreira, P. P.; Conway, L. J.; Cucciari, A.; Di Cataldo, S.; Giannessi, F.; Kogler, E.; Eleno, L. T.; Pickard, C. J.; Heil, C.; Boeri,

- L. Search for ambient superconductivity in the Lu-NH system. *Nat. Commun.* **2023**, *14*, 5367.
- (132) Lurezzi, R.; Kogler, E.; Di Cataldo, S.; Aichhorn, M.; Boeri, L.; Heil, C. Quantum lattice dynamics and their importance in ternary superhydride clathrates. *Commun. Phys.* **2023**, *6*, 298.
- (133) Xie, S.; Stewart, G.; Hamlin, J.; Hirschfeld, P.; Hennig, R. Functional form of the superconducting critical temperature from machine learning. *Phys. Rev. B* **2019**, *100*, No. 174513.
- (134) Xie, S.; Quan, Y.; Hire, A.; Deng, B.; DeStefano, J.; Salinas, I.; Shah, U.; Fanfarillo, L.; Lim, J.; Kim, J.; Stewart, G. R.; Hamlin, J. J.; Hirschfeld, P. J.; Hennig, R. G. Machine learning of superconducting critical temperature from Eliashberg theory. *npj Comput. Mater.* **2022**, *8*, 14.
- (135) Isayev, O.; Fourches, D.; Muratov, E. N.; Oses, C.; Rasch, K.; Tropsha, A.; Curtarolo, S. Materials cartography: representing and mining materials space using structural and electronic fingerprints. *Chem. Mater.* **2015**, *27*, 735–743.
- (136) Hamidieh, K. A data-driven statistical model for predicting the critical temperature of a superconductor. *Comput. Mater. Sci.* **2018**, *154*, 346–354.
- (137) Stanev, V.; Oses, C.; Kusne, A. G.; Rodriguez, E.; Paglione, J.; Curtarolo, S.; Takeuchi, I. Machine learning modeling of superconducting critical temperature. *npj Comput. Mater.* **2018**, *4*, 29.
- (138) Zeng, S.; Zhao, Y.; Li, G.; Wang, R.; Wang, X.; Ni, J. Atom table convolutional neural networks for an accurate prediction of compounds properties. *npj Comput. Mater.* **2019**, *5*, 84.
- (139) Konno, T.; Kurokawa, H.; Nabeshima, F.; Sakishita, Y.; Ogawa, R.; Hosako, I.; Maeda, A. Deep learning model for finding new superconductors. *Phys. Rev. B* **2021**, *103*, No. 014509.
- (140) Choudhary, K.; Garrity, K. Designing High- T_c Superconductors with BCS-inspired Screening, Density Functional Theory and Deep-learning. *npj Comput. Mater.* **2022**, *8*, 244.
- (141) Cerqueira, T. F.; Sanna, A.; Marques, M. A. Sampling the materials space for conventional superconducting compounds. *Adv. Mater.* **2024**, *36*, No. 2307085.
- (142) Tran, H.; Vu, T. N. Machine-learning approach for discovery of conventional superconductors. *Phys. Rev. Mater.* **2023**, *7*, No. 054805.
- (143) Zhang, J.; Zhu, Z.; Xiang, X.-D.; Zhang, K.; Huang, S.; Zhong, C.; Qiu, H.-J.; Hu, K.; Lin, X. Machine learning prediction of superconducting critical temperature through the structural descriptor. *J. Phys. Chem. C* **2022**, *126*, 8922–8927.
- (144) Matsumoto, K.; Horide, T. An acceleration search method of higher T_c superconductors by a machine learning algorithm. *Appl. Phys. Express* **2019**, *12*, No. 073003.
- (145) Peretti, C.; Bernot, K.; Guizouarn, T.; Laufek, F.; Vymazalová, A.; Bindi, L.; Sessoli, R.; Fanelli, D. From individual elements to macroscopic materials: in search of new superconductors via machine learning. *npj Comput. Mater.* **2023**, *9*, 71.
- (146) Ishikawa, T.; Miyake, T.; Shimizu, K. Materials informatics based on evolutionary algorithms: Application to search for superconducting hydrogen compounds. *Phys. Rev. B* **2019**, *100*, No. 174506.
- (147) Hutcheon, M. J.; Shipley, A. M.; Needs, R. J. Predicting novel superconducting hydrides using machine learning approaches. *Phys. Rev. B* **2020**, *101*, No. 144505.
- (148) Shipley, A. M.; Hutcheon, M. J.; Needs, R. J.; Pickard, C. J. High-throughput discovery of high-temperature conventional superconductors. *Phys. Rev. B* **2021**, *104*, No. 054501.
- (149) Wines, D.; Choudhary, K.; Biacchi, A. J.; Garrity, K. F.; Tavazza, F. High-throughput DFT-based discovery of next generation two-dimensional (2D) superconductors. *Nano Lett.* **2023**, *23*, 969–978.
- (150) Hai, Y.-L.; Jiang, M.-J.; Tian, H.-L.; Zhong, G.-H.; Li, W.-J.; Yang, C.-L.; Chen, X.-J.; Lin, H.-Q. Superconductivity Above 100 K Predicted in Carbon-Cage Network. *Adv. Sci.* **2023**, *10*, No. 2303639.
- (151) Song, P.; Hou, Z.; de Castro, P. B.; Nakano, K.; Hongo, K.; Takano, Y.; Maezono, R. High- T_c ternary metal hydrides, YKH_{12} and LaKH_{12} , discovered by machine learning. *arXiv* **2021**, DOI: [10.48550/arXiv.2103.00193](https://doi.org/10.48550/arXiv.2103.00193).
- (152) Le, T. D.; Noumeir, R.; Quach, H. L.; Kim, J. H.; Kim, J. H.; Kim, H. M. Critical temperature prediction for a superconductor: A variational bayesian neural network approach. *IEEE Trans Appl. Supercond.* **2020**, *30*, 1–5.
- (153) García-Nieto, P. J.; Garcia-Gonzalo, E.; Paredes-Sánchez, J. P. Prediction of the critical temperature of a superconductor by using the WOA/MARS, Ridge, Lasso and Elastic-net machine learning techniques. *Neural. Comput. Appl.* **2021**, *33*, 17131–17145.
- (154) Stanev, V.; Choudhary, K.; Kusne, A. G.; Paglione, J.; Takeuchi, I. Artificial intelligence for search and discovery of quantum materials. *Commun. Mater.* **2021**, *2*, 105.
- (155) Raviprasad, S.; Angadi, N. A.; Kothari, M. Tree Based Models for Critical Temperature Prediction of Superconductors. *2022 3rd International Conference for Emerging Technology (INSET)* **2022**, 1–5.
- (156) Revathy, G.; Rajendran, V.; Rashmika, B.; Sathish Kumar, P.; Parkavi, P.; Shynisha, J. Random Forest Regressor based superconductivity materials investigation for critical temperature prediction. *Mater. Today: Proc.* **2022**, *66*, 648.
- (157) Bai, Z.; Bhullar, M.; Akinpelu, A.; Yao, Y. Unveiling future superconductors through machine learning. *Mater. Today Phys.* **2024**, *43*, No. 101384.
- (158) Roter, B.; Dordevic, S. V. Predicting new superconductors and their critical temperatures using machine learning. *Physica C: Supercond. Appl.* **2020**, *575*, No. 1353689.
- (159) Roter, B.; Ninkovic, N.; Dordevic, S. V. Clustering superconductors using unsupervised machine learning. *Physica C: Supercond. Appl.* **2022**, *598*, No. 1354078.
- (160) Yamaguchi, K.; Asahi, R.; Sasaki, Y. SC-CoMICs: A superconductivity corpus for materials informatics. *Proceedings of the Twelfth Language Resources and Evaluation Conference* **2020**, 6753–6760.
- (161) Yamaguchi, K.; Asahi, R.; Sasaki, Y. Superconductivity information extraction from the literature: A new corpus and its evaluations. *Adv. Eng. Inform.* **2022**, *54*, No. 101768.
- (162) Foppiano, L.; Dieb, T. M.; Suzuki, A.; Ishii, M. Proposal for automatic extraction framework of superconductors related information from scientific literature. *IEICE Technol. Rep.* **2019**, 1–5.
- (163) Foppiano, L.; Dieb, S.; Suzuki, A.; Baptista de Castro, P.; Iwasaki, S.; Uzuki, A.; Echevarria, M. G. E.; Meng, Y.; Terashima, K.; Romary, L.; Takano, Y.; Ishii, M. SuperMat: construction of a linked annotated dataset from superconductors-related publications. *Sci. Technol. Adv. Mater.: Methods* **2021**, *1*, 34–44.
- (164) Foppiano, L.; Castro, P. B.; Ortiz Suarez, P.; Terashima, K.; Takano, Y.; Ishii, M. Automatic extraction of materials and properties from superconductors scientific literature. *Sci. Technol. Adv. Mater.: Methods* **2023**, *3*, No. 2153633.
- (165) Sommer, T.; Willa, R.; Schmalian, J.; Friederich, P. 3DSC - a dataset of superconductors including crystal structures. *Sci. Data* **2023**, *10*, 816.
- (166) Margine, E. R.; Giustino, F. Anisotropic migdal-eliasberg theory using wannier functions. *Phys. Rev. B* **2013**, *87*, No. 024505.
- (167) Poncé, S.; Margine, E. R.; Verdi, C.; Giustino, F. Electron–phonon coupling, transport and superconducting properties using maximally localized Wannier functions. *Comput. Phys. Commun.* **2016**, *209*, 116–133.
- (168) Giustino, F.; Cohen, M. L.; Louie, S. G. Electron-phonon interaction using Wannier functions. *Phys. Rev. B* **2007**, *76*, No. 165108.
- (169) Morel, P.; Anderson, P. W. Calculation of the Superconducting State Parameters with Retarded Electron-Phonon Interaction. *Phys. Rev.* **1962**, *125*, 1263–1271.
- (170) McMillan, W. L. Transition Temperature of Strong-Coupled Superconductors. *Phys. Rev.* **1968**, *167*, 331–344.
- (171) Dynes, R. McMillan's equation and the T_c of superconductors. *Solid State Commun.* **1972**, *10*, 615–618.
- (172) Allen, P. B.; Dynes, R. C. Transition temperature of strong-coupled superconductors reanalyzed. *Phys. Rev. B* **1975**, *12*, 905–922.

- (173) Esterlis, I.; Nosarzewski, B.; Huang, E. W.; Moritz, B.; Devereaux, T. P.; Scalapino, D. J.; Kivelson, S. A. Breakdown of the Migdal-Eliashberg theory: A determinant quantum Monte Carlo study. *Phys. Rev. B* **2018**, *97*, No. 140501.
- (174) Alexandrov, A. Breakdown of the Migdal-Eliashberg theory in the strong-coupling adiabatic regime. *Europhys. Lett.* **2001**, *56*, 92.
- (175) Hague, J.; d'Ambrumenil, N. Breakdown of Migdal-Eliashberg theory via catastrophic vertex divergence at low phonon frequency. *J. Low. Temp. Phys.* **2008**, *151*, 1149–1163.
- (176) Benedetti, P.; Zeyher, R. Holstein model in infinite dimensions at half-filling. *Phys. Rev. B* **1998**, *58*, No. 14320.
- (177) Yuzbashyan, E. A.; Altshuler, B. L. Breakdown of the Migdal-Eliashberg theory and a theory of lattice-fermionic superfluidity. *Phys. Rev. B* **2022**, *106*, No. 054518.
- (178) Dynes, R.; White, A.; Graybeal, J.; Gurne, J. Breakdown of Eliashberg theory for two-dimensional superconductivity in the presence of disorder. *Phys. Rev. Lett.* **1986**, *57*, 2195.
- (179) Hohenberg, P.; Kohn, W. Inhomogeneous Electron Gas. *Phys. Rev.* **1964**, *136*, B864–B871.
- (180) Kohn, W.; Sham, L. Self-Consistent Equations Including Exchange and Correlation Effects. *Phys. Rev.* **1965**, *140*, A1133–A1138.
- (181) Giannozzi, P.; et al. QUANTUM ESPRESSO: a modular and open-source software project for quantum simulations of materials. *J. Phys.: Condens. Matter* **2009**, *21*, No. 395502.
- (182) Giannozzi, P.; et al. Advanced capabilities for materials modelling with Quantum ESPRESSO. *J. Phys.: Condens. Matter* **2017**, *29*, No. 465901.
- (183) Gonze, X.; et al. ABINIT: First-principles approach to material and nanosystem properties. *Comput. Phys. Commun.* **2009**, *180*, 2582.
- (184) Gonze, X.; et al. A brief introduction to the ABINIT software package. *Zeit. Kristallogr.* **2005**, *220*, 558.
- (185) Gonze, X.; et al. Recent developments in the ABINIT software package. *Comput. Phys. Commun.* **2016**, *205*, 106–131.
- (186) Marsiglio, F.; Schossmann, M.; Carbotte, J. Iterative analytic continuation of the electron self-energy to the real axis. *Phys. Rev. B* **1988**, *37*, 4965.
- (187) Marini, G.; Marchese, G.; Profeta, G.; Sjakste, J.; Macheda, F.; Vast, N.; Mauri, F.; Calandra, M. EPIq: an open-source software for the calculation of electron-phonon interaction related properties. *Comput. Phys. Commun.* **2024**, *295*, No. 108950.
- (188) Margine, E.; Lambert, H.; Giustino, F. Electron-phonon interaction and pairing mechanism in superconducting Ca-intercalated bilayer graphene. *Sci. Rep.* **2016**, *6*, No. 21414.
- (189) Kuderowicz, G.; Wiendlocha, B. Strong-coupling superconductivity of the Heusler-type compound ScAu₂Al: Ab initio studies. *Phys. Rev. B* **2023**, *108*, No. 224501.
- (190) Errea, I.; Calandra, M.; Pickard, C. J.; Nelson, J.; Needs, R. J.; Li, Y.; Liu, H.; Zhang, Y.; Ma, Y.; Mauri, F. High-pressure hydrogen sulfide from first principles: A strongly anharmonic phonon-mediated superconductor. *Phys. Rev. Lett.* **2015**, *114*, No. 157004.
- (191) Akashi, R.; Kawamura, M.; Tsuneyuki, S.; Nomura, Y.; Arita, R. First-principles study of the pressure and crystal-structure dependences of the superconducting transition temperature in compressed sulfur hydrides. *Phys. Rev. B* **2015**, *91*, No. 224513.
- (192) Lejaeghere, K.; et al. Reproducibility in density functional theory calculations of solids. *Science* **2016**, *351*, aad3000.
- (193) Franceschetti, A.; Zunger, A. The inverse band-structure problem of finding an atomic configuration with given electronic properties. *Nature* **1999**, *402*, 60–63.
- (194) Sanchez-Lengeling, B.; Aspuru-Guzik, A. Inverse molecular design using machine learning: Generative models for matter engineering. *Science* **2018**, *361*, 360–365.
- (195) Gómez-Bombarelli, R.; Wei, J. N.; Duvenaud, D.; Hernández-Lobato, J. M.; Sánchez-Lengeling, B.; Sheberla, D.; Aguilera-Iparraguirre, J.; Hirzel, T. D.; Adams, R. P.; Aspuru-Guzik, A. Automatic chemical design using a data-driven continuous representation of molecules. *ACS Cent. Sci.* **2018**, *4*, 268–276.
- (196) Weymuth, T.; Reiher, M. Inverse quantum chemistry: Concepts and strategies for rational compound design. *Int. J. Quantum Chem.* **2014**, *114*, 823–837.
- (197) d'Avezac, M.; Luo, J.-W.; Chanier, T.; Zunger, A. Genetic-Algorithm Discovery of a Direct-Gap and Optically Allowed Superstructure from Indirect-Gap Si and Ge Semiconductors. *Phys. Rev. Lett.* **2012**, *108*, No. 027401.
- (198) Xiang, H. J.; Huang, B.; Kan, E.; Wei, S.-H.; Gong, X. G. Towards Direct-Gap Silicon Phases by the Inverse Band Structure Design Approach. *Phys. Rev. Lett.* **2013**, *110*, No. 118702.
- (199) Lombardo, T.; et al. Artificial intelligence applied to battery research: hype or reality? *Chem. Rev.* **2022**, *122*, 10899–10969.
- (200) Tabor, D. P.; Roch, L. M.; Saikin, S. K.; Kreisbeck, C.; Sheberla, D.; Montoya, J. H.; Dwarakanath, S.; Aykol, M.; Ortiz, C.; Tribukait, H.; Amador-Bedolla, C.; Brabec, C. J.; Maruyama, B.; Persson, K. A.; Aspuru-Guzik, A. Accelerating the discovery of materials for clean energy in the era of smart automation. *Nat. Rev. Mater.* **2018**, *3*, 5–20.
- (201) Tran, H.; Gurnani, R.; Kim, C.; Pilania, G.; Kwon, H.-K.; Lively, R.; Ramprasad, R. Design of Functional and Sustainable Polymers Assisted by Artificial Intelligence. *Nat. Rev. Mater.* **2024**, DOI: [10.1038/s41578-024-00708-8](https://doi.org/10.1038/s41578-024-00708-8).
- (202) Hu, M.; Tan, Q.; Knibbe, R.; Xu, M.; Jiang, B.; Wang, S.; Li, X.; Zhang, M.-X. Recent applications of machine learning in alloy design: A review. *Mater. Sci. Eng. R Rep.* **2023**, *155*, No. 100746.
- (203) Liu, X.; Zhang, J.; Pei, Z. Machine learning for high-entropy alloys: progress, challenges and opportunities. *Prog. Mater. Sci.* **2023**, *131*, No. 101018.
- (204) Mannodi-Kanakkithodi, A.; Pilania, G.; Huan, T. D.; Lookman, T.; Ramprasad, R. Machine Learning Strategy for the Accelerated Design of Polymer Dielectrics. *Sci. Rep.* **2016**, *6*, No. 20952.
- (205) Kim, C.; Batra, R.; Chen, L.; Tran, H.; Ramprasad, R. Polymer Design using Genetic Algorithm and Machine Learning. *Comput. Mater. Sci.* **2021**, *186*, No. 110067.
- (206) Batra, R.; Dai, H.; Huan, T. D.; Chen, L.; Kim, C.; Gutekunst, W. R.; Song, L.; Ramprasad, R. Polymers for Extreme Conditions Designed Using Syntax-Directed Variational Autoencoders. *Chem. Matter.* **2020**, *32*, 10489–10500.
- (207) Huan, T. D.; Sharma, V.; Rossetti, G. A.; Ramprasad, R. Pathways towards ferroelectricity in hafnia. *Phys. Rev. B* **2014**, *90*, No. 064111.
- (208) Tuoc, V. N.; Huan, T. D. Predicted Binary Compounds of Tin and Sulfur. *J. Phys. Chem. C* **2018**, *122*, 17067–17072.
- (209) Togo, A.; Oba, F.; Tanaka, I. First-principles calculations of the ferroelastic transition between rutile-type and CaCl₂-type SiO₂ at high pressures. *Phys. Rev. B* **2008**, *78*, No. 134106.
- (210) Monacelli, L.; Bianco, R.; Cherubini, M.; Calandra, M.; Errea, I.; Mauri, F. The stochastic self-consistent harmonic approximation: calculating vibrational properties of materials with full quantum and anharmonic effects. *J. Phys.: Condens. Matter* **2021**, *33*, No. 363001.
- (211) Semenok, D. V.; et al. Superconductivity at 253 K in lanthanum-yttrium ternary hydrides. *Mater. Today* **2021**, *48*, 18–28.
- (212) Stillinger, F. H. Exponential multiplicity of inherent structures. *Phys. Rev. E* **1999**, *59*, 48.
- (213) Amsler, M.; Flores-Livas, J. A.; Huan, T. D.; Botti, S.; Marques, M. A. L.; Goedecker, S. *Phys. Rev. Lett.* **2012**, *108*, No. 205505.
- (214) Huan, T. D.; Amsler, M.; Marques, M. A. L.; Botti, S.; Willand, A.; Goedecker, S. Low-energy polymeric phases of alanates. *Phys. Rev. Lett.* **2013**, *110*, No. 135502.
- (215) Huan, T. D.; Tuoc, V. N.; Minh, N. V. Layered structures of organic/inorganic hybrid halide perovskites. *Phys. Rev. B* **2016**, *93*, No. 094105.
- (216) Huang, X.; Duan, D.; Li, X.; Li, F.; Huang, Y.; Wu, G.; Liu, Y.; Zhou, Q.; Liu, B.; Cui, T. High-pressure polymorphism as a step towards high density structures of LiAlH₄. *Appl. Phys. Lett.* **2015**, *107*, No. 041906.

- (217) Wei, Y.; Nukala, P.; Salverda, M.; Matzen, S.; Zhao, H. J.; Momand, J.; Everhardt, A. S.; Agnus, G.; Blake, G. R.; Lecoer, P.; Kooi, B. J.; Iñiguez, J.; Dkhil, B.; Noheda, B. A rhombohedral ferroelectric phase in epitaxially strained $\text{Hf}_0.5\text{Zr}_0.5\text{O}_2$ thin films. *Nat. Mater.* **2018**, *17*, 1095–1100.
- (218) Qi, Y.; Singh, S.; Lau, C.; Huang, F.-T.; Xu, X.; Walker, F. J.; Ahn, C. H.; Cheong, S.-W.; Rabe, K. M. Stabilization of competing ferroelectric phases of HfO_2 under epitaxial strain. *Phys. Rev. Lett.* **2020**, *125*, No. 257603.
- (219) Glass, C. W.; Oganov, A. R.; Hansen, N. USPEX-Evolutionary crystal structure prediction. *Comput. Phys. Commun.* **2006**, *175*, 713–720.
- (220) Oganov, A. R.; Glass, C. W. Crystal structure prediction using ab initio evolutionary techniques: Principles and applications. *J. Chem. Phys.* **2006**, *124*, No. 244704.
- (221) Wang, Y.; Lv, J.; Zhu, L.; Ma, Y. CALYPSO A method for crystal structure prediction. *Comput. Phys. Commun.* **2012**, *183*, 2063–2070.
- (222) Pickard, C. J.; Needs, R. J. Ab initio random structure searching. *J. Phys.: Condens. Matter* **2011**, *23*, No. 053201.
- (223) Lonie, D. C.; Zurek, E. XtalOpt An open-source evolutionary algorithm for crystal structure prediction. *Comput. Phys. Commun.* **2011**, *182*, 372–387.
- (224) Hajinazar, S.; Thorn, A.; Sandoval, E. D.; Kharabadez, S.; Kolmogorov, A. N. MAISE: Construction of neural network interatomic models and evolutionary structure optimization. *Comput. Phys. Commun.* **2021**, *259*, No. 107679.
- (225) Goedecker, S. Minima hopping: An efficient search method for the global minimum of the potential energy surface of complex molecular systems. *J. Chem. Phys.* **2004**, *120*, 9911.
- (226) Amsler, M.; Goedecker, S. Crystal structure prediction using the minima hopping method. *J. Chem. Phys.* **2010**, *133*, No. 224104.
- (227) Sun, Y.; Lv, J.; Xie, Y.; Liu, H.; Ma, Y. Route to a Superconducting Phase above Room Temperature in Electron-Doped Hydride Compounds under High Pressure. *Phys. Rev. Lett.* **2019**, *123*, No. 097001.
- (228) Zhong, X.; Sun, Y.; Itaya, T.; Xu, M.; Liu, H.; Hemley, R. J.; Chen, C.; Ma, Y. Prediction of above-room-temperature superconductivity in lanthanide/actinide extreme superhydrides. *J. Am. Chem. Soc.* **2022**, *144*, 13394–13400.
- (229) Zhang, H.; Jin, X.; Lv, Y.; Zhuang, Q.; Liu, Y.; Lv, Q.; Bao, K.; Li, D.; Liu, B.; Cui, T. High-temperature superconductivity in compressed solid silane. *Sci. Rep.* **2015**, *5*, 8845.
- (230) Feng, J.; Grochala, W.; Jarón, T.; Hoffmann, R.; Bergara, A.; Ashcroft, N. Structures and potential superconductivity in SiH_4 at high pressure: En route to “metallic hydrogen”. *Phys. Rev. Lett.* **2006**, *96*, No. 017006.
- (231) Pickard, C. J.; Needs, R. High-pressure phases of silane. *Phys. Rev. Lett.* **2006**, *97*, No. 045504.
- (232) Yao, Y.; Tse, J.; Ma, Y.; Tanaka, K. Superconductivity in high-pressure SiH_4 . *Europhys. Lett.* **2007**, *78*, No. 37003.
- (233) Strobel, T. A.; Ganesh, P.; Somayazulu, M.; Kent, P.; Hemley, R. J. Novel Cooperative Interactions and Structural Ordering in $\text{H}_2\text{S}-\text{H}_2$. *Phys. Rev. Lett.* **2011**, *107*, No. 255503.
- (234) Huang, X.; Wang, X.; Duan, D.; Sundqvist, B.; Li, X.; Huang, Y.; Yu, H.; Li, F.; Zhou, Q.; Liu, B.; Cui, T. High-temperature superconductivity in sulfur hydride evidenced by alternating-current magnetic susceptibility. *Natl. Sci. Rev.* **2019**, *6*, 713–718.
- (235) Einaga, M.; Sakata, M.; Ishikawa, T.; Shimizu, K.; Eremets, M. I.; Drozdov, A. P.; Troyan, I. A.; Hirao, N.; Ohishi, Y. Crystal structure of the superconducting phase of sulfur hydride. *Nat. Phys.* **2016**, *12*, 835–838.
- (236) Nakao, H.; Einaga, M.; Sakata, M.; Kitagaki, M.; Shimizu, K.; Kawaguchi, S.; Hirao, N.; Ohishi, Y. Superconductivity of pure H_3S synthesized from elemental sulfur and hydrogen. *J. Phys. Soc. Jpn.* **2019**, *88*, No. 123701.
- (237) Osmond, I.; Moulding, O.; Cross, S.; Muramatsu, T.; Brooks, A.; Lord, O.; Fedotenko, T.; Buhot, J.; Friedemann, S. Clean-limit superconductivity in $1 \text{ m}^{-3} \text{ m}^3 \text{ H}_3\text{S}$ synthesized from sulfur and hydrogen donor ammonia borane. *Phys. Rev. B* **2022**, *105*, No. L220502.
- (238) Struzhkin, V.; Li, B.; Ji, C.; Chen, X.-J.; Prakapenka, V.; Greenberg, E.; Troyan, I.; Gavriliuk, A.; Mao, H.-k. Superconductivity in La and Y hydrides: Remaining questions to experiment and theory. *Matter Radiat. Extremes* **2020**, *5*, No. 028201.
- (239) Zhou, D.; Semenok, D. V.; Duan, D.; Xie, H.; Chen, W.; Huang, X.; Li, X.; Liu, B.; Oganov, A. R.; Cui, T. Superconducting praseodymium superhydrides. *Sci. Adv.* **2020**, *6*, No. eaax6849.
- (240) Wang, Y.; Wang, K.; Sun, Y.; Ma, L.; Wang, Y.; Zou, B.; Liu, G.; Zhou, M.; Wang, H. Synthesis and superconductivity in yttrium superhydrides under high pressure. *Chin. Phys. B* **2022**, *31*, No. 106201.
- (241) Bhattacharyya, P.; et al. Imaging the Meissner effect in hydride superconductors using quantum sensors. *Nature* **2024**, *627*, 73–79.
- (242) Shao, M.; Chen, S.; Chen, W.; Zhang, K.; Huang, X.; Cui, T. Superconducting ScH_3 and LuH_3 at megabar pressures. *Inorg. Chem.* **2021**, *60*, 15330–15335.
- (243) Kim, D. Y.; Scheicher, R. H.; Mao, H.-k.; Kang, T. W.; Ahuja, R. General trend for pressurized superconducting hydrogen-dense materials. *Proc. Natl. Acad. Sci. U.S.A.* **2010**, *107*, 2793–2796.
- (244) Wei, Y.-K.; Yuan, J.-N.; Khan, F. I.; Ji, G.-F.; Gu, Z.-W.; Wei, D.-Q. Pressure induced superconductivity and electronic structure properties of scandium hydrides using first principles calculations. *RSC Adv.* **2016**, *6*, 81534–81541.
- (245) Troyan, I. A.; et al. Non-Fermi-Liquid Behavior of Superconducting SnH_4 . *Adv. Sci.* **2023**, *10*, No. 2303622.
- (246) He, X.; et al. Superconductivity discovered in niobium polyhydride at high pressures. *Mater. Today Phys.* **2024**, *40*, No. 101298.
- (247) Huang, G.; Peng, D.; Luo, T.; Chen, L.-C.; Dalladay-Simpson, P.; Cao, Z.-Y.; Gorelli, F. A.; Zhong, G.-H.; Lin, H.-Q.; Chen, X.-J. Synthesis of superconducting phase of $\text{La}_0.5\text{Ce}_0.5\text{H}_{10}$ at high pressures. *J. Phys.: Condens. Matter* **2024**, *36*, No. 075702.
- (248) Chen, L.-C.; Luo, T.; Cao, Z.-Y.; Dalladay-Simpson, P.; Huang, G.; Peng, D.; Zhang, L.-L.; Gorelli, F. A.; Zhong, G.-H.; Lin, H.-Q.; Chen, X.-J. Synthesis and superconductivity in yttrium-cerium hydrides at high pressures. *Nat. Commun.* **2024**, *15*, 1809.
- (249) Cross, S.; Buhot, J.; Brooks, A.; Thomas, W.; Kleppe, A.; Lord, O.; Friedemann, S. High-temperature superconductivity in La_4H_{23} below 100 GPa. *Phys. Rev. B* **2024**, *109*, No. L020503.
- (250) Smits, F. Measurement of sheet resistivities with the four-point probe. *Bell Syst. Technol. J.* **1958**, *37*, 711–718.
- (251) Miccoli, I.; Edler, F.; Pfniür, H.; Tegenkamp, C. The 100th anniversary of the four-point probe technique: the role of probe geometries in isotropic and anisotropic systems. *J. Phys.: Condens. Matter* **2015**, *27*, No. 223201.
- (252) De Launay, J. The isotope effect in superconductivity. *Phys. Rev.* **1954**, *93*, 661.
- (253) Garland, J. W., Jr Isotope effect in superconductivity. *Phys. Rev. Lett.* **1963**, *11*, 114.
- (254) Goldfarb, R. B.; Lelental, M.; Thompson, C. In *Magnetic Susceptibility of Superconductors and Other Spin Systems*; Hein, R. A., Francavilla, R. A., Liebenberg, D. H., Eds.; Plenum Press: New York, 1991; Chapter 2, pp 49–80.
- (255) Struzhkin, V. V.; Mao, H.-k. Magnetic Methods in Studies of New Superconducting Hydrides in a Diamond Anvil Cell. *Natl. Sci. Rev.* **2024**, *11*, No. nwae005.
- (256) Troyan, I.; Gavriliuk, A.; Rüffer, R.; Chumakov, A.; Mironovich, A.; Lyubutin, I.; Perekalin, D.; Drozdov, A. P.; Eremets, M. I. Observation of superconductivity in hydrogen sulfide from nuclear resonant scattering. *Science* **2016**, *351*, 1303–1306.
- (257) Ho, K. O.; Wong, K. C.; Leung, M. Y.; Pang, Y. Y.; Leung, W. K.; Yip, K. Y.; Zhang, W.; Xie, J.; Goh, S. K.; Yang, S. Recent developments of quantum sensing under pressurized environment using the nitrogen vacancy (NV) center in diamond. *J. Appl. Phys.* **2021**, *129*, No. 241101.

- (258) Werthamer, N.; Helfand, E.; Hohenberg, P. Temperature and purity dependence of the superconducting critical field, H_c c 2. III Electron spin and spin-orbit effects. *Phys. Rev.* **1966**, *147*, 295.
- (259) Minkov, V.; Ksenofontov, V.; Bud'ko, S.; Talantsev, E.; Eremets, M. Magnetic flux trapping in hydrogen-rich high-temperature superconductors. *Nat. Phys.* **2023**, *19*, 1293.
- (260) Ashcroft, N. W. Metallic hydrogen: A high-temperature superconductor? *Phys. Rev. Lett.* **1968**, *21*, 1748.
- (261) Chen, X.-J.; Struzhkin, V. V.; Song, Y.; Goncharov, A. F.; Ahart, M.; Liu, Z.; Mao, H.-k.; Hemley, R. J. Pressure-induced metallization of silane. *Proc. Natl. Acad. Sci. U.S.A.* **2008**, *105*, 20–23.
- (262) Strobel, T. A.; Goncharov, A. F.; Seagle, C. T.; Liu, Z.; Somayazulu, M.; Struzhkin, V. V.; Hemley, R. J. High-pressure study of silane to 150 GPa. *Phys. Rev. B* **2011**, *83*, No. 144102.
- (263) Chen, X.-J.; Wang, J.-L.; Struzhkin, V. V.; Mao, H.-k.; Hemley, R. J.; Lin, H.-Q. Superconducting behavior in compressed solid SiH₄ with a layered structure. *Phys. Rev. Lett.* **2008**, *101*, No. 077002.
- (264) Martinez-Canales, M.; Oganov, A. R.; Ma, Y.; Yan, Y.; Lyakhov, A. O.; Bergara, A. Novel structures and superconductivity of silane under pressure. *Phys. Rev. Lett.* **2009**, *102*, No. 087005.
- (265) Jin, X.; Meng, X.; He, Z.; Ma, Y.; Liu, B.; Cui, T.; Zou, G.; Mao, H.-k. Superconducting high-pressure phases of disilane **2010**, *107*, 9969–9973.
- (266) Flores-Livas, J. A.; Amsler, M.; Lenosky, T. J.; Lehtovaara, L.; Botti, S.; Marques, M. A.; Goedecker, S. High-pressure structures of disilane and their superconducting properties. *Phys. Rev. Lett.* **2012**, *108*, No. 117004.
- (267) Li, Y.; Hao, J.; Liu, H.; Li, Y.; Ma, Y. The metallization and superconductivity of dense hydrogen sulfide. *J. Chem. Phys.* **2014**, *140*, No. 174712.
- (268) Cho, A. Stinky hydrogen sulfide smashes superconductivity record. *Science* **2015**, DOI: 10.1126/science.aad1628.
- (269) Geballe, Z. M.; Liu, H.; Mishra, A. K.; Ahart, M.; Somayazulu, M.; Meng, Y.; Baldini, M.; Hemley, R. J. Synthesis and stability of lanthanum superhydrides. *Angew. Chem., Int. Ed.* **2018**, *130*, 696–700.
- (270) Liu, H.; Naumov, I. I.; Geballe, Z. M.; Somayazulu, M.; Tse, J. S.; Hemley, R. J. Dynamics and superconductivity in compressed lanthanum superhydride. *Phys. Rev. B* **2018**, *98*, No. 100102.
- (271) Sun, D.; Minkov, V. S.; Mozaffari, S.; Sun, Y.; Ma, Y.; Chariton, S.; Prakapenka, V. B.; Eremets, M. I.; Balicas, L.; Balakirev, F. F. High-temperature superconductivity on the verge of a structural instability in lanthanum superhydride. *Nat. Commun.* **2021**, *12*, 6863.
- (272) Kruglov, I. A.; Semenok, D. V.; Song, H.; Szczęśniak, R.; Wrona, I. A.; Akashi, R.; Davari Esfahani, M. M.; Duan, D.; Cui, T.; Kvashnin, A. G.; Oganov, A. R. Superconductivity of LaH₁₀ and LaH₁₆ polyhydrides. *Phys. Rev. B* **2020**, *101*, No. 024508.
- (273) Song, P.; Hou, Z.; Nakano, K.; Hongo, K.; Maezono, R. Potential high-T_c superconductivity in YCeH_x and LaCeH_x under pressure. *Mater. Today Phys.* **2022**, *28*, No. 100873.
- (274) Salke, N. P.; Davari Esfahani, M. M.; Zhang, Y.; Kruglov, I. A.; Zhou, J.; Wang, Y.; Greenberg, E.; Prakapenka, V. B.; Liu, J.; Oganov, A. R.; Lin, J.-F. Synthesis of clathrate cerium superhydride CeH₉ at 80–100 GPa with atomic hydrogen sublattice. *Nat. Commun.* **2019**, *10*, 4453.
- (275) Materials Genome Initiative. 2011 (accessed 2019-07-01).
- (276) Jain, A.; Ong, S. P.; Hautier, G.; Chen, W.; Richards, W. D.; Dacek, S.; Cholia, S.; Gunter, D.; Skinner, D.; Ceder, G.; Persson, K. A. Commentary: The Materials Project: A materials genome approach to accelerating materials innovation. *APL Mater.* **2013**, *1*, No. 011002.
- (277) Saal, J. E.; Kirklin, S.; Aykol, M.; Meredig, B.; Wolverton, C. Materials design and discovery with high-throughput density functional theory: the open quantum materials database (OQMD). *JOM* **2013**, *65*, 1501–1509.
- (278) Taylor, R. H.; Rose, F.; Toher, C.; Levy, O.; Yang, K.; Buongiorno Nardelli, M.; Curtarolo, S. A RESTful API for exchanging materials data in the AFLOWLIB.org consortium. *Comput. Mater. Sci.* **2014**, *93*, 178–192.
- (279) Agrawal, A.; Choudhary, A. Deep materials informatics: Applications of deep learning in materials science. *MRS Commun.* **2019**, *9*, 779–792.
- (280) Lee, J.; Asahi, R. Transfer learning for materials informatics using crystal graph convolutional neural network. *Comput. Mater. Sci.* **2021**, *190*, No. 110314.
- (281) Batzner, S.; Musaelian, A.; Sun, L.; Geiger, M.; Mailoa, J. P.; Kornbluth, M.; Molinari, N.; Smidt, T. E.; Kozinsky, B. E(3)-equivariant graph neural networks for data-efficient and accurate interatomic potentials. *Nat. Commun.* **2022**, *13*, 2453.
- (282) Kaba, O.; Ravanbakhsh, S. Equivariant networks for crystal structures. *arXiv* **2022**, DOI: 10.48550/arXiv.2211.15420.
- (283) Gong, X.; Li, H.; Zou, N.; Xu, R.; Duan, W.; Xu, Y. General framework for E(3)-equivariant neural network representation of density functional theory Hamiltonian. *Nat. Commun.* **2023**, *14*, 2848.
- (284) Kuenneth, C.; Ramprasad, R. polyBERT: a chemical language model to enable fully machine-driven ultrafast polymer informatics. *Nat. Commun.* **2023**, *14*, 4099.
- (285) Gurnani, R.; Kuenneth, C.; Toland, A.; Ramprasad, R. Polymer informatics at scale with multitask graph neural networks. *Chem. Mater.* **2023**, *35*, 1560–1567.
- (286) Fan, W.; Geerts, F. *Foundations of Data Quality Management*; Springer International Publishing: Cham, Switzerland, 2012; pp 93–118.
- (287) Vu, T. N.; Nayak, S. K.; Nguyen, N. T. T.; Alpay, S. P.; Tran, H. Atomic configurations for materials research: A case study of some simple binary compounds. *AIP Adv.* **2021**, *11*, No. 045120.
- (288) Tuoc, V. N.; Nguyen, N. T.; Sharma, V.; Huan, T. D. Probabilistic Deep Learning Approach for Targeted Hybrid Organic-Inorganic Perovskites. *Phys. Rev. Mater.* **2021**, *5*, No. 125402.
- (289) Bergerhoff, G.; Hundt, R.; Sievers, R.; Brown, I. The inorganic crystal structure data base. *J. Chem. Inf. Comput. Sci.* **1983**, *23*, 66–69.
- (290) Ward, L.; Agrawal, A.; Choudhary, A.; Wolverton, C. A general-purpose machine learning framework for predicting properties of inorganic materials. *npj Comput. Mater.* **2016**, *2*, No. 16028.
- (291) Breiman, L. Random forests. *Mach. Learn.* **2001**, *45*, 5–32.
- (292) Tuoriniemi, J.; Juntunen-Nurmilaukas, K.; Uusvuori, J.; Pentti, E.; Salmela, A.; Sebedash, A. Superconductivity in lithium below 0.4 millikelvin at ambient pressure. *Nature* **2007**, *447*, 187–189.
- (293) Matthias, B. *Progress in Low Temperature Physics*; Elsevier, 1957; Vol. 2, Chapter 5, pp 138–150.
- (294) Buzea, C.; Robbie, K. Assembling the puzzle of superconducting elements: a review. *Supercond. Sci. Technol.* **2005**, *18*, R1.
- (295) Kuz'min, V.; Artemenko, A. G.; Muratov, E. N. Hierarchical QSAR technology based on the Simplex representation of molecular structure. *J. Comp. Aided Mol. Des.* **2008**, *22*, 403–421.
- (296) Kohonen, T. Essentials of the self-organizing map. *Neural Netw.* **2013**, *37*, 52–65.
- (297) Van der Maaten, L.; Hinton, G. Visualizing data using t-SNE. *Journal of Machine Learning Research* **2008**, *9*, 2579–2605.
- (298) Chen, T.; Guestrin, C. Xgboost: A scalable tree boosting system. *arXiv* **2016**, DOI: 10.48550/arXiv.1603.02754.
- (299) Kuenneth, C.; Rajan, A. C.; Tran, H.; Chen, L.; Kim, C.; Ramprasad, R. Polymer Informatics with Multi-Task Learning. *Patterns* **2021**, *2*, No. 100238.
- (300) Kuenneth, C.; Lalonde, J.; Marrone, B. L.; Iverson, C. N.; Ramprasad, R.; Pilania, G. Bioplastic Design using Multitask Deep Neural Networks. *Commun. Mater.* **2022**, *3*, 96.
- (301) Gražulis, S.; Daškevič, A.; Merkys, A.; Chateigner, D.; Lutterotti, L.; Quirós, M.; Serebryanyaya, N. R.; Moeck, P.; Downs, R. T.; Le Bail, A. Crystallography Open Database (COD): an open-access collection of crystal structures and platform for world-wide collaboration. *Nucleic Acids Res.* **2012**, *40*, D420–D427.
- (302) Winiarski, M. J.; Wiendlocha, B.; Golęb, S.; Kushwaha, S. K.; Wiśniewski, P.; Kaczorowski, D.; Thompson, J. D.; Cava, R. J.; Klimczuk, T. Superconductivity in CaBi₂. *Phys. Chem. Chem. Phys.* **2016**, *18*, 21737–21745.

- (303) Wold, S.; Sjöström, M.; Eriksson, L. PLS-regression: a basic tool of chemometrics. *Chemometr. Intell. Lab. Syst.* **2001**, *58*, 109–130.
- (304) De, S.; Bartók, A. P.; Csányi, G.; Ceriotti, M. Comparing molecules and solids across structural and alchemical space. *Phys. Chem. Chem. Phys.* **2016**, *18*, 13754–13769.
- (305) Smola, A. J.; Schölkopf, B. A tutorial on support vector regression. *Stat. Comput.* **2004**, *14*, 199–222.
- (306) Friedman, J. H. Greedy function approximation: a gradient boosting machine. *Annals of Statistics* **2001**, *29*, 1189–1232.
- (307) Choudhary, K.; DeCost, B. Atomistic line graph neural network for improved materials property predictions. *npj Comput. Mater.* **2021**, *7*, 185.
- (308) Ward, L.; et al. Matminer: An open source toolkit for materials data mining. *Comput. Mater. Sci.* **2018**, *152*, 60–69.
- (309) Williams, C. K. I.; Rasmussen, C. E. In *Advances in Neural Information Processing Systems 8*; Touretzky, D. S., Mozer, M. C., Hasselmo, M. E., Eds.; MIT Press: Cambridge, MA, 1995.
- (310) Rasmussen, C. E., Williams, C. K. I., Eds. *Gaussian Processes for Machine Learning*; MIT Press: Cambridge, MA, 2006.
- (311) De Breuck, P.-P.; Hautier, G.; Rignanese, G.-M. Materials property prediction for limited datasets enabled by feature selection and joint learning with MODNet. *npj Comput. Mater.* **2021**, *7*, 83.
- (312) Alexandria database. <https://alexandria.icams.rub.de>.
- (313) Behler, J.; Parrinello, M. Generalized Neural-Network Representation of High-Dimensional Potential-Energy Surfaces. *Phys. Rev. Lett.* **2007**, *98*, No. 146401.
- (314) Bartók, A. P.; Payne, M. C.; Kondor, R.; Csányi, G. Gaussian Approximation Potentials: The Accuracy of Quantum Mechanics, without the Electrons. *Phys. Rev. Lett.* **2010**, *104*, No. 136403.
- (315) Bartók, A. P.; De, S.; Poelking, C.; Bernstein, N.; Kermode, J. R.; Csányi, G.; Ceriotti, M. Machine learning unifies the modeling of materials and molecules. *Sci. Adv.* **2017**, *3*, No. e1701816.
- (316) Thompson, A. P.; Swiler, L. P.; Trott, C. R.; Foiles, S. M.; Tucker, G. K. Spectral neighbor analysis method for automated generation of quantum-accurate interatomic potentials. *J. Comput. Phys.* **2015**, *285*, 316–330.
- (317) Chen, C.; Deng, Z.; Tran, R.; Tang, H.; Chu, I.-H.; Ong, S. P. Accurate force field for molybdenum by machine learning large materials data. *Phys. Rev. Mater.* **2017**, *1*, No. 043603.
- (318) Shapeev, A. V. Moment tensor potentials: A class of systematically improvable interatomic potentials. *Multiscale Model. Simul.* **2016**, *14*, 1153–1173.
- (319) Gubaev, K.; Podryabinkin, E. V.; Hart, G. L.; Shapeev, A. V. Accelerating high-throughput searches for new alloys with active learning of interatomic potentials. *Comput. Mater. Sci.* **2019**, *156*, 148–156.
- (320) Zhang, L.; Han, J.; Wang, H.; Car, R.; Weinan, E. Deep potential molecular dynamics: a scalable model with the accuracy of quantum mechanics. *Phys. Rev. Lett.* **2018**, *120*, No. 143001.
- (321) Matlantis. <https://matlantis.com/>.
- (322) Pickard, C. J. Ephemeral data derived potentials for random structure search. *Phys. Rev. B* **2022**, *106*, No. 014102.
- (323) Ouyang, R.; Curtarolo, S.; Ahmetcik, E.; Scheffler, M.; Ghiringhelli, L. M. SISSO: A compressed-sensing method for identifying the best low-dimensional descriptor in an immensity of offered candidates. *Phys. Rev. Mater.* **2018**, *2*, No. 083802.
- (324) Choi, H. J.; Louie, S. G.; Cohen, M. L. Anisotropic Eliashberg theory for superconductivity in compressed and doped MgB₂. *Phys. Rev. B* **2009**, *79*, No. 094518.
- (325) Calandra, M.; Profeta, G.; Mauri, F. Adiabatic and nonadiabatic phonon dispersion in a Wannier function approach. *Phys. Rev. B* **2010**, *82*, No. 165111.
- (326) Kong, Y.; Dolgov, O.; Jepsen, O.; Andersen, O. Electron-phonon interaction in the normal and superconducting states of MgB₂. *Phys. Rev. B* **2001**, *64*, No. 020501.
- (327) Bohnen, K.-P.; Heid, R.; Renker, B. Phonon dispersion and electron-phonon coupling in MgB₂ and AlB₂. *Phys. Rev. Lett.* **2001**, *86*, 5771.
- (328) Choi, H. J.; Roundy, D.; Sun, H.; Cohen, M. L.; Louie, S. G. First-principles calculation of the superconducting transition in MgB₂ within the anisotropic Eliashberg formalism. *Phys. Rev. B* **2002**, *66*, No. 020513.
- (329) Chandrasekaran, A.; Kamal, D.; Batra, R.; Kim, C.; Chen, L.; Ramprasad, R. Solving the electronic structure problem with machine learning. *npj Comput. Mater.* **2019**, *5*, 22.
- (330) Li, H.; Wang, Z.; Zou, N.; Ye, M.; Xu, R.; Gong, X.; Duan, W.; Xu, Y. Deep-learning density functional theory Hamiltonian for efficient ab initio electronic-structure calculation. *Nat. Comput. Sci.* **2022**, *2*, 367–377.
- (331) Scherbela, M.; Reisenhofer, R.; Gerard, L.; Marquetand, P.; Grohs, P. Solving the electronic Schrödinger equation for multiple nuclear geometries with weight-sharing deep neural networks. *Nat. Comput. Sci.* **2022**, *2*, 331–341.
- (332) del Rio, B. G.; Phan, B.; Ramprasad, R. A deep learning framework to emulate density functional theory. *npj Comput. Mater.* **2023**, *9*, 158.
- (333) Del Rio, B. G.; Kuenneth, C.; Tran, H. D.; Ramprasad, R. An Efficient Deep Learning Scheme To Predict the Electronic Structure of Materials and Molecules: The Example of Graphene-Derived Allotropes. *J. Phys. Chem. A* **2020**, *124*, 9496–9502.
- (334) Li, H.; Tang, Z.; Fu, J.; Dong, W.-H.; Zou, N.; Gong, X.; Duan, W.; Xu, Y. Deep-learning density functional perturbation theory. *Phys. Rev. Lett.* **2024**, *132*, No. 096401.
- (335) Lüders, M.; Marques, M.; Lathiotakis, N.; Floris, A.; Profeta, G.; Fast, L.; Continenza, A.; Massidda, S.; Gross, E. Ab initio theory of superconductivity. I. Density functional formalism and approximate functionals. *Phys. Rev. B* **2005**, *72*, No. 024545.
- (336) Marques, M.; Lüders, M.; Lathiotakis, N.; Profeta, G.; Floris, A.; Fast, L.; Continenza, A.; Gross, E.; Massidda, S. Ab initio theory of superconductivity. II Application to elemental metals. *Phys. Rev. B* **2005**, *72*, No. 024546.
- (337) Sanna, A.; Pellegrini, C.; Gross, E. Combining Eliashberg theory with density functional theory for the accurate prediction of superconducting transition temperatures and gap functions. *Phys. Rev. Lett.* **2020**, *125*, No. 057001.
- (338) Li, Z.; Antonius, G.; Chan, Y.-H.; Louie, S. G. Electron-phonon coupling from GW perturbation theory: Practical workflow combining BerkeleyGW, ABINIT, and EPW. *Comput. Phys. Commun.* **2024**, *295*, No. 109003.
- (339) ChatGPT. <https://chat.openai.com/chat>.
- (340) Llama. <https://llama.meta.com/>.
- (341) Dagdelen, J.; Dunn, A.; Lee, S.; Walker, N.; Rosen, A. S.; Ceder, G.; Persson, K. A.; Jain, A. Structured information extraction from scientific text with large language models. *Nat. Commun.* **2024**, *15*, 1418.
- (342) Zheng, Z.; Zhang, O.; Borgs, C.; Chayes, J. T.; Yaghi, O. M. ChatGPT chemistry assistant for text mining and the prediction of MOF synthesis. *J. Am. Chem. Soc.* **2023**, *145*, 18048–18062.
- (343) Cadden-Zimansky, P.; Wei, J.; Chandrasekhar, V. Cooper-pair-mediated coherence between two normal metals. *Nat. Phys.* **2009**, *5*, 393–397.
- (344) Balestrieri, R.; Pesenti, J.; LeCun, Y. Learning in high dimension always amounts to extrapolation. *arXiv* **2021**, DOI: [10.48550/arXiv.2110.09485](https://doi.org/10.48550/arXiv.2110.09485).